Winter 2010

Constrained Optimal Orbit Design for Earth Observation

Sharon D. Vtipil
Old Dominion University

CONSTRAINED OPTIMAL ORBIT DESIGN FOR EARTH OBSERVATION

by

Sharon D. Vtipil
B.S. May 1997, United States Naval Academy
M.E. December 2000, University of Florida

A Dissertation Submitted to the Faculty of
Old Dominion University in Partial Fulfillment of the
Requirement for the Degree of

DOCTOR OF PHILOSOPHY

AEROSPACE ENGINEERING

OLD DOMINION UNIVERSITY
December 2010

Approved by:

_____
Brett A. Newman (Chairman)

_____
Robert L. Ash (Member)

_____
John Adam (Member)

ABSTRACT

CONSTRAINED OPTIMAL ORBIT DESIGN FOR EARTH OBSERVATION

Sharon D. Vtipil
Old Dominion University, 2010
Chairman: Dr. Brett A. Newman

The purpose of this dissertation is to demonstrate user requirements for a satellite observation mission can be used to determine a constrained optimal orbit based on observation site requirements, observation condition restraints, and sensor characteristics. The typical Earth observation satellite is first designed according to an appropriate orbit; then the observation requirements are used to develop a target schedule. The new design process outlines the development of the appropriate orbit by incorporating user requirements at the forefront of mission planning, not after an orbit has been selected. This research shows how to map the user requirements into constraints for the cost function and optimization process. A global case study with variations demonstrates the effectiveness of the design process. Additionally, a case study is performed for a regional or clustered set of targets. Finally, a lifecycle analysis tests the orbit in a full perturbation environment to evaluate the changes in the ideal orbital elements over time without orbit maintenance or corrections.

This dissertation is dedicated to my precious son Daniel with whom I started this journey and my beloved daughter Gabrielle who is just starting her own journey.

ACKNOWLEDGEMENTS

My appreciation for making this dissertation possible first goes to Dr. Newman for allowing me the freedom to pursue my passion and whose guidance has been invaluable. My deepest gratitude goes to my parents who taught me to dream big, my husband for his unwavering support, and to my math teacher Ms. Bell who challenged me to learn not just memorize. I would also like to thank Dr. Adam and Dr. Ash, members of my dissertation committee, for their guidance and encouragement. To God be the glory.

TABLE OF CONTENTS

Chapter-Section Page

LIST OF TABLES.....ix

LIST OF FIGURES.....x

1. INTRODUCTION.....1

1.1 Problem Motivation.....1

1.2 Literature Review.....5

1.2.1 Orbital Mechanics.....5

1.2.2 Orbital Propagation.....9

1.2.3 Perturbations.....11

1.2.4 Orbit Design.....13

1.2.5 Scheduling Options.....15

1.2.6 Optimization.....16

1.2.7 Problem Statement.....18

1.2.8 Assumptions.....19

1.3 Dissertation Outline.....20

2. ORBIT DESIGN METHODOLOGY.....21

2.1 Introduction.....21

2.2 Design Process.....21

2.3 Mission Requirements.....23

2.4 Bounding the Problem.....24

2.5 Optimization Parameters.....28

2.6 Lifecycle Analysis.....29

3. REPEATING GROUND TRACK CONCEPTS.....31

3.1 Repeating Methods.....31

3.2 Condition for Repeating Ground Tracks.....33

3.2.1 Flower Constellation.....36

3.2.2 Epicyclic Motion Repeat Ground Track Orbit.....39

3.2.3 Modified Flower Constellation.....42

3.2.4 Simplified Repeat Groundtrack.....46

3.3 Method Comparisons.....48

3.3.1 Semi-Major Axis Comparison.....48

3.3.2 Computational Time Comparison.....54

3.3.3 Residual Comparison.....60

3.3.4 Comparison Conclusions.....67

4. OPTIMIZATION PROCESS.....70

4.1 Optimization Cost Function.....70

4.2 Optimization Process.....79

4.3 Genetic Algorithm Optimality.....82

5. UNMODELED ON-ORBIT PERTURBATIONS.....87

5.1 Introduction to Space Surveillance.....87

5.2 Cowell's Formulation.....89

5.3 Disturbing Functions.....90

5.3.1 Non-Spherical Earth.....90

5.3.2 Aerodynamic Drag.....99

5.3.3 Solar Radiation.....101

5.3.4 Third Body Effects.....102

5.4 Employing Perturbations.....104

6. CASE STUDY RESULTS.....105

6.1 Global Case Study.....105

6.1.1 Global Baseline.....106

6.1.2 Minimum Duration Variation.....109

6.1.3 Revisit Rate Variation.....111

6.1.4 Lighting Condition Variation.....114

6.1.5 Maximum Sun Angle Variation.....117

6.1.6 Field of View Variation.....119

6.1.7 Slew Variation.....122

6.1.8 Resolution Altitude Variation.....124

6.2 Regional Case Study.....126

6.3 Lifecycle Analysis.....129

7. CONCLUSIONS.....143

7.1 Conclusions.....143

7.2 Recommendations.....144

REFERENCES.....145

VITA.....152

LIST OF TABLES

Table		Page
4.1	Orbital Elements for Population Sizes 20, 100, 250, and 500	86
6.1	Global Observation Sites	105
6.2	Case Study Baseline and Variations	106
6.3	Global Baseline Schedule	107
6.4	Minimum Duration Variation Schedule	109
6.5	Revisit Rate Variation Schedule	112
6.6	Lighting Condition Variation Schedule	115
6.7	Maximum Sun Angle Variation Schedule	118
6.8	Field of View Variation Schedule	120
6.9	Slew Variation Schedule	122
6.10	Resolution Altitude Variation Schedule	124
6.11	Regional Observation Sites	126
6.12	Regional Case Schedule	127
6.13	Satellite Description	129
6.14	First Repetition Cycle Schedule	141
6.15	Tenth Repetition Cycle Schedule	142

LIST OF FIGURES

Figure		Page
1.1a	Keplerian Orbital Elements	7
1.1b	Keplerian Orbital Elements	8
2.1	Information Flow for Orbital Design Based on User Requirements	22
2.2	Mapping Mission Requirements	25
2.3	Mapping Secondary Requirements	27
3.1	Inertial vs. Reference Orbits	33
3.2	Perturbing Elements for Repeating Ground Tracks	34
3.3	Epicyclic Motion	39
3.4	Inclination vs. Semi-Major Axis for FC Methods, τ = ½	50
3.5	Inclination vs. Semi-Major Axis for ERO Methods, τ =	50
3.6	Inclination vs. Semi-Major Axis for MFC Methods, τ = ½	51
3.7	Inclination vs. Semi-Major Axis for FC Methods, τ = ¼	51
3.8	Inclination vs. Semi-Major Axis for ERO Methods, τ = ¼	52
3.9	Inclination vs. Semi-Major Axis for MFC Methods, τ = ¼	52
3.10	Inclination vs. Semi-Major Axis for FC Methods, τ = 1/16	53
3.11	Inclination vs. Semi-Major Axis for ERO Methods, τ = 1/16	53
3.12	Inclination vs. Semi-Major Axis for MFC Methods, τ = 1/16	54
3.13	Computational Times for FC, τ = ½	56
3.14	Computational Times for ERO, τ = ½	56
3.15	Computational Times for MFC, τ = ½	57
3.16	Computational Times for FC, τ = ¼	57

3.17 Computational Times for ERO, τ = ¼.....58

3.18 Computational Times for MFC, τ = ¼.....58

3.19 Computational Times for FC, τ = 1/16.....59

3.20 Computational Times for ERO, τ = 1/16.....59

3.21 Computational Times for MFC, τ = 1/16.....60

3.22 Function Value for FC, τ = ½.....61

3.23 Function Value for ERO, τ = ½.....62

3.24 Function Value for EROr, τ = ½.....62

3.25 Function Value for MFC, τ = ½.....63

3.26 Function Value for FC, τ = ¼.....63

3.27 Function Value for ERO, τ = ¼.....64

3.28 Function Value for EROr, τ = ¼.....64

3.29 Function Value for MFC, τ = ¼ 65

3.30 Function Value for FC, τ = 1/16.....65

3.31 Function Value for ERO, τ = 1/16.....66

3.32 Function Value for EROr, τ = 1/16.....66

3.33 Function Value for MFC, τ = 1/16.....67

4.1 Satellite Position and Geometry.....71

4.2 Optimal Orbit for Highest Resolution Cost Function for Two Sites.....72

4.3 Optimal Orbit for Highest Resolution Cost Function for 20 Sites.....73

4.4 Optimal Orbit for Maximum Observation Time Cost Function for 20 Sites.....73

4.5 Crossover.....81

4.6 Cost Function Value for Population Sizes 20, 100, 250, and 500.....83

4.7 Generations for Population Sizes 20, 100, 250, and 500.....84

4.8 Run Times for Population Sizes 20, 100, 250, and 500.....84

5.1 Orbital Model Information Flow.....87

5.2 Non-Spherical Earth Geometry.....91

5.3 Zonal Harmonics.....95

5.4 Sectorial Harmonics.....95

5.5 Tesseral Harmonics.....96

5.6 Geocentric vs. Geodetic Coordinates.....98

5.7 Satellite Altitude.....99

6.1 Global Baseline Ground Trace.....108

6.2 Minimum Duration Variation Ground Trace.....110

6.3 Revisit Rate Variation Ground Trace.....113

6.4 Lighting Condition Variation Ground Trace.....116

6.5 Maximum Sun Angle Variation Ground Trace.....119

6.6 Field of View Variation Ground Trace.....121

6.7 Slew Variation Ground Trace.....123

6.8 Resolution Altitude Variation Ground Trace.....125

6.9 Regional Case Ground Trace.....128

6.10 Longitude of Ascending Node over Time.....130

6.11 Argument of Perigee over Time.....131

6.12 Inclination over Time.....132

6.13 True Anomaly over Time.....133

6.14 Height of Perigee over Time.....134

6.15 Semi-Major Axis over Time.....135

6.16 Eccentricity over Time.....136

6.17 Cost Function Value over Time.....137

6.18 Perturbed Ground Trace.....138

6.19 Perturbed Orbit Polar View.....139

6.20 Perturbed Orbit Equatorial View.....140

CHAPTER 1

INTRODUCTION

1.1 Problem Motivation

To obtain the ultimate view, the human has pursued the high ground. The first high ground was terrestrial; the hill, mountain, or cliff. This advantageous view served as a look out for approaching visitors whether friend or foe. The high ground provided a military advantage to see the battlefield for maneuvering troops or political advantage of viewing one's realm. Humans also learned to build towers as tall as their engineering skills allowed reaching into the sky to gain an aerial view.[1] Towers are an integral part of fortresses for lookouts and serve as lighthouses to lead ships to safety.

As technology advanced, the high ground became the sky. The first recorded use of the sky as the high ground was in 1794 when a French officer used a hot air balloon to watch Austrian army troop movements.[2] On December 17, 1903, in Kitty Hawk, North Carolina, man first achieved powered flight.[3] Wilbur Wright expressed his belief in a letter "For some years I have been afflicted with the belief that flight is possible to man."[4] Orville Wright was "proud that he and his brother had made something of themselves, and had used their own wits and their modest resources to change the future; that of all the giants who had come before, he and Wilbur alone had the gumption and the know-how to succeed with their frail machine of sticks and canvas on the remote stretch of sand at Kitty Hawk."[5] Airplanes quickly found their purpose for providing aerial reconnaissance. By 1910 Britain, France, and Germany recognized the value of winged aircraft for reconnaissance.[4] Whereas cavalry scouts on the ground might be gone for

days, airplanes could cover more ground in hours instead of days, much better than a lieutenant gripping a church steeple.[5] As early as 1914, the first cameras were employed on British squadron aircraft becoming the first photoreconnaissance aircraft.[6] "The first really successful air reconnaissances were made, not on the Western Front, but in East Prussia, where the Germans were withstanding the advance of superior numbers of Russian troops in late 1914. During the decisive Battle of Tannenberg an unexpected Russian attack was reported by *Fliegerabteilung 14*; the crew of the third machine of that unit to observe the enemy movement, Lts. Canter and Mertens, made a personal report to Generals Hindenburg and Ludendorff at headquarters, and the Russians were later forced to withdraw."[6] In battle, these eyes in the sky could scout out advancing armies and provide critical data for development of battle maneuvers.

Airplanes also found civilian usefulness for this high ground. In 1919, the first aerial surveying and mapping operations began with the U.S. Coast and Geodetic survey of Atlantic City.[4] Even in peacetime operations, aircraft were employed for special missions to gain insight into an opponent's realm. For example in 1956 President Eisenhower authorized the U-2, a new reconnaissance aircraft, to overfly the Soviet Union.[7] The U-2 was designed to fly fifteen thousand feet higher than any Soviet fighter or missile and be undetectable.[8] Eisenhower ordered the U-2 to be a civilian effort because he was immensely concerned that a military incursion into Soviet airspace could ignite a war.[8] He was concerned about the rudimentary character of intelligence estimates of the Soviet Union military stature. He wanted to develop policies based on estimates of the actual situation, not speculation.[9] In a few flights, the images brought back by the U-2 showed the Soviets were not racing ahead of the US in development of

the heavy bombers.[8] Eisenhower stopped the overflights when the Soviets shot down a U-2 on 1 May 1960.[10] Speaking on the achievements of the U-2, Eisenhower noted the program "produced intelligence of critical importance to the United States" and "perhaps as important as the positive information-what the Soviets did have- was the negative information it produced-what the Soviets did not have."[8] Today airborne sensors continue to provide valuable information for a multitude of surveillance and reconnaissance missions.

In understanding the advantage of high ground, humans pushed forward to the ultimate high ground, space. Eisenhower looked to higher heights where platforms could not be shot down.[7] He wanted freedom in space.

> ...by establishing principle of freedom of space, the as-yet-untested doctrine that terrestrial laws, including traditional claims of sovereign airspace, did not extend into space. The Eisenhower administration knew this novel legal issue was pivotal. If the Soviet Union or other nations asserted that their restricted national airspace extended above the atmosphere, the operation of any kind of satellites, whether civilian or military, would be impeded...[8]

The Russians first entered this realm of space with the launch of the satellite *Sputnik* in 1957.[11] Sputnik was only 58 centimeters in diameter and weighed only 84 kilograms.[1] The Americans quickly answered the Russians with the launch of *Explorer 1* on 31 January 1958.[1] The precedence of satellite overflight was quickly established.[7] Also, the concept of remote sensing satellite overflight was acknowledged when the Soviet leader Khrushchev said "he did not care how many satellites flew over his territory" and that "anyone might take all the pictures he wished from satellites over Soviet territory."[8] As Eisenhower desired, the satellite reconnaissance missions were less vulnerable to being

shot down than were U2. Satellites quickly found the new high ground, space, advantageous for reconnaissance and surveillance missions.

The idea of looking down on the Earth's surface to obtain information describes remote sensing. Formally, remote sensing is defined as "the practice of deriving information about the Earth's land and water surfaces using images acquired from an overhead perspective, using electromagnetic radiation in one or more regions of the electromagnetic spectrum, reflected or emitted from the Earth's surface."[9] Employing overhead platforms for remote sensing is well stated by the following explanation:

> Space-based systems in appropriate orbital deployments provide worldwide coverage and frequent access to specific Earth locations, including those denied to terrestrial-based forces, on a recurring basis. Unconstrained by political boundaries, satellites deployed in specific orbits and in sufficient numbers maintain a continuous presence over enemy [and friendly] territory....Although space systems provide global coverage, some can be focused to provide information on specific areas of interest, which can improve situational awareness and planning tempo and can enable information dominance for all friendly military forces.[12]

Corona was the first American military program to put this philosophy into action. The data provided key intelligence on Soviet programs, including missile complexes, test ranges, ship deployments, aircraft operations, and atomic weapons storage facilities.[10] The Corona series, a secret military intelligence imagery space-based platform, took over 800,000 images from 1960 to 1972.[10]

Even though secret military reconnaissance missions may continue, satellites have also taken their place in the civilian realm. Views from space enable sensors to gather information about crops and natural resources greatly facilitating farmers and resource managers.[13] Space-based imagery enables map development to see changes in a given area or to reveal unfamiliar terrain.[14,15] These imagery products are used in developing

agriculture management, forestry practices, disaster relief operations, fire-fighting, and urban planning.[10] Also, an eye can be kept on potential adversaries for troop movements and violations of international treaties.[14] During wartime, space-based sensors provide photoreconnaissance and radar data to locate and identify targets.[7] Whether for military or civilian purposes, space has enabled enhanced missions for reconnaissance and surveillance.

The pursuit of the high ground has led man to better understand his environment and surroundings. From military to civilian missions the field of remote sensing, observing from a distance, continues to grow. This research explores the challenge of determining an optimal orbit for observing a given set of desired ground locations. This orbit can be used in the mission design process of a new satellite or to maneuver a current on-orbit satellite. The purpose of this research is for better employment of space-based Earth observing sensors.

1.2 Literature Review

1.2.1 Orbital Mechanics

The basis of understanding the newest domain of high ground, space, lies with the study of orbital dynamics, the study of motion of one body revolving around another body. The governing laws were first understood by the great scientists like Johann Kepler and Isaac Newton. Kepler studied precise astronautical observations provided by Tycho Brahe,[3] and from these studies of this data, Kepler discovered three important orbital laws.[16]

1. The orbit of each planet is an ellipse with the Sun at one focus.

2. The line joining the planet to the Sun sweeps out equal areas in equal times.
3. The square of the period of a planet is proportional to the cube of its mean distance to the Sun.

Each orbit is described by three main components: size, shape, and orientation. These three main components are often quantified by the classical orbital elements or Keplerian orbital elements. The first five elements describe the orbit while the sixth element places the satellite along the orbit. The six orbital elements include:[14]

1. Semi-Major axis: describes the orbit's size. This variable is half the distance of the major (long) axis.
2. Eccentricity: describes the orbit's shape. For Earth satellites, the orbit will be either circular where eccentricity is zero or elliptical where eccentricity is between zero and one.
3. Inclination: one of three elements to describe the orbit's position. This variable is the tilt of the orbit with respect to the Earth's equatorial plane.
4. Longitude of Ascending Node: one of three elements to describe the orbit's position. This variable is the swivel of the orbit with respect to the Earth's equatorial plane. This angle is measured from the vernal equinox to the ascending node, the point in the orbit where the satellite goes from below the equator to above the equator.
5. Argument of Perigee: one of the three elements to describe the orbit's position. This variable is the angle from the ascending node to perigee, the point of the orbit closest to the Earth.

6. True Anomaly: describes the satellite's position. This variable is the angle from perigee to the satellite position.

Together these six elements describe the satellite's orbit (Figure 1.1a) and its location on the orbit (Figure 1.1b).

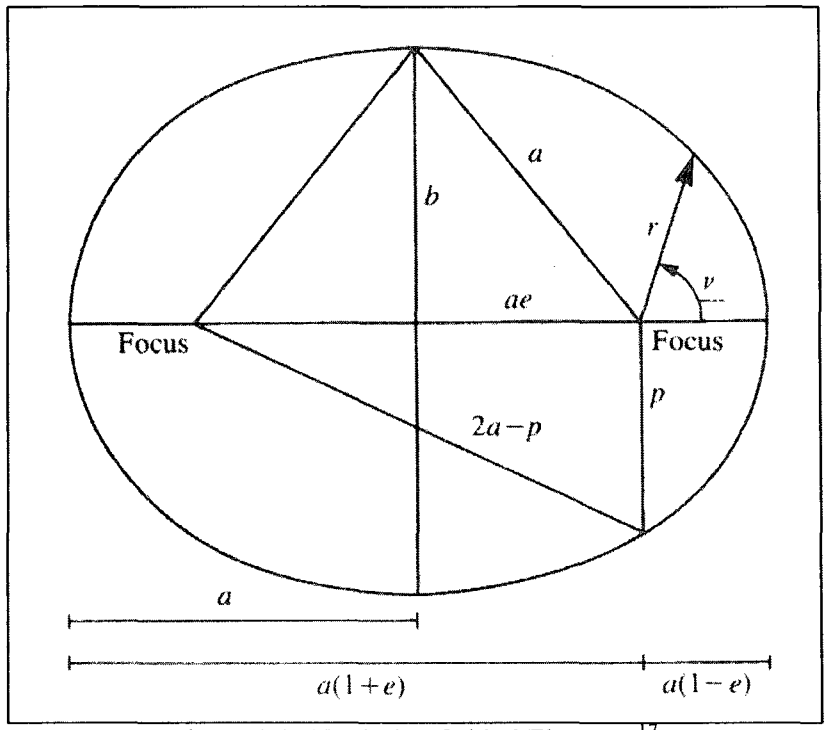

Figure 1.1a Keplerian Orbital Elements[17]

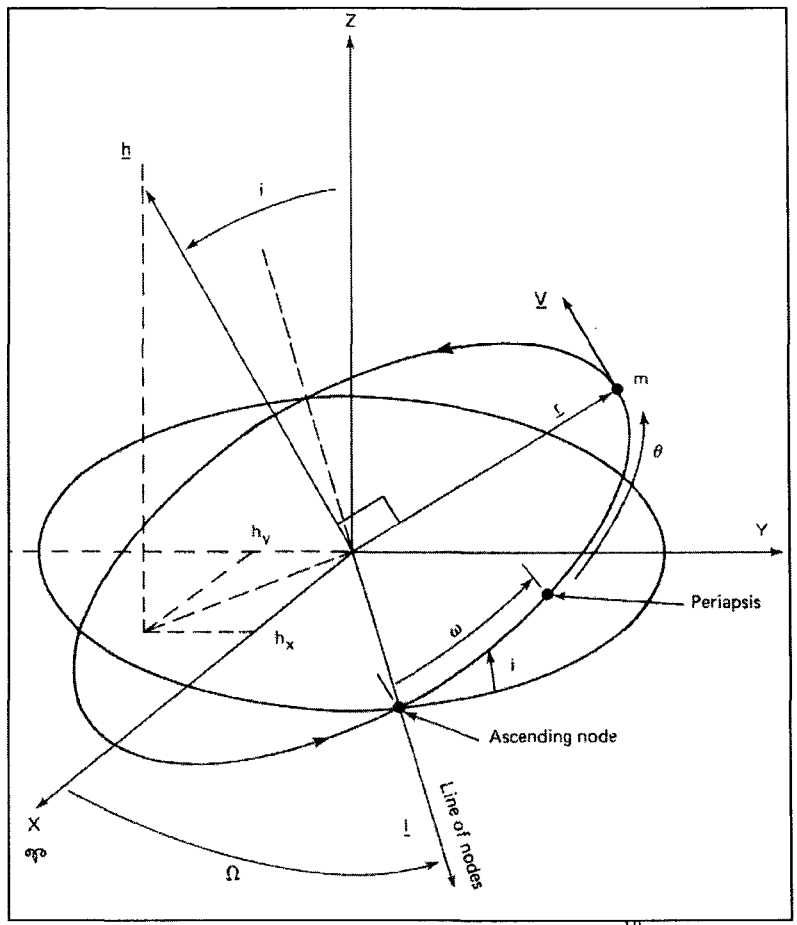

Figure 1.1b Keplerian Orbital Elements[18]

Another way to describe the motion of one body around another is to use the position and velocity vectors at a given time reference. Note the correlation of the three components of each of the position and velocity vectors for a total of six elements to the six Keplerian orbital elements needed to fully describe orbital motion. In fact, the choice of orbital elements or position and velocity vectors may depend on the situation. Additionally, transformations between the two sets of elements are available.

While Kepler was able to describe the kinematics of motion, Newton was able to describe the dynamics of motion.[16] Newton's three laws of motion include:

1. Every body continues in its state of rest, or of uniform motion in a right [straight] line, unless it is compelled to change that state by forces impressed upon it.
2. The change of motion is proportional to the motive force impressed and is made in the direction of the right line in which that force is impressed.
3. To every action there is always opposed an equal reaction: or, the mutual actions of two bodies upon each other are always equal and direction to contrary parts.

While Kepler and Newton laid the foundation of understanding for orbital motion, Konstantin Tsiolkovskii, father of astronautics, paved the way for man to reach the stars through his groundwork in modern rocketry. He calculated a spacecraft would need to obtain a velocity of 7 km/sec to enter orbit around the Earth. He proposed the concept of a multistage rocket and presented discussions of weightlessness, artificial satellites, and space stations.[11] Others like Robert Goddard, Wernher von Braun, and Sergei Korolev brought rocketry to fruition. Although man has achieved the dream of reaching the heavens to look down upon our planet, the intricacies of orbital mechanics are still sought.

1.2.2 Orbital Propagation

Several methods are available for orbital propagation, some use ideal conditions and others take into consideration special circumstances such as perturbations. Under ideal conditions, the two body Lagrange Coefficients method is quite useful to propagate the orbit. Also, numerical integration algorithms may be used for ideal conditions and for special circumstances. Various strategies to deal with perturbations are also available, each having their own advantages and disadvantages.

The two body Lagrange Coefficient procedure is based on the position and velocity vectors of the orbiting body in an ideal, unperturbed situation. This method, also known as the Lagrange F and G functions, uses position and velocity vectors in terms of orbital plane coordinates. Propagation is based on true anomaly not time. However to be useful for mission analysis or design, true anomaly must be ultimately related back to time. The updated position and velocity vectors are determined by the transition matrix of F, G, F_t, and G_t Lagrangian coefficients and initial position and velocity vectors.[19] This method is a fast way to propagate along the orbital path for undisturbed motion.

Another method of orbital propagation is to use Cowell's formulation based on second-order differential equations. Cowell's formulation determines the overall acceleration by adding perturbing accelerations to the two-body equation of motion.[16] By using rectangular coordinates, perturbations can be added linearly as desired. Numerical integration can incorporate the disturbed or perturbed motion through the use of calculus of finite differences to accomplish the integration.[16] Various methods are available for performing the finite difference, most notably are Euler's method, Taylor's method, and the Runge-Kutta method.[20] These are single step methods that do not require back values to start the integrator. Multistep methods are available such as the Adams-Bashforth formula but they require a single step or starting method.[20] This research employs the Runge-Kutta fourth-order method with Cowell's rectangular formation. The fourth-order Runge-Kutta alogorithm evaluates the state derivative function (first order differential equations form) at four different points along an estimated trajectory. These four evaluations are used to find a final estimate from a weighted average.[16] One main disadvantage of this method is that error will continue to grow through propagation.

However, using an appropriate time step for orbital integration, it can be shown that the fourth order Runge-Kutta method is sufficient for orbital propagation within a reasonable time frame.

1.2.3 Perturbations

Kepler and Newton allowed for the development of idealized two body motion. However, actual satellite motion is not idealized; it is in an ever changing environment. One example of these intricacies is the study of perturbations within orbital mechanics. Perturbations are defined as the "deviations from a normal, idealized, or undisturbed motion."[16] Some perturbations are secular while others are periodic, both short and long term.[21, 22] The main perturbations of interest in relation to this dissertation are non-spherical Earth effects, aerodynamic drag, solar pressure, and third body effects.

The Earth is not a perfect homogeneous sphere. Rather, it slightly bulges at the equator with flattening at the poles.[21] This flattening is called oblateness. The Earth's radius at the equator is about 22 km more than the radius of the poles. Therefore, to treat the Earth as spherically symmetric with uniform density does not accurately describe its gravitational force.[14] Therefore, the shape of the Earth can be described as a geoid, an imaginary surface to which a level is parallel and plumb bob perpendicular to which the real surface of the Earth's elevation is measured.[1] This perturbed gravitational force is conservative.[14] The satellite's acceleration can be found through the gradient of a geopotential function.[21]

The Earth's atmosphere decreases with altitude but still has an impact as far as 1000 km up.[14] This thin air interacts with satellites causing resistance to motion and

dissipation to energy, and this interaction is called aerodynamic drag. Drag causes the satellite to slow down through a non-conservative force and must be considered in complete perturbation modeling.[23] Satellites in lower Earth orbits are more affected by aerodynamic drag than satellites at higher altitudes. The upper atmosphere is difficult to model due to many variables such as the mean free path between particles, day-night cycle, solar cycles, and fluctuation of the magnetic field. Also, drag is difficult to model due to the satellite's drag coefficient and cross sectional area.[14, 24]

Solar radiation causes pressure on satellites. This effect is more pronounced in lightweight, large cross sectional area satellites. Solar radiation pressure is also more pronounced on higher altitude satellites.[21] Solar radiation pressure is a non-conservative force and is also difficult to model due to fluctuating solar radiation and the satellite's cross sectional area that faces the Sun.[16]

Third body effects are perturbation due to the gravitational influence of other bodies within the idealized two body sphere of influence. For Earth orbit applications, the two main bodies are the Moon and Sun. Satellites in higher altitudes are more affected by third body perturbations. Third body perturbations are conservative since they are based on gravitational attraction.[16]

Fortunately, each of these four perturbations can be modeled to help understand its effect on the nominal orbit. These perturbations can be modeled independently as in this research. While this research uses basic models described in detail in Section 5.3, more complete models are available. For example the non-spherical Earth standard is the World Geodetic System 1984 with the gravitational field model the Earth Gravitational Model 1996.[25] The Jacchia-Bowman 2006 model incorporates satellite drag

measurements and solar flux estimates for a significantly improved satellite drag model.[26] Like aerodynamics drag models, solar radiation models are also dependent on improved satellite measurements. Third body models are based on the accuracy of the third body position. The Jet Propulsion Laboratory offers very precise planetary ephemerides while the *Astronomical Almanac* offers simpler, yet fairly accurate models.[16] The perturbation models can be incorporated into sophisticated models to more accurately assess their overall impact. Section 5.1 describes the two main models developed over the years that are still in use, the Position and Partials as functions of Time (PPT3) and the Simplified General Perturbations (SPG4).[27]

These four main perturbations, aerodynamic drag, solar radiation, third body effects, and non-spherical Earth, must be considered when choosing an orbit for a particular mission. Many satellites with Earth observation missions are often placed in similar orbits because of these perturbations. This research incorporates the most significant non-spherical Earth effect in the orbit design process and assesses the effects of the other perturbation sources on the orbit lifecycle.

1.2.4 Orbit Design

To view the Earth from the high ground of space, sensor platforms have been placed in special orbits to best achieve their mission. Orbits are generally described by three main categories: low-Earth orbit (LEO), mid-Earth orbit (MEO), or geosynchronous orbit (GEO). LEO is defined by orbits with an altitude below 800 km. MEO ranges from about 800 km to 30,000 km. GEO is around 35,780 km and these orbits have periods equal to the Earth's rotation.[16] Most Earth observation missions are either LEO or GEO.

Low altitudes provide increased instrument performance since it is closer to the Earth's surface.[21] However, the amount of Earth's surface that can be viewed in any given instance is relatively limited. One trade off in LEO is the relatively short dwell time over a target; however, because of the shorter orbit period, the revisit rate is also more frequent.[7] The cost associated with LEO launches is less because less propellant is needed for lower orbits.[21]

GEO provides a relatively fixed view over a given region. It can view nearly 40% of the Earth's surface. However, because of the greater distance, the satellite sensors are less able to refine target coordinates.[7] Another advantage of GEO is the longer lifetimes being much less affected by aerodynamic drag. But the cost associated with GEO launches is much greater.[21]

Two specialized orbits employed frequently are the Sun-synchronous orbit and the repeat ground track orbit.[28] The Sun-synchronous orbit, a LEO, enables certain ground lighting conditions by maintaining a constant orientation towards the Sun.[16] The orbit takes the satellite over the poles providing coverage of the globe by successive orbits.[29] The repeat ground track orbit may be applied to any altitude orbit and provides a periodic revisit over a particular ground location. The repeat ground track does exactly as its name implies, it retraces its ground track over a certain time interval.[16] After considering the advantages and disadvantages of the many orbit possibilities, mission planners choose an appropriate orbit category for a given satellite mission. The repeat ground track orbit type is emphasized in the dissertation research. Within a particular category, efforts to design a specific orbit are still necessary, and this is a major thrust of the research incorporating user requirements and optimization principles.

1.2.5 Scheduling Options

Once an orbit has been selected for the satellite, the sensor can be tasked at particular times in the orbit to view specific ground locations for information collection. Consider each tasking of gathering information on a specific ground location as a "job." Scheduling takes three main questions into account:[30]

1. Which jobs make the schedule?
2. What order should they be in (order in time)?
3. What is the exact start and stop time for each scheduled job?

There are many scheduling options available, each taking into account varying considerations or constraints. These constraints are well described:

> These constraints include requirements on the instruments used to collect the data, and duration and ordering constraints associated with the data collecting, recording, and downlinking tasks. In addition, SSR [solid state recorder] capacity, and constraints on communications equipment such as satellite antennae and ground stations must be satisfied. There may also be set-up steps associated with particular operations, like establishing a data link prior to downlink, or aiming an instrument prior to data acquisition. These steps generate further temporal and ordering constraints. A request can also involve coordinating activities among different satellites. For example, a stereo image will involve multiple sensing events of the same location at different viewing angles. In other cases, adequate spectral coverage may require the use of two or more instruments to sense the same land area, or to sense both land use and atmospheric conditions. Finally, scientists may want to image the same area at different times of day.[31]

Each scheduling algorithm must determine which considerations are most appropriate, hence the numerous algorithms available to provide an "optimized" schedule for a satellite mission. For example some satellite schedules take into account multiple sensors on one platform.[32] Other algorithms are designed for multiple sensors on multiple platforms for a company that has a number of satellites to manage.[31] Other

schedules must consider tasking an area that requires multiple images for complete coverage.[33] This research investigates the problem of only one sensor on one platform.

Algorithms may employ different methods to solve for the satellite schedule. Two popular methods are constructive and evolutionary algorithms. The constructive method builds a schedule using rules to select jobs allocating resources if available.[30] This method is fairly fast and straightforward. The evolutionary algorithm evaluates numerous permutations to determine the best allocation.[34] This method requires permutations to evolve to create more fit solutions and therefore is inherently more complex and time consuming. This research is based on the constructive Priority Dispatch (PD) algorithm for a Window Constraint Packing (WCP) problem. A WCP strategy uses a given amount of time, divided into discreet time intervals forming a timeline, to accomplish a specific number of jobs. PD logic is the method used to assign the jobs to the timeline which schedules the jobs according to priority and slack, the number of opportunities available for that job to be scheduled.[30]

1.2.6 Optimization

In his textbook, Goldberg states "Optimization: Seeks to improve performance towards some optimal point or points…two parts: (1) we seek improvement to approach some (2) optimal point. There is a clear distinction between the process of improvement and the destination or optimum itself."[35]

Optimization begins with an objective in mind, a quantitative measure of the system performance.[36] The characteristics of the system that are used to optimize the performance are called variables and may be restricted, or constrained.[36] This research addresses a constrained optimization problem because parameter bounds are imposed on

the system variables. Modeling the system objective, variables, and constraints is the first step in the optimization process. Once the system is modeled, an optimization approach or method can be applied to solve the problem. Regardless of which method is chosen for the optimization process, it should possess the following characteristics:[36]

1. Robustness: They should perform well on a wide variety of problems in their class, for all reasonable values of the starting point.
2. Efficiency: They should not require excessive computer time or storage.
3. Accuracy: They should be able to identify a solution with precision, without being overly sensitive to errors in the data or the arithmetic rounding errors that occur when the algorithm is implemented on a computer.

Solutions may be local, the point at which the objective function is optimized compared to other feasible nearby points, or the solution may be global, the point most optimized among all feasible points.[36] A few techniques are available to find the global optimum; however, no method can guarantee a solution that is the absolute, single, unique global optimum without searching the entire domain. Popular techniques include genetic algorithm, neural network, particle swarm optimization, and simulated annealing. The genetic algorithm is based on natural selection and genetics while neural network techniques mimic the computing power of interconnected processors.[37] Particle swarm optimization methods were developed by researching the motion of bird flocks searching for food.[38] Simulated annealing is based on the process of cooling of solids.[37] This research desires a global solution to the proposed problem and therefore implements the genetic algorithm (GA) optimization process. The GA approach does not use the system variables directly, but instead uses a coded version of the variables.[35] This codification allows the GA to search through the entire feasible region to find a global solution.

1.2.7 Problem Statement

Many Earth observation satellite missions are designed sequentially where the first step is selection of a suitable orbit and then the satellite sensor is scheduled for collecting observations based on the suitable orbit. This design philosophy leads to a less than ideal system that under performs in the volume of data generated per unit of time and/or the duration of time consumed per unit of data. An integrated strategy would allow desired observations to drive the orbit design. This approach would place the priority of the mission, e.g., user requirements, at the forefront of the mission planning. Incorporating a robust scheduler into a design methodology would aid in finding a realistic strategy to bring user requirements to the forefront of the mission planning. User requirements in this dissertation refer to a request for performance that drives a system capability where as that capability entails numerous possibilities such as maximum observation coverage of requested surface targets, consistent observing angle from orbiting satellites, specific lighting conditions during observation periods, and flexibility of priority rank for each ground target. Additionally, the chosen sensor for the satellite will have certain limiting characteristics such as lighting conditions appropriate for sensor type, maximum altitude for quality sensor resolution, sensor field of view, and sensor slew angle. Sensor resolution as defined in this problem is spatial resolution, the fineness of the spatial detail visible on an image or how small an object can be to be identified on an image.[9]

This dissertation investigates a new methodology for constrained optimal orbit design for Earth observation. The purpose of this work is to provide a solid foundation for decision making for new Earth observing satellite mission designs. This design

methodology for finding an optimal orbit provides clearer insight into the requirements for the new satellite system and can be used to show how altering a mission requirement can affect the determined optimal orbit. Also, the methodology can be a useful tool in repositioning a current on-orbit satellite for improved observation coverage. While target selection is necessary on a daily basis[32] a satellite may need to be re-evaluated for orbital positioning. Optimal orbits generated from the proposed methodology may need to be refined according to additional system design concerns including orbit stability, orbital maneuvering fuel consumption, or launch site restrictions. Objectives of the research are to explore the feasibility of using requirements to drive the solution for an optimal orbit where constraints are placed on the process, as well as to formulate effective strategy, algorithms, and software to bring the design process to a state where practical and useful orbits can be generated in a reliable and efficient manner for a given set of requirements and constraints. These objectives have been achieved.

1.2.8 Assumptions

The development presented in this dissertation is for a single-vehicle, single-sensor satellite for one Earth-based elliptical orbit. Additionally, observations are assumed to require a recurring basis; therefore the orbit is based on a repeating ground track. Limited zonal effects are accounted for in determining the semi-major axis and identical perturbations are included in the orbit propagation which is needed to repetitively evaluate the cost function and therefore is iteratively run in the search process. The ground track coordinates are calculated as geodetic latitude and geocentric longitude. Orbital perturbations such as aerodynamic drag and solar radiation are also

not accounted for during the observation period. Also phenomena such as space weather or cloud cover are not considered in this analysis. The final orbit should be evaluated with a full perturbed propagation model. Needed modifications to maintain the desired orbital parameters are assumed to be small and achievable with satellite thrusters. Scheduling assumptions include no time is needed between observations for sensor functions and that the entire period of repetition is available for observing.

1.3 Dissertation Outline

This research work includes the design methodology for generating a constrained optimal orbit based on user requirements. Chapter 2 discusses this design methodology, mapping the mission requirements into parameters. Chapter 3 investigates the available repeating ground track methods and determines the best fit for this research. Chapter 4 describes the genetic algorithm optimization process, as well as the cost function developed for this problem, and has some insights into the "optimality" of this work. In Chapter 5, the unmodeled on-orbit perturbations of non-spherical Earth, aerodynamic drag, solar pressure, and third body effects are reviewed as well as the techniques employed in the lifecycle analysis. Chapter 6 presents the case study results for the baseline case and variations. Also, the lifecycle analysis of the orbital elements under full perturbations is demonstrated. Finally, Chapter 7 presents research conclusions.

CHAPTER 2

ORBIT DESIGN METHODOLOGY

2.1 Introduction

The concept of developing an orbit based on observation sites was first explored by Abdelkhalik and Mortari.[39] They proposed a solution based on an orbit that does not require maneuvering to visit all observation sites within a given time frame. Two different types of mission constraints are proposed to include maximum resolution which requires a predetermined semi-major axis and a maximum observation time which may not be necessary to acquire desired data. This research expands on their preliminary work by directly incorporating user requirements with a more sophisticated cost function and also shows that orbital altitude can be included as an optimized parameter.[40] This chapter steps through solving this problem of finding a constrained optimal orbit for Earth observation satellites based on user requirements by first outlining the design process. Then the problem is bounded based on mission requirements including observation requests and sensor characteristics. Next, the optimization parameters are described. Finally, the orbital lifecycle is discussed.

2.2 Design Process

Figure 2.1 outlines the information flow for the overall orbit design process. The process starts with the input by defining the user requirements. For Earth observing satellites, the most important measurement parameters are resolution, repetition interval, time of year for observations, and Sun angle.[41] The requirements subdivide into three

categories comprising observation site requirements, observation restraints, and sensor information. Each user requirement component is mapped into the optimizing parameter bounds or cost function components. The parameters are optimized through a search technique to find a minimum cost function value. The final algorithm output includes orbital elements of the constrained optimal orbit and the observation schedule for the ground targets. This design process is coded in Matlab using a modular concept so elements may easily be updated and the program could be incorporated with other programs.

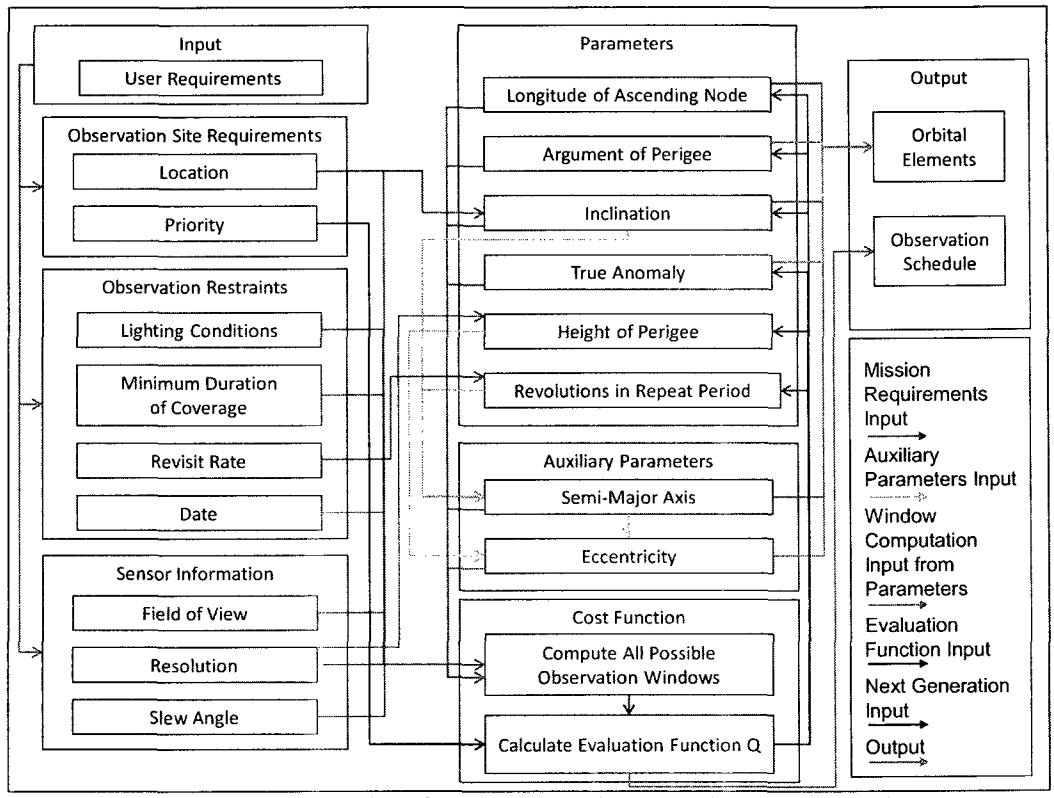

Figure 2.1 Information Flow for Orbital Design Based on User Requirements

2.3 Mission Requirements

The first step in this problem to finding an optimal orbit for an Earth observation satellite is to map the mission requirements into constraints. The mission requirements are divided into three parts: observation site requirements, observation condition restraints, and sensor characteristics.

Observation site requirements include the observation site's location and priority. The observation location consists of latitude and longitude. The site with the highest degree of latitude determines the minimum inclination bound, as indicated by the flow path in Figure 2.1. The latitude and longitude of each site are used to compute the windows of opportunity in the cost function. A window of opportunity is a time frame the observation site will be within view of the satellite sensor given the defined problem restraints. The second observation site requirement, observation priority, is a ranking from 1 to 5 with 5 being the highest priority. The priority is a weighting measure in the cost function.

The observation restraints include the minimum time duration of coverage, lighting condition, revisit rate, and start date. The minimum time duration of coverage sets the minimum time needed to complete an observation and is used in the cost function computation. The lighting condition includes the maximum allowable Sun angle for the observation. The Sun angle is measured from the nadir line of the satellite-observation site to the Sun-observation site line. Lighting condition is used in computing possible windows of opportunities. The revisit rate is the number of revolutions the Earth completes in its rotating cycle as viewed from the precessing orbital plane[42] which is approximately the number of days at which the target needs to be repeatedly observed.

The revisit rate is used to calculate the minimum and maximum values of the orbital revolutions in the repetition cycle. The date is the start of the first period of repetition given in Julian format. The date is extremely important for sensors that depend on specific lighting conditions.

The sensor parameters include the sensor field of view (FOV), slew angle, and maximum altitude of sensor for desired resolution. The FOV is measured from nadir to the edge of view and is used for determining windows of opportunity. The slew angle, also used for determining the windows of opportunity, is the angle the middle of the sensor can move off the satellite's nadir. The maximum altitude of the sensor for desired resolution provides the maximum height of the sensor for an allowable resolution. Sensor resolution as defined in this problem is spatial resolution, the fineness of the spatial detail visible on an image or how small an object can be and still be identifiable on an image.[9] If the sensor is above this altitude, the observation quality is reduced. The resolution determines the maximum allowable height of perigee.

2.4 Bounding the Problem

From the given mission requirements, the bounds for this problem are developed. Each of the mission requirements maps into the problem conditions as shown below in Figure 2.2. Note the maximum altitude for minimum sensor resolution does not specify the orbit semi-major axis or the maximum height of apogee. The mission requirement on resolution only determines the maximum allowable height of perigee. This map allows for an orbit to be more elliptical where at other points in the trajectory the satellite may reach altitudes above this maximum ceiling for resolution. Penalizing the observation

quality above the desired resolution height is taken into account through a cost function weighting measure and is further described in the cost function section. This implementation allows increased design flexibility that would otherwise be overly constraining.

Mission Requirements		Problem Definition
Revisit Rate	→	Earth Revolutions in Repeat Cycle, d
Observation Site Latitude	→	Minimum Inclination, i_{min}
Maximum Altitude for Desired Sensor Resolution	→	Maximum Height of Perigee, h_{pmax}

Figure 2.2 Mapping Mission Requirements

The mission requirements lead to auxiliary requirements for the semi-major axis and eccentricity. The semi-major axis, a, is determined using the Epicyclic motion Repeating ground track Orbit (ERO) concept by Aorpimai and Palmer[42] based on the inclination, i, and similitude parameter, τ; the number of Earth rotations for a period of repetition divided by the number of orbits in the period of repetition.[39] An efficient method of employing the ERO concept is to use a polynomial equation shown in Equation (2.1) for finding the valid semi-major axis root which is the single real, positive root within a valid semi-major axis range of low Earth to geosynchronous orbits.[43]

$$\{\tau(\zeta a^4 + \eta a^2 - \theta + \lambda) - \gamma a^2 + \delta + \varepsilon\}^2 - \beta^2 a^{11} = 0 \qquad (2.1)$$

where

$$\beta = \frac{\omega_E}{J_2 R_E^2 \sqrt{\mu}}$$

$$\gamma = \frac{3}{2}\cos(i)$$

$$\delta = \frac{15}{16}\frac{J_4}{J_2} R_E^2 \cos(i)\{4 - 7\sin^2(i)\}$$

$$\varepsilon = \frac{3}{8}\frac{(J_2)^2}{J_2} R_E^2 \cos(i)\{11 - 20\sin^2(i)\}$$

$$\zeta = \frac{1}{J_2 R_E^2}$$

$$\eta = 3 - \frac{15}{4}\sin^2(i)$$

$$\theta = \frac{15}{16}\frac{J_4}{J_2} R_E^2 \left\{\frac{34}{5} - 25\sin^2(i) + \frac{77}{4}\sin^4(i)\right\}$$

$$\lambda = \frac{3}{16}\frac{(J_2)^2}{J_2} R_E^2 \{14 + 17\sin^2(i) - 35\sin^4(i)\}$$

and

$$R_E = 6378.1363\,\text{km}$$

$$\omega_E = 7.29211585530 \times 10^{-5}\ \text{rad/s}$$

$$\mu = 398600.4415\,\text{km}^3/\text{s}^2$$

$$J_2 = 0.0010826269$$

$$J_4 = -0.0000016204$$

In Equation (2.1), R_E is the mean radius of the Earth, ω_E is the rotation rate of the Earth, J_2 is the second zonal gravitational harmonic coefficient, J_4 is the fourth zonal gravitational harmonic coefficient, and μ is the Earth gravitational parameter. Additionally, the eccentricity, e, of the orbit is based on the semi-major axis and height of perigee, h_p, as shown in Equation (2.2).[39]

$$e = 1 - \frac{R_E + h_p}{a} \tag{2.2}$$

These auxiliary requirements map into the problem definition as shown in Figure 2.3. These mappings also appear in the signal flow paths as indicated in Figure 2.1.

Auxiliary Requirements		Problem Definition
Inclination and Period of Repetition	→	Semi-Major Axis, a
Height of Perigee and Semi-Major Axis	→	Eccentricity, e

Figure 2.3 Mapping Secondary Requirements

Equation (2.1) is based on a near circular orbit as well as the assumption $n = (\mu/a^3)^{1/2}$ where n is the mean motion. Implications are that orbital propagation using nonlinear simulation with perturbations, although close, will not lead to high precision ground track closer. Therefore the ERO solution needs to be refined to account for the eccentric orbit and mean motion assumption using the Simplified Repeat Groundtrack (SRG) method by Collins.[44] Equation (2.3) and the mean motion expression $n = (\mu/a^3)^{1/2}$ may be solved using a two step iteration Newton method with the ERO determined semi-major axis and given inclination, eccentricity, and similitude parameter.* Ground track closure is typically very precise after employing this refinement process.

$$\chi^3 + Q\chi^7 - \frac{\omega_E}{\tau} = 0 \tag{2.3}$$

where

$$\chi = n^{1/3}$$

$$Q = \frac{3}{2} J_2 \frac{R_E^2}{\mu^{2/3}} \psi$$

and

* Recommendation from Dr. Paul Cefola, Personal Correspondence, September 2009.

$$\psi = 3\left(1-e^2\right)^{-\frac{3}{2}}\left(\frac{1}{3}-\frac{1}{2}\sin(i)^2\right)-\frac{1}{\left(1-e^2\right)^2}\left(\frac{1}{2}-\frac{5}{2}\cos(i)^2\right)-\frac{1/\tau}{\left(1-e^2\right)^2}\cos(i)$$

2.5 Optimization Parameters

The optimization process used for this design methodology is the genetic algorithm. The genetic algorithm allows the logic program to search over the entire parameter space in an efficient manner. The search for an optimal orbit will rely on six parameters: inclination, longitude of ascending node, argument of perigee, true anomaly, the height of perigee, and number of revolutions of the orbit in the period of repetition. These parameters are adjusted by the genetic algorithm to best achieve the objectives and simultaneously satisfy the constraints.

The inclination, i, has a minimum bound determined by the maximum observation site latitude. This constraint ensures the satellite will pass overhead the observation site since the orbit's inclination determines the highest latitude the satellite can reach.[14] The maximum inclination bound is preset at 105 deg to allow for the possibility of polar orbits and Sun synchronous missions in the search domain. The longitude of ascending node, Ω, has no physical restrictions and is set for the full range from 0 to 360 deg. Additionally, the argument of perigee, ω, and true anomaly, θ, range from 0 to 360 deg. The height of perigee, h_p, ranges from a minimum set altitude for avoiding significant orbital decay to a maximum altitude where the sensor is still within a desired resolution as given in the mission requirements. Additionally, the radius of perigee is constrained to be equal to or less than the semi-major axis to ensure an elliptical orbit.

The number of revolutions in the orbit in the period of repetition, k, is based on the similitude parameter, τ, from 0.0625 to 1. The similitude parameter is the number of

Earth rotations for a period of repetition divided by the number of orbits in the period of repetition given in Equation (2.4).[39]

$$\tau = d / k \tag{2.4}$$

The parameter k allows for the altitude of the orbit to range from the very minimum low Earth orbit when the similitude parameter is 0.0625 to the highest altitude of a geosynchronous orbit when the similitude parameter is 1 given by Equation (2.5).

$$k_{\min} = d/1$$

$$k_{\max} = d/0.0625 \tag{2.5}$$

Within this well defined constraint problem, the altitude of the orbit is not preset and only bounded to ensure physically feasible orbits avoiding hyperbolic or parabolic orbits, orbits that penetrate the Earth, or complex number solutions. The shape of the orbit is not limited to circular or near circular solutions but may also include elliptical solutions. Additionally, the solution can range across a wide variety of inclination values.

Chapter 4 describes the cost function and optimization process used to determine an optimal solution for this design method.

2.6 Lifecycle Analysis

Once an optimal solution is determined, its orbital parameters are evaluated to determine the solution's effective life. As part of the design process, it is essential to know how long to expect the orbital elements to hold up under perturbations. This research assumes satellite thrusters can overcome the effects of perturbations to maintain the desired optimal orbit solution found in the optimization algorithm.[45] However, the

required level of orbit maintenance is an important characteristic to evaluate for design purposes. The lifecycle analysis shows how the orbital elements are affected over time without the thruster corrections and thus indirectly evaluates this characteristic. The initial solution orbital elements are propagated using perturbations of non-spherical Earth, aerodynamic drag, solar radiation pressure, and third body effects from the Sun and Moon. These propagations are described in detail in Chapter 5. In intervals of the repetition period, the orbital elements and cost function are graphed over time to see how the solution holds up with the additional perturbations previously mentioned. Results are presented in Chapter 6.

CHAPTER 3

REPEATING GROUND TRACK CONCEPTS

3.1 Repeating Methods

For many Earth observation satellites, an ideal orbit designed in the presence of perturbations is based on a repeating ground track which allows for specific observations to be scheduled on a routine basis or with the same sensing conditions. Two recent methods for finding a repeat ground track are available. Unfortunately each method is based on different assumptions and parameters, and has their own set of limitations on the type of orbit for which the method should be applied. In order to bridge these differences and limitations and provide a comparison for evaluating the merits and/or deficiencies, a third method is developed.

The first method for generating repeat ground tracks is the Flower Constellation (FC) concept by Mortari, Wilkins, and Bruccoleri.[46, 47] The FC method is based on the Keplerian orbital elements: semi-major axis, eccentricity, inclination, longitude of the ascending node, argument of perigee, and the mean anomaly. The main advantage of this method is a general applicability to any elliptic eccentricity based on a specified perigee height. Unfortunately, the FC method only considers the second order zonal effects, that is J_2 effects. The second method provides a repeating ground track based on epicyclic motion theory by Aorpimai and Palmer.[42] The Epicyclic motion Repeating ground track Orbit (ERO) concept is based on two polar elements (radius and argument of latitude) and two orbital elements (inclination and longitude of the ascending node).[48] This method was developed for near circular orbits and therefore does not use eccentricity or

require a specified height of perigee. The ERO method includes the J_2 term like the FC method, but also uses the J_4 first order and J_2 second order terms. These different perturbation models, variable sets, and orbit families make comparison between the methods difficult.

The new method is an extension or modification of the FC method and is denoted by MFC. In order to bridge the gap between the limitation of the FC framework using only the J_2 term and the ERO limitation for near circular orbits, the Flower Constellation procedure is modified to include the J_4 and J_2^2 terms. In addition to these three methods, a fourth Simplified Repeat Groundtrack (SRG) method by Collins[44] is re-introduced. The SRG approach is based on the Keplerian orbital elements with the J_2 perturbation term like the FC method. However, this method requires more specific inputs than the FC method.

In the following sections, mathematical conditions for repeating ground tracks using the FC and ERO techniques are reviewed, a modified FC method is developed, and the SRG technique is applied as a refinement process. The modified FC method is applied to several examples and results are compared with the corresponding FC and ERO results. The FC, MFC, and ERO conditions are solved through numerical and polynomial methods for computational comparison. Finally, conclusions from these examples and results are drawn to support the selection of one of the methods for use in an orbit design optimization algorithm.[49]

3.2 Condition for Repeating Ground Tracks

For an orbit to have a repeating ground track, the period of repetition T_r is related to the nodal period of the satellite T_Ω and nodal period of Greenwich $T_{\Omega G}$ by Equation (3.1).[46]

$$T_r = N_p T_\Omega = N_d T_{\Omega G} \tag{3.1}$$

N_p is the number of revolutions along the orbit in one period of repetition and N_d is the number of sidereal days the Earth completes during the period of repetition.[46] Note N_p and N_d are integers. Figure 3.1 shows the relationship of the inertial frame orbits to the rotating Earth reference frame orbit.

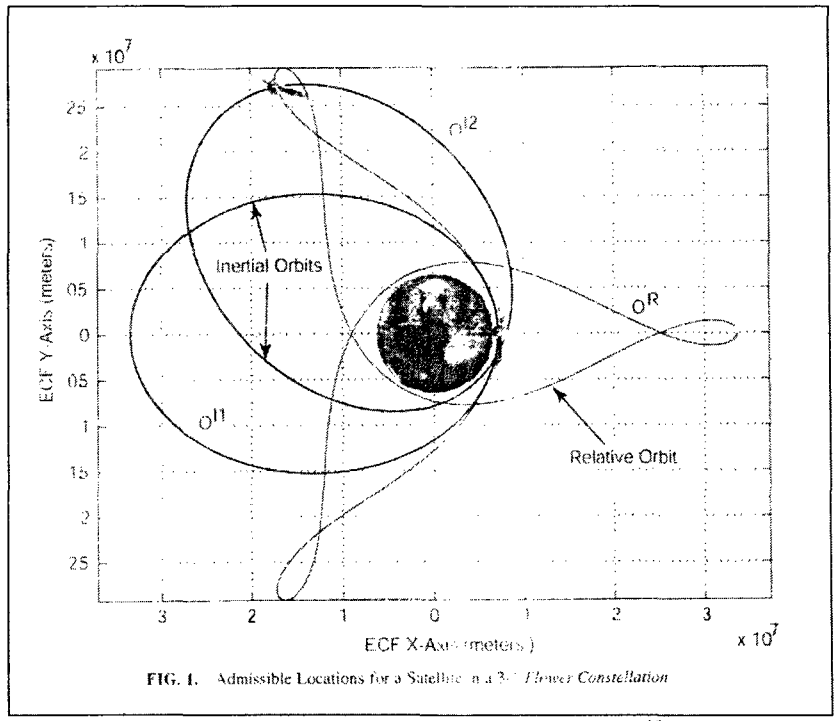

Figure 3.1 Inertial vs. Reference Orbits[46]

The geometry underlying this condition is illustrated in Figure 3.2. Equation (3.1) simply states that the time for the westward progression of the ground track to complete one revolution and the time for the northward penetration of the ground track to also

complete one revolution constitute a rational number. By expressing the nodal periods to depend on the orbital elements, Equation (3.1) is converted to a more useful form.

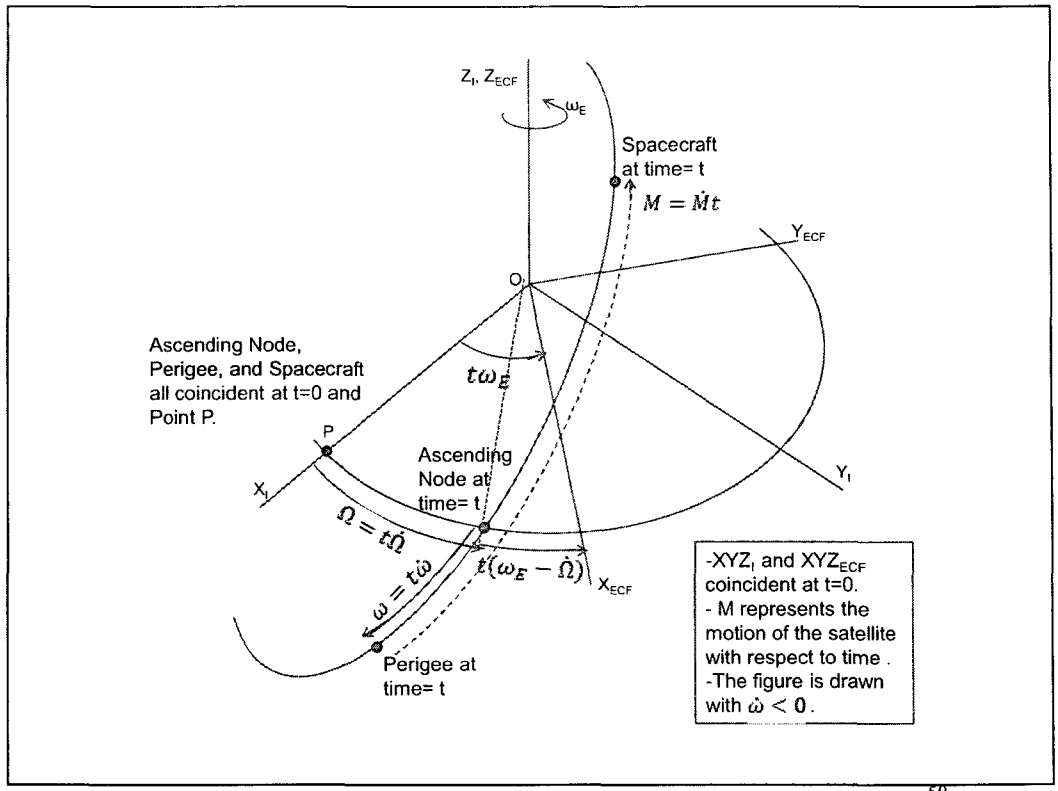

Figure 3.2 Perturbing Elements for Repeating Ground Tracks[50]

The nodal period T_Ω is related to the satellite's anomalistic period T by Equation (3.2) where $\dot{M}$ denotes the rate of change in the mean anomaly due to nominal motion and perturbations and $\dot{\omega}$ is the rate of change in the argument of perigee.

$$T_\Omega = \frac{2\pi}{\dot{M} + \dot{\omega}} \tag{3.2}$$

The current mean anomaly, M, in Figure 3.2 represents the motion of the spacecraft with respect to time. M is related to the initial mean anomaly, M_o, by Equation (3.3)[16]

$$M = M_o + nt \tag{3.3}$$

where n is the satellite's mean motion. The rate of change of the current mean anomaly is related to the rate of change of the initial mean anomaly through Equation (3.4).[16]

$$\dot{M} = \dot{M}_o + n \tag{3.4}$$

The anomalistic period T is similarly related to the mean motion in Equation (3.5).

$$T = \frac{2\pi}{n} \tag{3.5}$$

Now Equation (3.2) can be rewritten in terms of the anomalistic period in Equation (3.6).

$$T_\Omega = \frac{2\pi}{n + \dot{M}_o + \dot{\omega}} = T\left(1 + \frac{\dot{M}_o + \dot{\omega}}{n}\right)^{-1} \tag{3.6}$$

Figure 3.2 represents the perturbing elements appearing in Equation (3.6) as a function of time for the satellite.

The nodal period of Greenwich is provided as in Equation (3.7)

$$T_{\Omega G} = \frac{2\pi}{\omega_E - \dot{\Omega}} \tag{3.7}$$

where the Earth's rotational rate is ω_E = 7.29211585530 × 10^{-5} rad/s. The nodal regression of the orbital plane is $\dot{\Omega}$. Referring back to Figure 3.2, $T_{\Omega G}$ physically represents the time required for the Greenwich meridian to depart from the ascending node and return to its perturbed ($\dot{\Omega}$) location. Substituting these expressions for the nodal period of the satellite and nodal period of Greenwich into Equation (3.1) and rearranging for the similitude parameter, $\tau = N_s/N_p$, yields Equation (3.8).

$$\tau = \frac{\omega_E - \dot{\Omega}}{n + \dot{M}_o + \dot{\omega}} \tag{3.8}$$

This equation is the fundamental necessary requirement in usable form for repeating ground tracks and is the foundation for any repeating ground track mission design

method, including the FC and ERO methods. For a specified similitude τ, the equation will be solved for the unknown orbital parameterization variables in the various methodologies.

3.2.1 Flower Constellation

The Flower Constellation concept was developed by Mortari, Wilkins, and Bruccoleri to group existing constellations and orbits with three common characteristics:[46]

1. Identical orbit shape. Anomalistic period, argument of perigee, height of perigee, and inclination are common across the orbit family.
2. Compatible periods. The orbital period is evaluated in such a way as to yield a perfectly repeated ground track.
3. Equally spaced nodes. Tracks crossing the equatorial plane at the nodes for each satellite in a complete Flower Constellation are displaced equally.

Examples include the Walker constellation, Molniya orbits, and geosynchronous orbits. The common framework also allows for the development of new constellations with these same characteristics. A full FC may have multiple orbits, but this dissertation will only develop one orbit with a repeating ground track. Therefore, characteristics 1 and 3 will not be investigated in this research. The development in this dissertation is categorized as an "incomplete" FC since only one satellite for one orbit is addressed, not multiple orbits or a multi-satellite orbit.

The FC method is based on the Keplerian orbital elements: semi-major axis, eccentricity, inclination, longitude of the ascending node, argument of perigee, and the

mean anomaly. The main advantage of this method is a general applicability for any eccentricity which is a product of a specified height of perigee. Unfortunately, the FC method only considers the second order zonal effects, that is J_2 effects.[51] The FC concept uses geopotential perturbation theory, but the second order zonal effects only change the argument of perigee, longitude of the ascending node, and mean anomaly[46] as applied in Equations (3.9), (3.10), and (3.11).

$$\dot{\omega} = \frac{3nR_E{}^2 J_2}{4p^2}\left\{4 - 5\sin^2(i)\right\} \tag{3.9}$$

$$\dot{\Omega} = -\frac{3nR_E{}^2 J_2}{2p^2}\cos(i) \tag{3.10}$$

$$\dot{M}_o = \frac{-3nR_E{}^2 J_2\sqrt{1-e^2}}{4p^2}\left\{3\sin^2(i) - 2\right\} \tag{3.11}$$

Equations (3.9)-(3.11) are derived by a standard variation of parameters technique applied to the orbital elements. In these expressions, R_E = 6378.1363 km for the Earth radius, p is the semi-parameter, i is the inclination, e is the eccentricity, and J_2 is the Earth gravitational perturbation parameter.

Express eccentricity, semi-parameter, and mean motion in terms of the semi-major axis a and perigee height above Earth's surface h_p as given[46] in Equations (3.12), (3.13), and (3.14)

$$e = 1 - \frac{R_E + h_p}{a} \tag{3.12}$$

$$p = 2(R_E + h_p) - \frac{(R_E + h_p)^2}{a} \tag{3.13}$$

$$n = \sqrt{\frac{\mu}{a^3}} \tag{3.14}$$

where μ = 3.986004415 × 10^5 km^3/s^2 for the Earth's gravitational constant. Substituting Equations (3.9)-(3.14) into the similitude expression yields Equation (3.15)[50]

$$\tau = \frac{\omega_E + 2A(a)\cos(i)}{\sqrt{\frac{\mu}{a^3}} + A(a)\left[\sqrt{1-\left(1-\frac{R_E+h_p}{a}\right)^2}\left\{2-3\sin^2(i)\right\}+\left\{4-5\sin^2(i)\right\}\right]} \tag{3.15}$$

where

$$A(a) = \frac{3\sqrt{\frac{\mu}{a^3}}R_E{}^2 J_2}{4\left(2(R_E+h_p)-\frac{(R_E+h_p)^2}{a}\right)^2}$$

Equation (3.15) will be used to compute the semi-major axis for specific inclination and perigee height that result in a repeat ground track. For computational advantages, Equation (3.15) can be converted to the polynomial equation given in Equation (3.16).[50]

$$4\mu\phi a^2 y(a)^2 x(a) = \left[\omega_E^2 a^3 x(a)^4 - \phi a^2 x(a) - \mu y(a)^2\right]^2 \tag{3.16}$$

where

$$\beta = 2-3\sin^2(i)$$

$$\delta = \frac{3R_E^2 J_2}{4}$$

$$\gamma = 4-5\sin^2(i)$$

$$\phi = \mu\tau^2\delta^2\beta^2$$

$$x(a) = ap$$

$$y(a) = \tau\left[x(a)^2 + \delta\gamma a^2\right] - 2\delta\cos(i)a^2$$

From Equation (3.16) the semi-major axis can be determined for a given inclination and specified height of perigee.

3.2.2 Epicyclic Motion Repeat Ground Track Orbit

The second method provides a repeating ground track based on epicyclic motion theory by Aorpimai and Palmer.[42] The Epicyclic Motion Repeating Ground Track Orbit concept is based on two polar elements (radius and argument of latitude) and two orbital elements (inclination and longitude of the ascending node). The argument of latitude replaces the argument of perigee and mean anomaly. See Figure 3.3 for the epicycle geometry. ERO includes the J_2 term like the FC, but also uses the J_4 first order and J_2 second order terms. This method was developed for near circular orbits with an eccentricity less than the order of J_2 and therefore does not use eccentricity or require a specified height of perigee.[52]

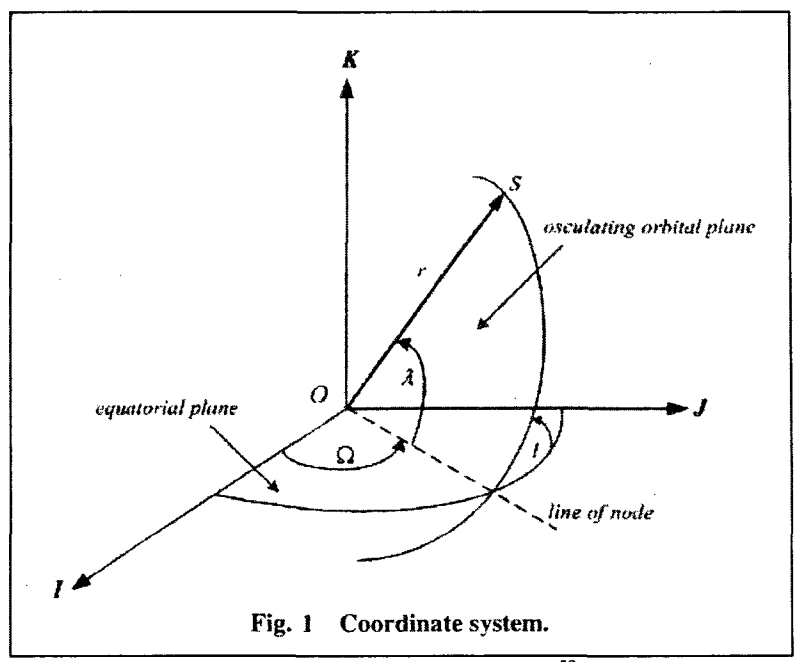

Figure 3.3 Epicyclic Motion[53]

The ERO basis has a very similar development of perturbation theory to the FC method but uses the argument of latitude instead of the argument of perigee and mean anomaly.[42] This choice is consistent with the near-circular assumption and omits eccentricity. The ERO development is different from other published techniques because only a mean orbital radius is defined. A mean orbital plane or other mean elements are not defined in the ERO technique.[53] The ERO semi-major axis, a, is designed to satisfy the energy relation Equation (3.17).

$$\varepsilon = -\left(\frac{\mu}{2a}\right) \tag{3.17}$$

ε is the total orbital specific energy for the satellite and is constant for an axisymmetric gravitational potential. The semi-major axis for a circular orbit and epicycle frequency, n_e, satisfy $a^3 n_e^2 = \mu$. The nodal frequency used in the FC method is related to the epicycle anomalistic frequency through the relation seen in Equation (3.18)[53]

$$\frac{2\pi}{T_\Omega} = (1+\kappa)n_e \tag{3.18}$$

where κ is the secular change in argument of latitude.

Equation (3.19) provides the basic ERO repeating ground track condition equivalent to Equation (3.8).

$$\frac{d}{k} = \frac{\frac{\omega_E}{n_e} - \upsilon}{1+\kappa} \tag{3.19}$$

Parameters d and k are analogous to FC parameters N_d and N_p and v is the secular change in ascending node. Using the defined terms of v and κ,[53] where

$$\kappa = \frac{3}{4}J_2\left(\frac{R_E}{a}\right)^2\left(4-5\sin^2(i)\right)-\frac{3}{64}J_4\left(\frac{R_E}{a}\right)^4\left(136-500\sin^2(i)+385\sin^4(i)\right)+\frac{3}{16}J_2^2\left(\frac{R_E}{a}\right)^4\left(14+17\sin^2(i)-35\sin^4(i)\right) \tag{3.20}$$

and

$$\nu = -\frac{3}{2}J_2\left(\frac{R_E}{a}\right)^2\cos(i)+\frac{15}{16}J_4\left(\frac{R_E}{a}\right)^4\cos(i)\left(4-7\sin^2(i)\right)+\frac{3}{8}J_2^2\left(\frac{R_E}{a}\right)^4\cos(i)\left(11-20\sin^2(i)\right) \tag{3.21}$$

the repeat condition can be written in terms of semi-major axis and inclination[42] given in Equation (3.22) using J_2, J_4, and J_2^2 perturbations.

$$\frac{d}{k} = \frac{\frac{\omega_E}{J_2}\sqrt{\frac{a^3}{\mu}}\left(\frac{a}{R_E}\right)^2+\frac{3}{2}cos(i)-\frac{15}{16}\frac{J_4}{J_2}\left(\frac{R_E}{a}\right)^2cos(i)\left(4-7sin^2(i)\right)-\frac{3}{8}\frac{(J_2)^2}{J_2}\left(\frac{R_E}{a}\right)^2cos(i)\left(11-20sin^2(i)\right)}{\left(\frac{a}{R_E}\right)^2\frac{1}{J_2}+\left(3-\frac{15}{4}sin^2(i)\right)-\frac{15}{16}\frac{J_4}{J_2}\left(\frac{R_E}{a}\right)^2\left(\frac{34}{5}-25sin^2(i)+\frac{77}{4}sin^4(i)\right)+\frac{3}{16}\frac{(J_2)^2}{J_2}\left(\frac{R_E}{a}\right)^2\left(14+17sin^2(i)-35sin^4(i)\right)} \tag{3.22}$$

This equation can be used to determine the semi-major axis for a given inclination using a numerical solver.[42]

For computational advantages, Equation (3.22) can be converted to the polynomial equation given in Equation (3.23).[50]

$$\{\tau(\zeta a^4+\eta a^2-\theta+\lambda)-\gamma a^2+\delta+\varepsilon\}^2-\beta^2 a^{11}=0 \tag{3.23}$$

where

$$\beta = \frac{\omega_E}{J_2 R_E^2\sqrt{\mu}}$$

$$\gamma = \frac{3}{2}cos(i)$$

$$\delta = \frac{15}{16}\frac{J_4}{J_2}R_E^2\,cos(i)\left\{4-7sin^2(i)\right\}$$

$$\varepsilon = \frac{3}{8}\frac{(J_2)^2}{J_2}R_E^2\,cos(i)\left\{11-20sin^2(i)\right\}$$

$$\zeta = \frac{1}{J_2 R_E^2}$$

$$\eta = 3 - \frac{15}{4}\sin^2(i)$$

$$\theta = \frac{15}{16}\frac{J_4}{J_2}R_E^2\left\{\frac{34}{5} - 25\sin^2(i) + \frac{77}{4}\sin^4(i)\right\}$$

$$\lambda = \frac{3}{16}\frac{(J_2)^2}{J_2}R_E^2\left\{14 + 17\sin^2(i) - 35\sin^4(i)\right\}$$

3.2.3 Modified Flower Constellation

The Modified Flower Constellation uses a similar development as the basic Flower Constellation approach, except the MFC method includes additional gravitational terms in the variations in argument of perigee, longitude of the ascending node, and mean anomaly. This enhancement allows for additional perturbation terms in order to compare with the ERO while retaining eccentricity and the ability to address non-circular orbits.[50] Adding the J_4 and J_2^2 terms[16] yields the following variational expressions in Equations (3.24)-(3.26).

$$\dot{\omega} = \frac{3nJ_2R_E^{\,2}}{4p^2}\left\{4 - 5\sin^2(i)\right\} + \frac{9nJ_2^{\,2}R_E^{\,4}}{384p^4}\left\{56e^2 + \left(760 - 36e^2\right)\sin^2(i) - \left(890 + 45e^2\right)\sin^4(i)\right\}$$
$$- \frac{15nJ_4R_E^{\,4}}{128p^4}\left\{64 + 72e^2 - \left(248 + 252e^2\right)\sin^2(i) + \left(196 + 189e^2\right)\sin^4(i)\right\} \tag{3.24}$$

$$\dot{\Omega} = \frac{-3J_2R_E^{\,2}n\cos(i)}{2p^2} + \frac{3J_2^{\,2}R_E^{\,4}n\cos(i)}{32p^4}\left\{12 - 4e^2 - \left(80 + 5e^2\right)\sin^2(i)\right\}$$
$$+ \frac{15J_4R_E^{\,4}n\cos(i)}{32p^4}\left\{8 + 12e^2 - \left(14 + 21e^2\right)\sin^2(i)\right\} \tag{3.25}$$

$$\dot{M}_o = \frac{3J_2 R_E^{\,2} n\sqrt{1-e^2}}{4p^2}\left\{2-3\sin^2(i)\right\} + \frac{3nJ_2^{\,2}R_E^{\,4}}{512p^4\sqrt{1-e^2}}\left\{\begin{matrix}320e^2-280e^4+\left(1600-1568e^2+328e^4\right)\sin^2(i)\\ +\left(-2096+1072e^2+79e^4\right)\sin^4(i)\end{matrix}\right\} - \frac{45J_4R_E^{\,4}e^2n\sqrt{1-e^2}}{128p^4}\left\{-8+40\sin(i)-35\sin^2(i)\right\} \tag{3.26}$$

Once again substitute Equations (3.24)-(3.26) into the basic condition for a repeating ground track in Equation (3.8). Also replace e, p, and n as given in Equations (3.12)-(3.14) to yield the equation that is used to determine the semi-major axis for a given inclination and perigee height. The MFC formulation preserves eccentricity like the FC and includes the additional J_4 and J_2^2 terms like the ERO. The MFC condition is given in Equation (3.27).

$$\tau = \frac{\omega_E + \sqrt{\frac{\mu}{a}}\left(2\cos(i)\delta\frac{a}{x^2}-\varepsilon\frac{a^3}{x^4}+\varsigma\frac{a}{x^3}\right)}{\sqrt{\frac{\mu}{a}}\left[\frac{1}{a}+h\delta\frac{\sqrt{x}}{x^2}+s\gamma\frac{\sqrt{x}}{x^3}\left(\frac{a^2}{x}-1\right)+j\delta\frac{a}{x^2}+\eta\frac{a^3}{x^4}-\phi\frac{a}{x^3}+\lambda\frac{a^4}{x^4\sqrt{x}}-\upsilon\frac{a^2}{x^3\sqrt{x}}+q\beta\frac{1}{x^2\sqrt{x}}\right]} \tag{3.27}$$

where

$$x = x(a) = ap$$

$$\delta = \frac{3R_E^2J_2}{4}$$

$$\beta = \frac{3R_E^4J_2^2}{1536}$$

$$\gamma = \frac{15R_E^4J_4}{128}$$

$$\varepsilon = b\beta + f\gamma + d\beta + g\gamma$$

$$\varsigma = d\beta + g\gamma$$

$$\eta = v\beta + t\gamma + w\beta + u\gamma$$

$$\phi = w\beta + u\gamma$$

$$\lambda = (q + k + m)\beta$$

$$\upsilon = (2q + m)\beta$$

$$b = 48\cos(i)\{12 - 80\sin(i)^2\}$$

$$d = 48\cos(i)\{-4 - 5\sin(i)^2\}$$

$$f = 4\cos(i)\{8 - 14\sin(i)^2\}$$

$$g = 4\cos(i)\{12 - 21\sin(i)^2\}$$

$$h = 2 - 3\sin(i)^2$$

$$j = 4 - 5\sin(i)^2$$

$$k = 3\{1600\sin(i)^2 - 2096\sin(i)^4\}$$

$$m = 3\{320 - 1568\sin(i)^2 + 1072\sin(i)^4\}$$

$$q = 3\{-280 + 328\sin(i)^2 + 79\sin(i)^4\}$$

$$s = 3\{8 - 40\sin(i) + 35\sin(i)^2\}$$

$$t = -\{64 - 248\sin(i)^2 + 196\sin(i)^4\}$$

$$u = -\{72 - 252\sin(i)^2 + 189\sin(i)^4\}$$

$$v = 12\{760\sin(i)^2 - 890\sin(i)^4\}$$

$$w = 12\{56 - 36\sin(i)^2 - 45\sin(i)^4\}$$

The MFC condition can also be transformed into a polynomial equation given in Equation (3.28).[43]

$$\left\{\tau^2\mu E(a)^2 - \omega_E^2 a^3 x(a)^9 - \mu x(a)[D(a) - \tau F(a)]^2\right\}^2 - 4\omega_E^2\mu a^3 x(a)^{10}[D(a) - \tau F(a)]^2 = 0 \tag{3.28}$$

where

$$x(a) = ap$$

$$D(a) = 2\cos(i)\delta a^2 x^2 - \varepsilon a^4 + \varsigma a^2 x$$

$$E(a) = h\delta a x^3 + s\gamma a^3 x - s\gamma a x^2 + \lambda a^5 - \upsilon a^3 x + q\beta a x^2$$

$$F(a) = x^4 + j\delta a^2 x^2 + \eta a^4 - \phi a^2 x$$

$$\delta = \frac{3R_E^2 J_2}{4}$$

$$\beta = \frac{3R_E^4 J_2^2}{1536}$$

$$\gamma = \frac{15R_E^4 J_4}{128}$$

$$\varepsilon = b\beta + f\gamma + d\beta + g\gamma$$

$$\varsigma = d\beta + g\gamma$$

$$\eta = v\beta + t\gamma + w\beta + u\gamma$$

$$\phi = w\beta + u\gamma$$

$$\lambda = (q + k + m)\beta$$

$$\upsilon = (2q + m)\beta$$

$$b = 48\cos(i)\{12 - 80\sin(i)^2\}$$

$$d = 48\cos(i)\{-4 - 5\sin(i)^2\}$$

$$f = 4\cos(i)\{8 - 14\sin(i)^2\}$$

$$g = 4\cos(i)\{12 - 21\sin(i)^2\}$$

$$h = 2 - 3\sin(i)^2$$

$$j = 4 - 5\sin(i)^2$$

$$k = 3\{1600\sin(i)^2 - 2096\sin(i)^4\}$$

$$m = 3\left\{320 - 1568\sin(i)^2 + 1072\sin(i)^4\right\}$$

$$q = 3\left\{-280 + 328\sin(i)^2 + 79\sin(i)^4\right\}$$

$$s = 3\left\{8 - 40\sin(i) + 35\sin(i)^2\right\}$$

$$t = -\left\{64 - 248\sin(i)^2 + 196\sin(i)^4\right\}$$

$$u = -\left\{72 - 252\sin(i)^2 + 189\sin(i)^4\right\}$$

$$v = 12\left\{760\sin(i)^2 - 890\sin(i)^4\right\}$$

$$w = 12\left\{56 - 36\sin(i)^2 - 45\sin(i)^4\right\}$$

Additional terms in the element rate changes may be added as appropriate. A second modified Flower Constellation (MFC2) procedure includes the J_6 terms.[16] This term was added to determine the degree of change between the FC, the MFC, and the MFC2. Since J_8 (1.426810879194179e-011) is two orders of magnitude less than J_6 (6.083464988806001e-009),[25] and the difference in the MFC and MFC2 techniques are so small,[50] this investigation does not include terms beyond J_2, J_4, and J_2^2.

3.2.4 Simplified Repeat Groundtrack

Another method of evaluating the repeat ground track condition is to use a simplified form of Equation (3.8) with only the J_2 term.[44] This method is different from the FC method in that eccentricity is given, rather than being a function of the perigee height and semi-major axis. Equation (3.8) may be written as below.

$$n\left(1 + \frac{3}{2}J_2\frac{R_E^2}{a^2}\psi\right) - \frac{\omega_E}{\tau} = 0 \tag{3.29}$$

where

$$\psi = 3\left(1-e^2\right)^{-\frac{3}{2}}\left(\frac{1}{3} - \frac{1}{2}\sin(i)^2\right) - \frac{1}{\left(1-e^2\right)^2}\left(\frac{1}{2} - \frac{5}{2}\cos(i)^2\right) - \frac{1/\tau}{\left(1-e^2\right)^2}\cos(i)$$

Let

$$Q = \frac{3}{2} J_2 \frac{R_E^2}{\mu^{2/3}} \psi \tag{3.30}$$

and

$$\chi = n^{1/3} \tag{3.31}$$

so that Equation (3.29) becomes

$$\chi^3 + Q\chi^7 - \frac{\omega_E}{\tau} = 0 \tag{3.32}$$

Equation (3.32) can be easily solved using a two step iteration Newton method with a close guess semi-major axis and given inclination, eccentricity, and similitude parameter.[†]

The SRG refinement method is needed because the FC, ERO, and MFC methods all make the assumption $n = (\mu/a^3)^{1/2}$, which is not true under perturbation and introduces error in the computed semi-major axis. Although simulating the perturbed orbital motion with such values leads to a ground trace that is approximately closed, in many cases the accuracy is not sufficient. Given a starting condition for a from either the FC, ERO, or MFC methods, Equation (3.32) is used to find $\chi(n)$ directly and $n = (\mu/a^3)^{1/2}$ is used to find the corresponding a, leading to the two step iteration procedure. Usually only two iterations are needed for convergence. Ground track closure with these results is nearly always satisfactory.

[†] Recommendation from Dr. Paul Cefola, Personal Correspondence, September 2009.

3.3 Method Comparisons

The method comparison focuses on evaluating the four processes to discover the most efficient method for finding a semi-major axis for a given inclination, similitude parameter, and perigee height. The equations for repeating ground track conditions for FC, ERO, MFC, and SRG are the basis for comparing the four methods. The FC, ERO, and MFC equations are first used to find the semi-major axis for a given inclination, similitude parameter, and perigee height. The SRG method needs a close guess initial semi-major axis as well as given eccentricity, inclination, and similitude parameter. Thus, the method comparison uses the SRG method to refine the semi-major axis determined by the FC, ERO, and MFC methods and these refined methods are called FCr, EROr, and MFCr respectively.

3.3.1 Semi-Major Axis Comparison

A grid pattern is laid with ranging inclinations and eccentricity for three cases for $\tau = ½$ (12 hour period), $\tau = ¼$ (6 hour period), and $\tau = 1/16$ (90 minute period). For $\tau = ½$, e ranges from 0 to 0.68. For $\tau = ¼$, e ranges from 0 to 0.28. For $\tau = 1/16$, $e \approx 0$. Inclination ranges from 0 to 100 degrees at a step interval of 5 degrees for all three cases. Figures 3.4-3.12 show the results for the inclination versus semi-major axis for each of the FC, ERO, and MFC methods in comparison to the SRG refinement. In all three cases the SRG refinement for each method converges to the same result, and the unrefined MFC method closely approximates this result. This behavior shows that using the FC or ERO method with the SRG refinement leads to the same semi-major axis as determined by the MFC method without need for refinement.

A few additional comments are given on Figures 3.4-3.12 before moving on. For the τ = ½ case, note all FC semi-major axis curves over the family of eccentricities coalesce at the inclination of 90 deg. This behavior is likely related to the cos(i) numerator term in Equation (3.15) vanishing at this critical inclination. Also note the unrefined and refined curves for each eccentricity intersect precisely at 60 deg inclination. For this value of i, each $\sin^2(i)$ factor in the denominator in Equation (3.15) equates to ± 0.25, while in Equation (3.29) both $\sin^2(i)$ and $\cos^2(i)$ factors within parameter ψ become ± 0.125 (including multiplying the term 3) at i = 60 deg. The noted intersections in Figure 3.4 correlate with this term cancelling. Similar features are observed in the FC method for τ = ¼ and 1/16 in Figures 3.7 and 3.10. Finally note that the refined curves for all three methods (Figures 3.4-3.6) intersect near i = 30 deg for τ = ½ but there is no similar intersection for τ = ¼ and 1/16 (Figures 3.7-3.12). For τ = ½ and i = 30 deg, the $\sin^2(i)$ factor in Equation (3.29) becomes + 0.625 while the combined $\cos^2(i)$ and cos(i) factor gives -1/0.622, again causing an approximate cancellation of terms (i.e., elimination of the eccentricity parameter) thus inducing the intersection of curves. When $\tau \neq$ ½, this alignment is diffused.

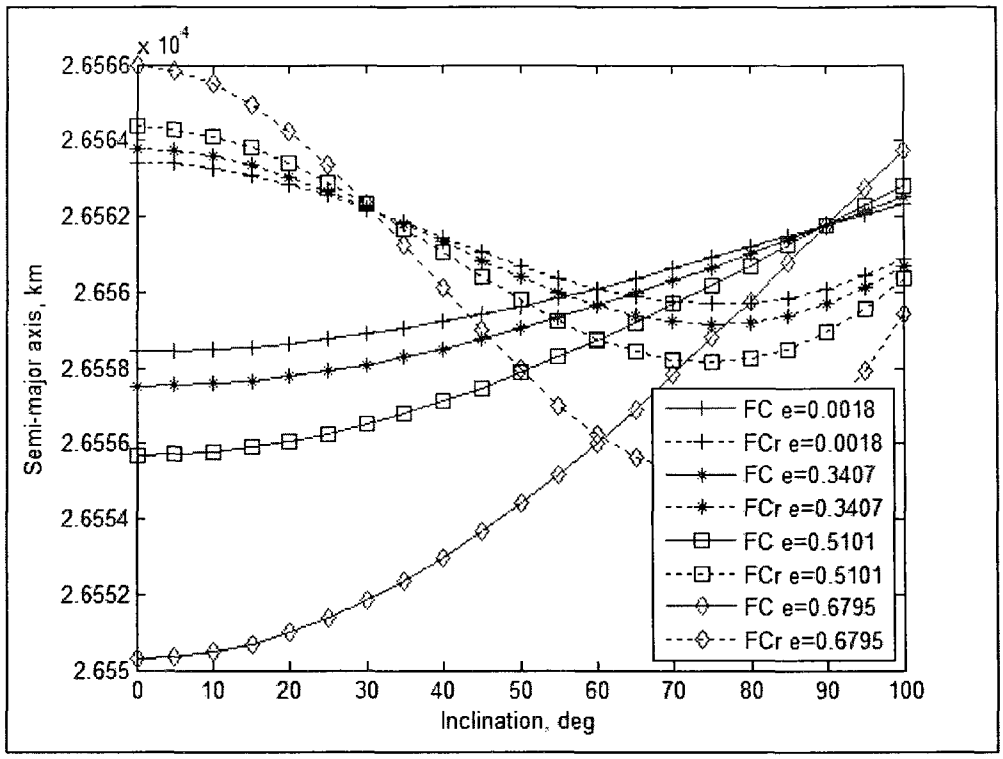

Figure 3.4 Inclination vs. Semi-Major Axis for FC Methods $\tau = ½$

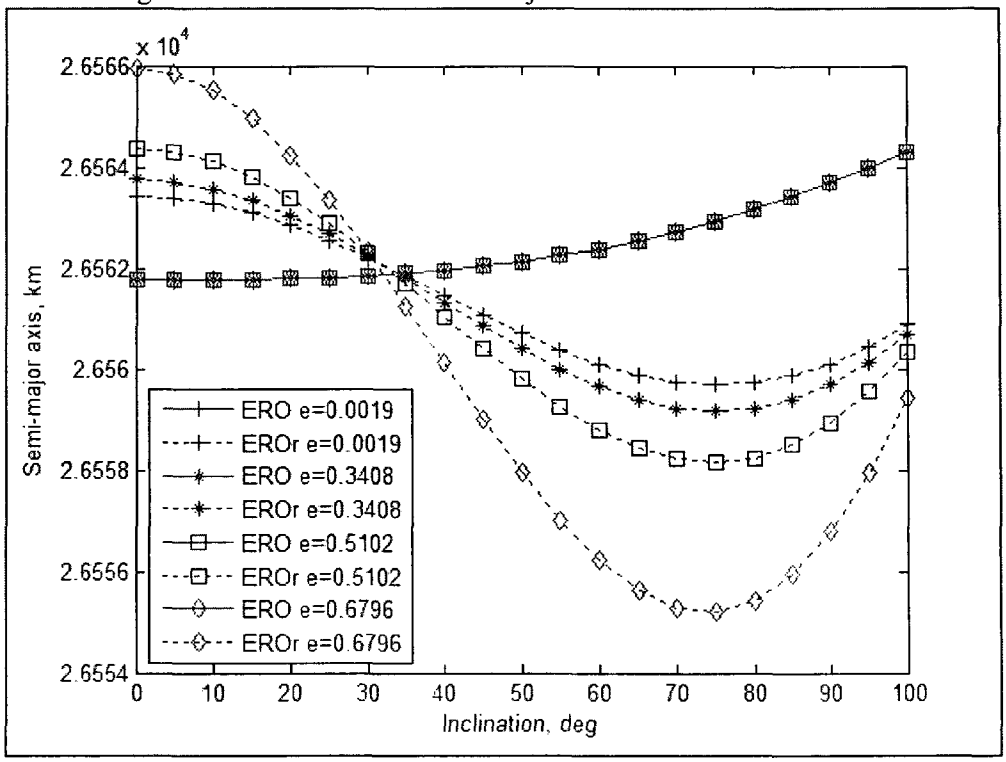

Figure 3.5 Inclination vs. Semi-Major Axis for ERO Methods $\tau = ½$

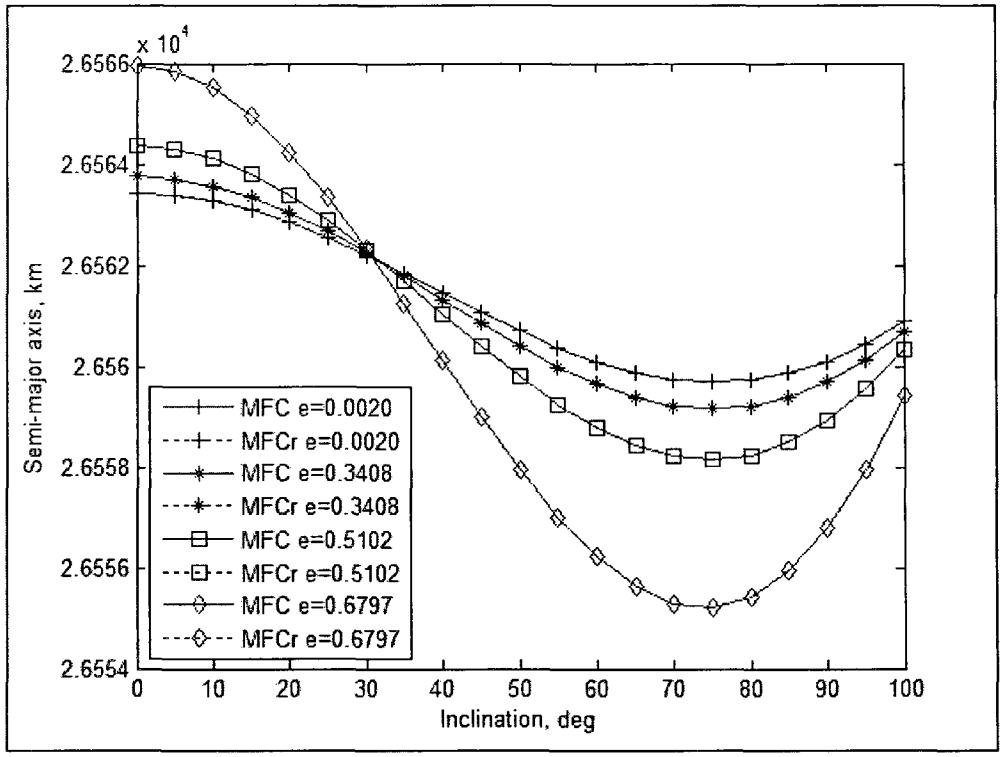

Figure 3.6 Inclination vs. Semi-Major Axis for MFC Methods $\tau = ½$

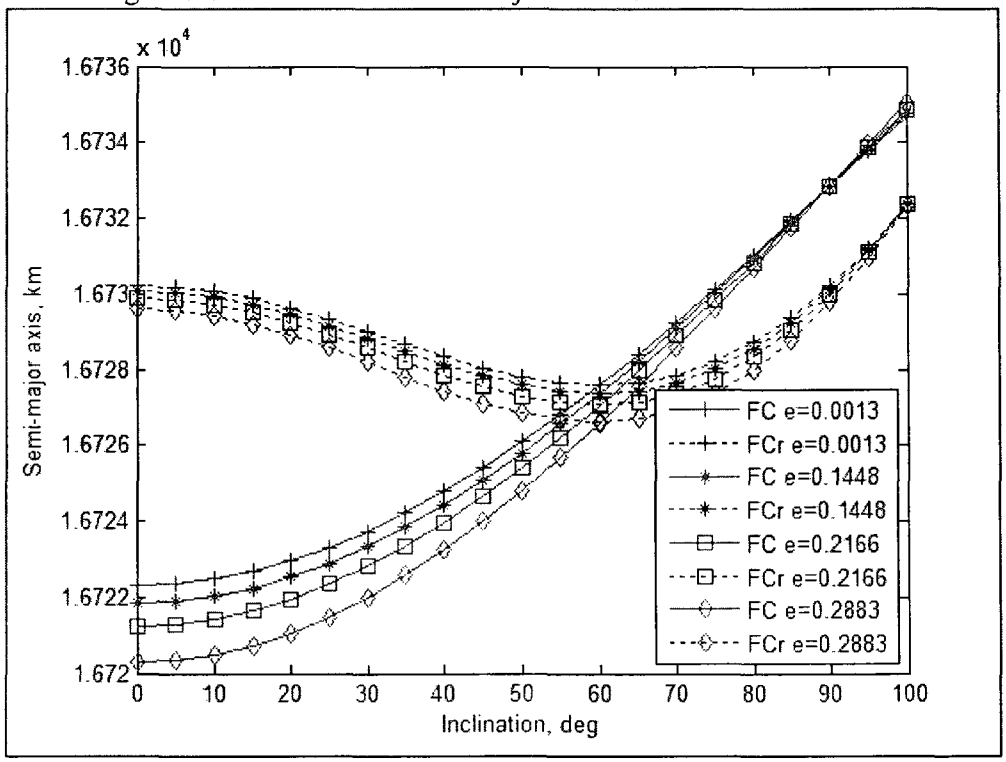

Figure 3.7 Inclination vs. Semi-Major Axis for FC Methods $\tau = ¼$

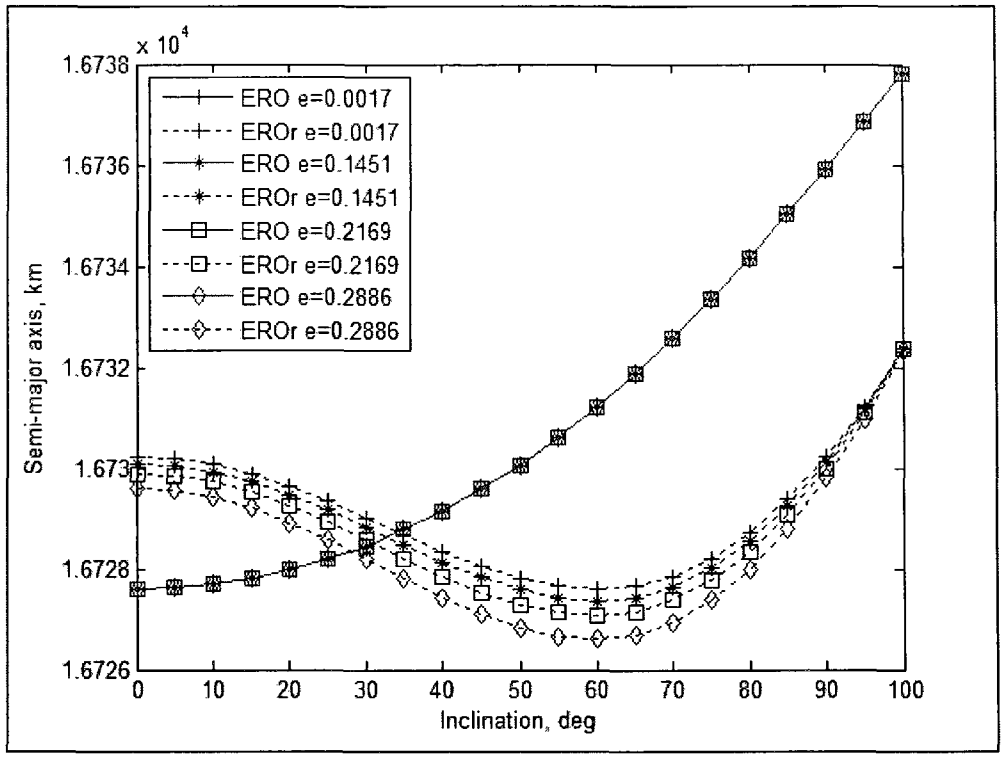

Figure 3.8 Inclination vs. Semi-Major Axis for ERO Methods $\tau = ¼$

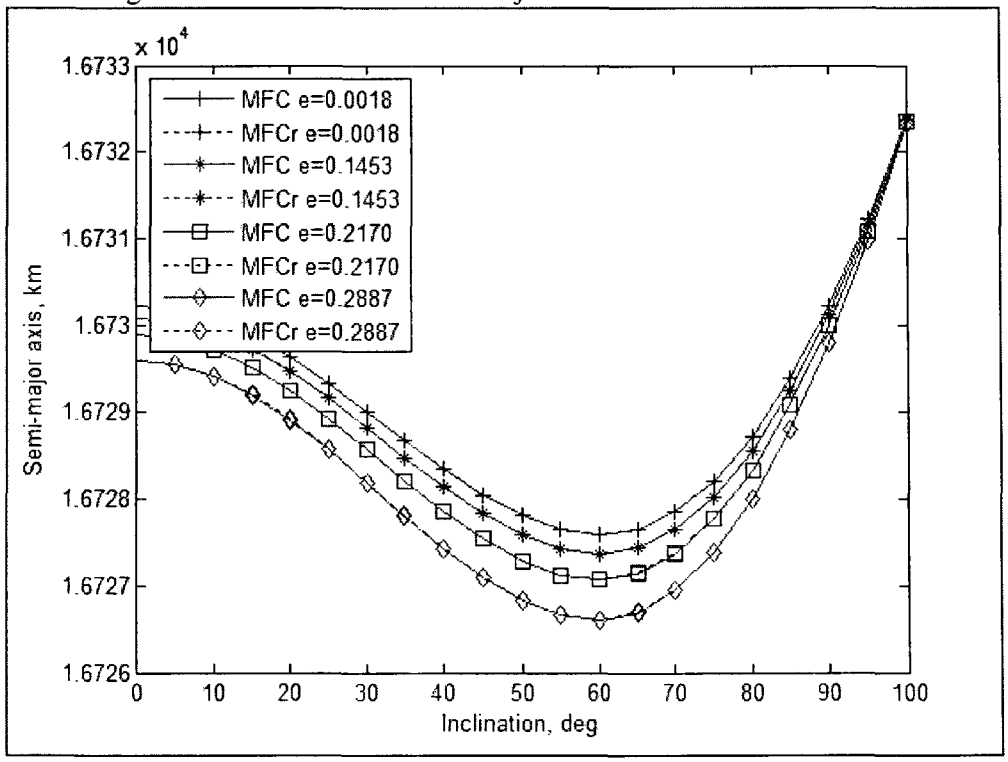

Figure 3.9 Inclination vs. Semi-Major Axis for MFC Methods $\tau = ¼$

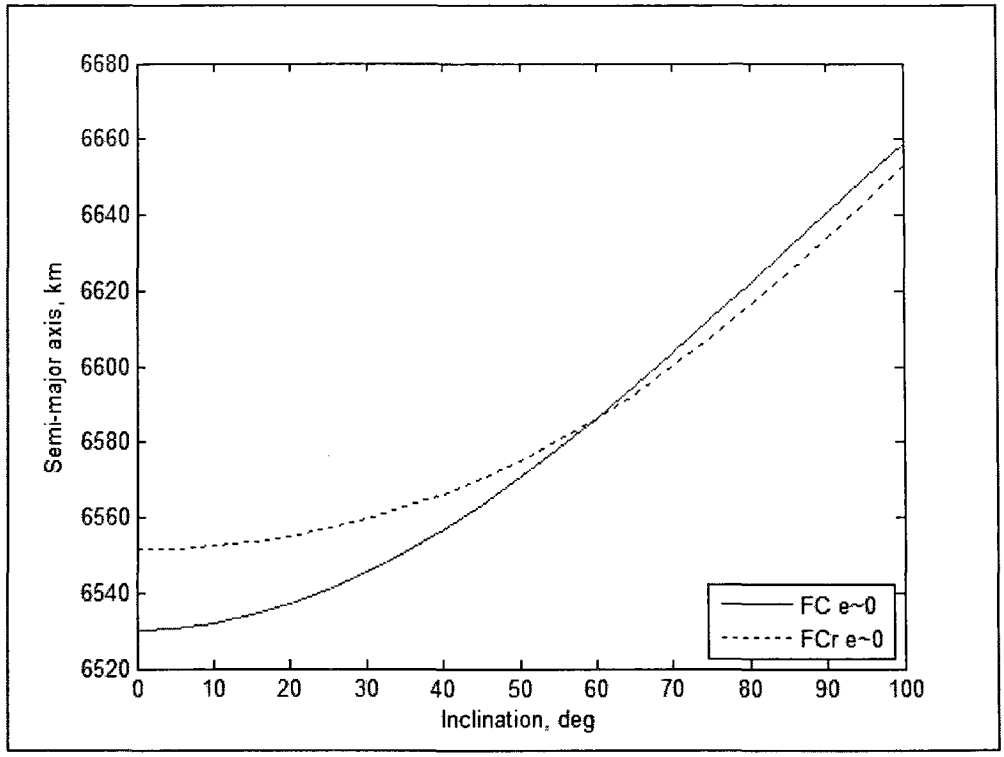

Figure 3.10 Inclination vs. Semi-Major Axis for FC Methods $\tau = 1/16$

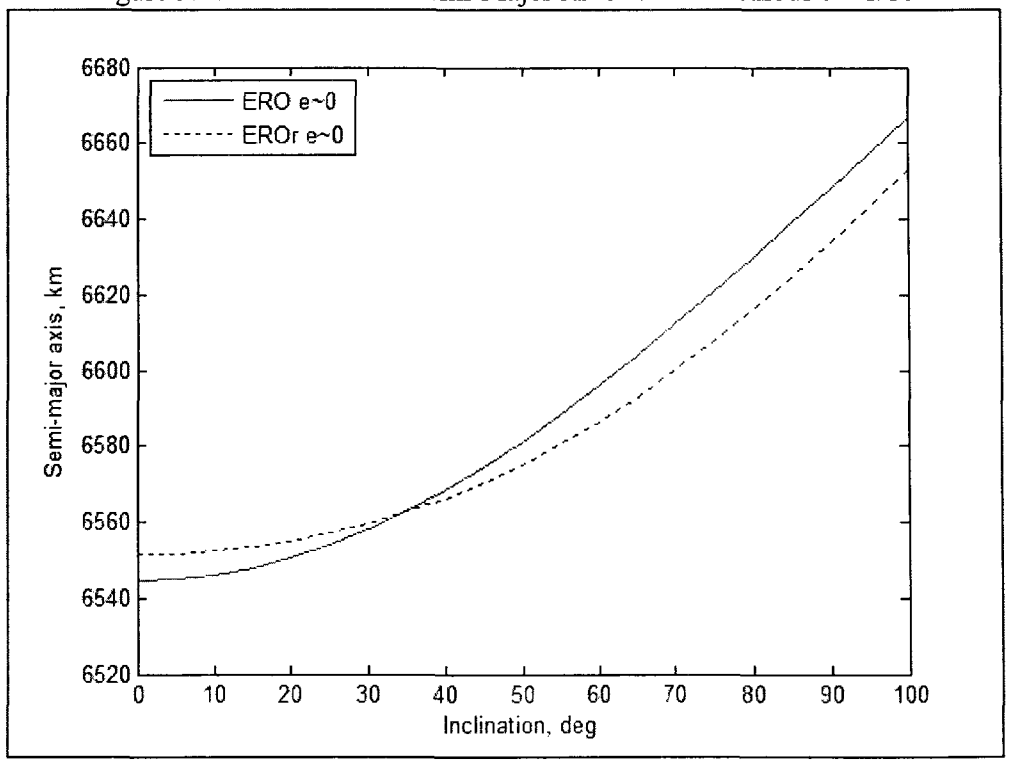

Figure 3.11 Inclination vs. Semi-Major Axis for ERO Methods $\tau = 1/16$

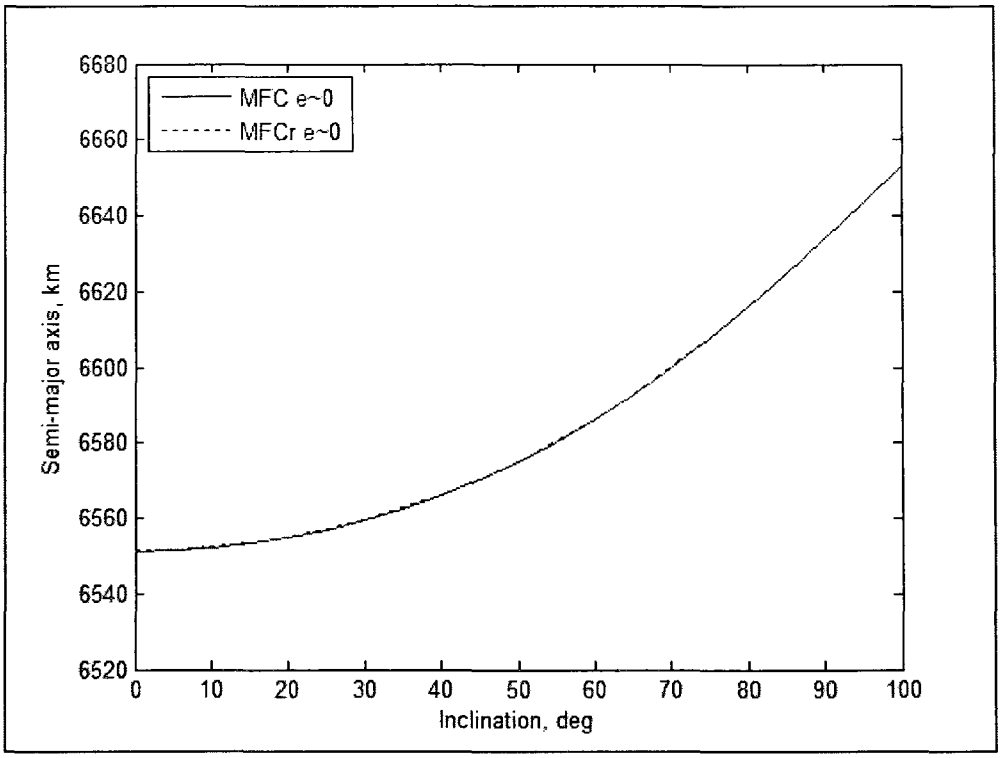

Figure 3.12 Inclination vs. Semi-Major Axis for MFC Methods $\tau = 1/16$

3.3.2 Computational Time Comparison

A second part of the method comparison focused on the computational time needed to find the semi-major axis for a given inclination, similitude parameter, and perigee height. Once again, the ERO equation is based only on inclination and similitude parameter (near circular orbit). The same three cases for $\tau = ½$ (12 hour period), $\tau = ¼$ (6 hour period), and $\tau = 1/16$ (90 minute period) are also used in comparing the computational time. The first computational time is found through using an algebraic numerical solver, the Newton method for this comparison, for the semi-major axis using Equations (3.15), (3.22), and (3.27). A realistic choice for a first guess of the semi-major axis leads to an appropriate root. The second process leading to a second computational

time is from the corresponding polynomial equations. Here all roots must be examined to determine the appropriate root. The FC and MFC polynomial equations can lead to multiple roots within a valid orbital range (from low orbital altitudes to a geosynchronous altitude). Therefore the valid roots must be further examined to find the appropriate root. Since finding the valid roots for the FC and MFC methods is complex, the SRG refinement with a two step iteration process is only applied to the ERO method. Figures 3.13-3.21 show the results for computational time for the two different processes for each τ based on the FC, ERO, and MFC approaches. Computational times are found using the "tic" and "toc" commands in Matlab. Each run represents an inclination and eccentricity pair, and a total of 105 pairs for τ = ½ and ¼ were considered, but only 63 pairs were used in the τ = 1/16 case.

The polynomial root finding approach consistently outperformed the algebraic Newton iteration approach with regards to computational time. A single run using the polynomial equation formulation consistently required 0.001 s or less to complete, while the algebraic equation formulation often took 3 to 5 times longer. When using the algebraic Newton iteration approach, due to the larger number of terms to evaluate (J_4, J_2^2), the ERO and MFC runs approximately took 0.003 to 0.005 s while the simpler FC runs usually took 0.002 s of computational time.

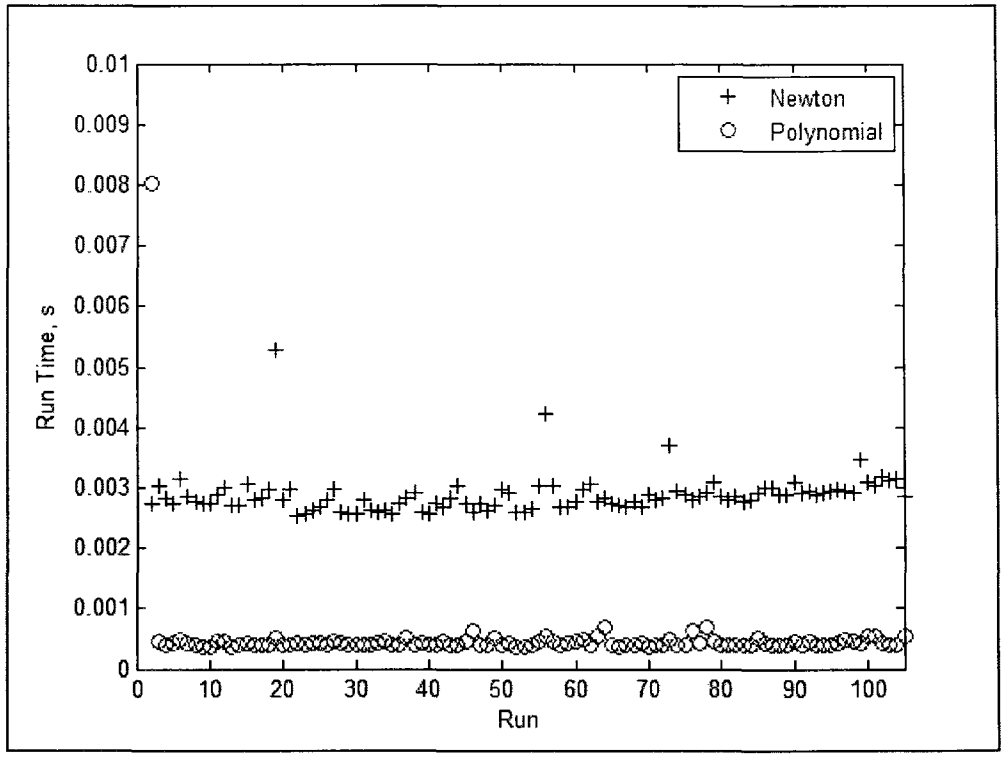

Figure 3.13 Computational Times for FC, $\tau = \frac{1}{2}$

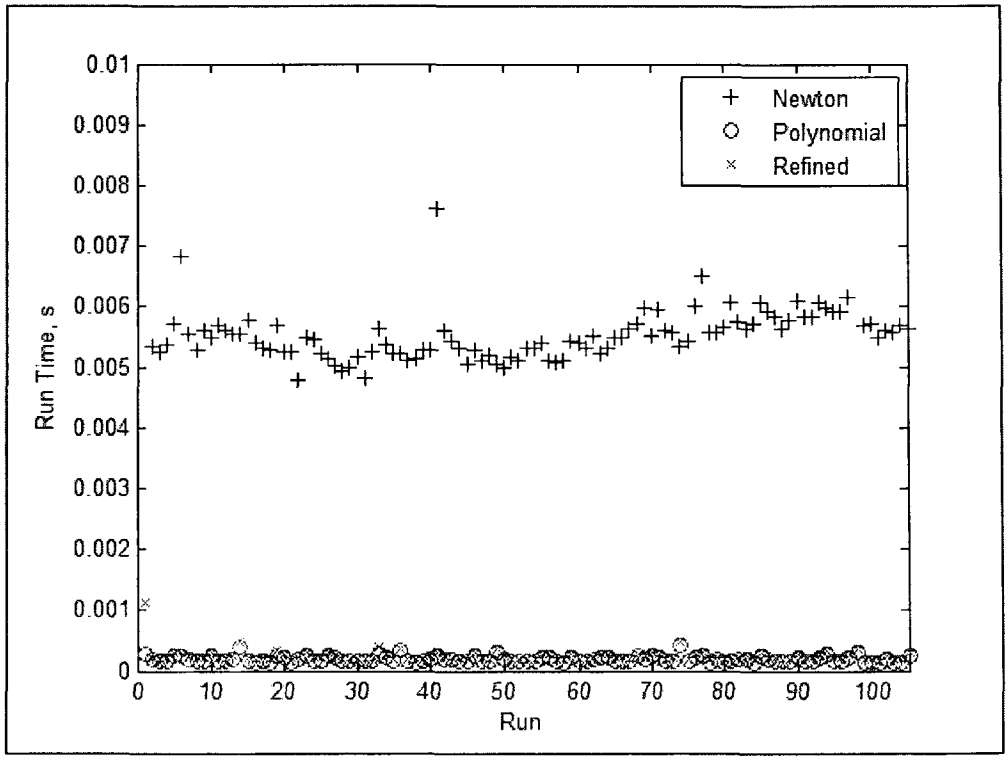

Figure 3.14 Computational Times for ERO, $\tau = \frac{1}{2}$

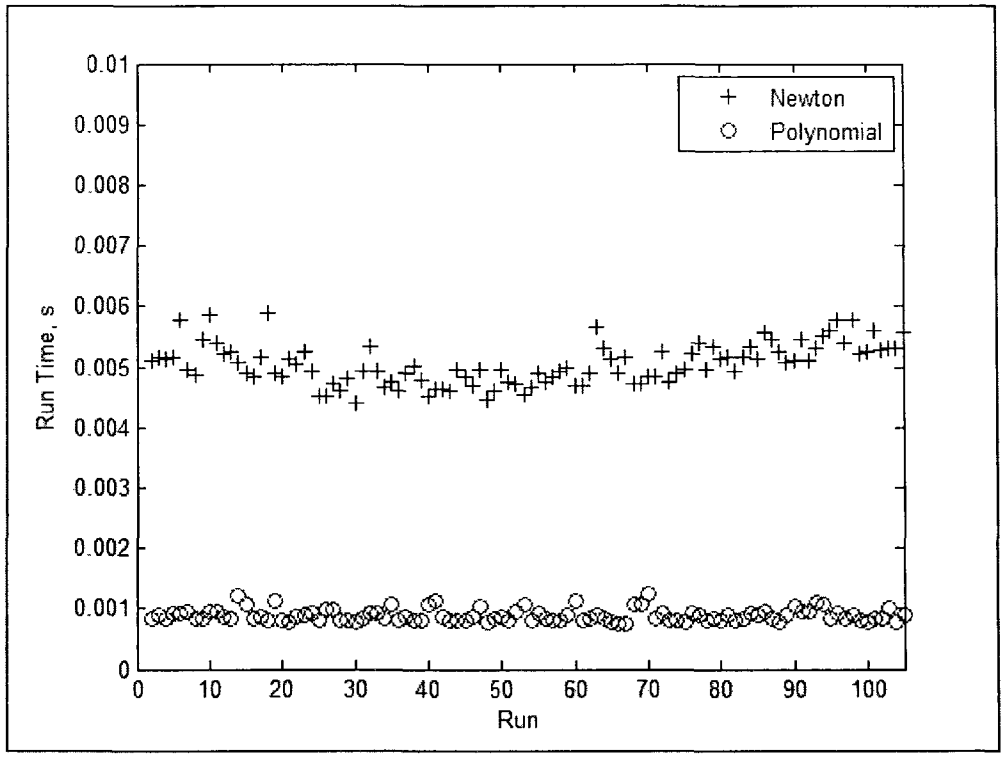

Figure 3.15 Computational Times for MFC, $\tau = ½$

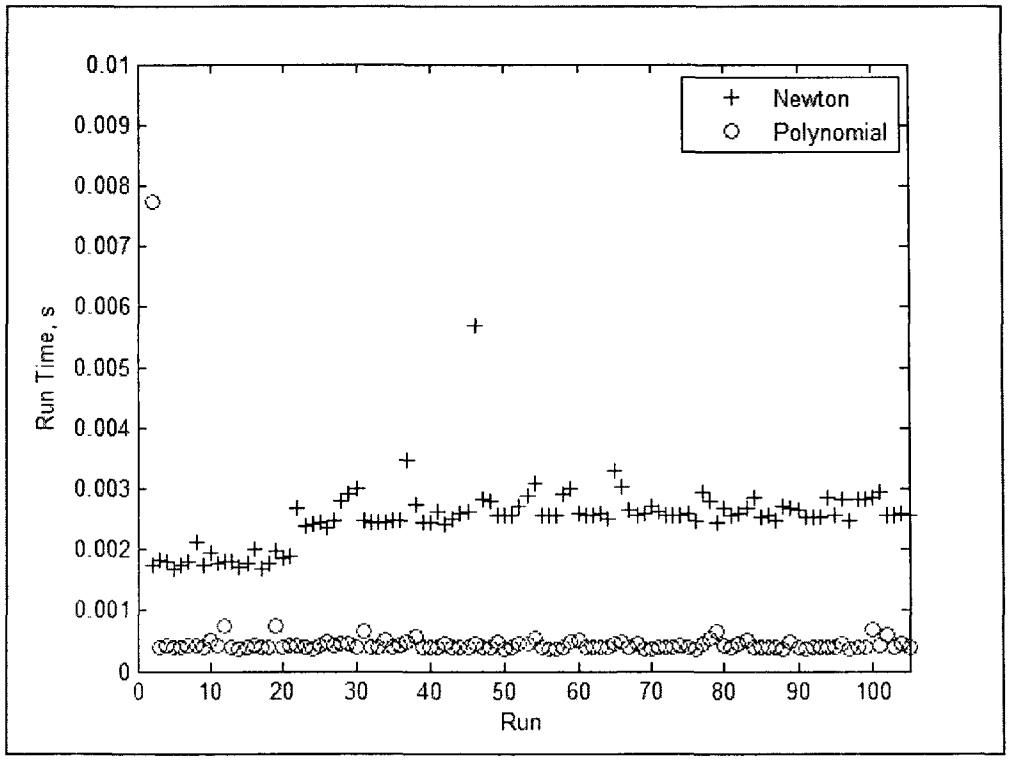

Figure 3.16 Computational Times for FC, $\tau = ¼$

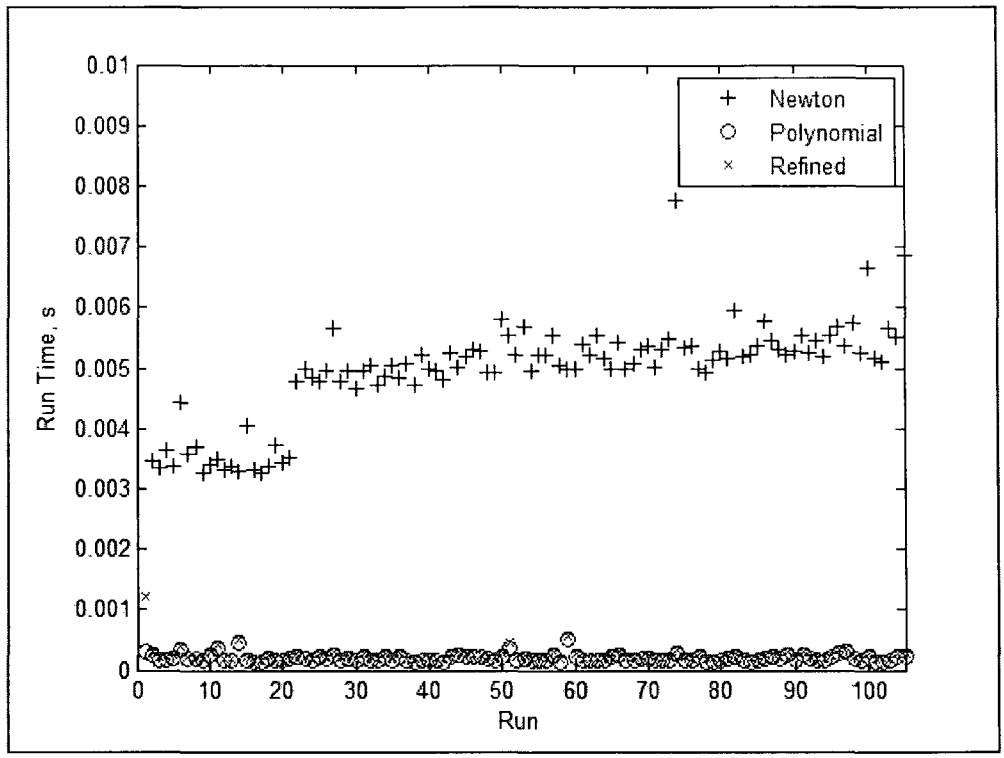

Figure 3.17 Computational Times for ERO, $\tau =$ ¼

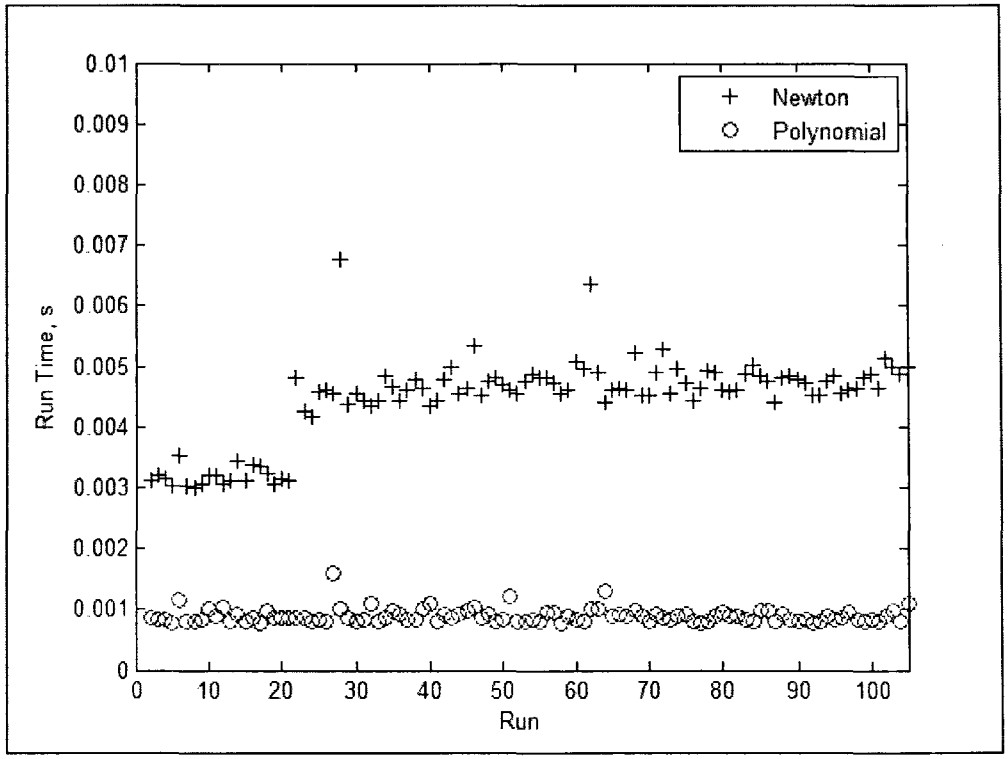

Figure 3.18 Computational Times for MFC, $\tau =$ ¼

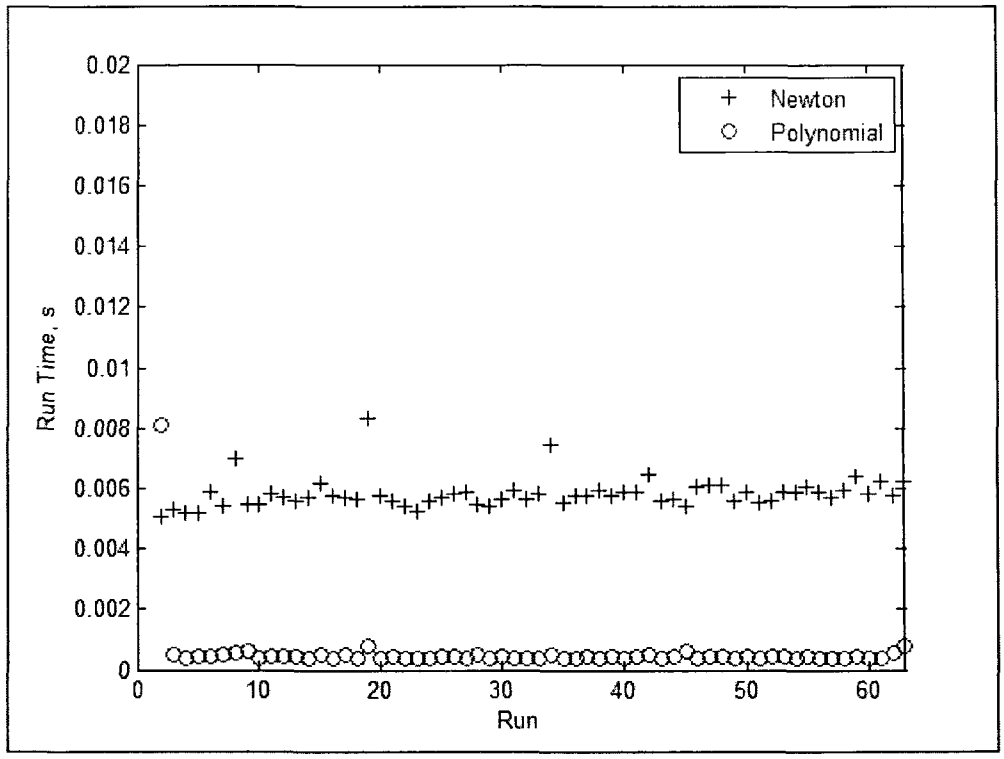

Figure 3.19 Computational Times for FC, $\tau = 1/16$

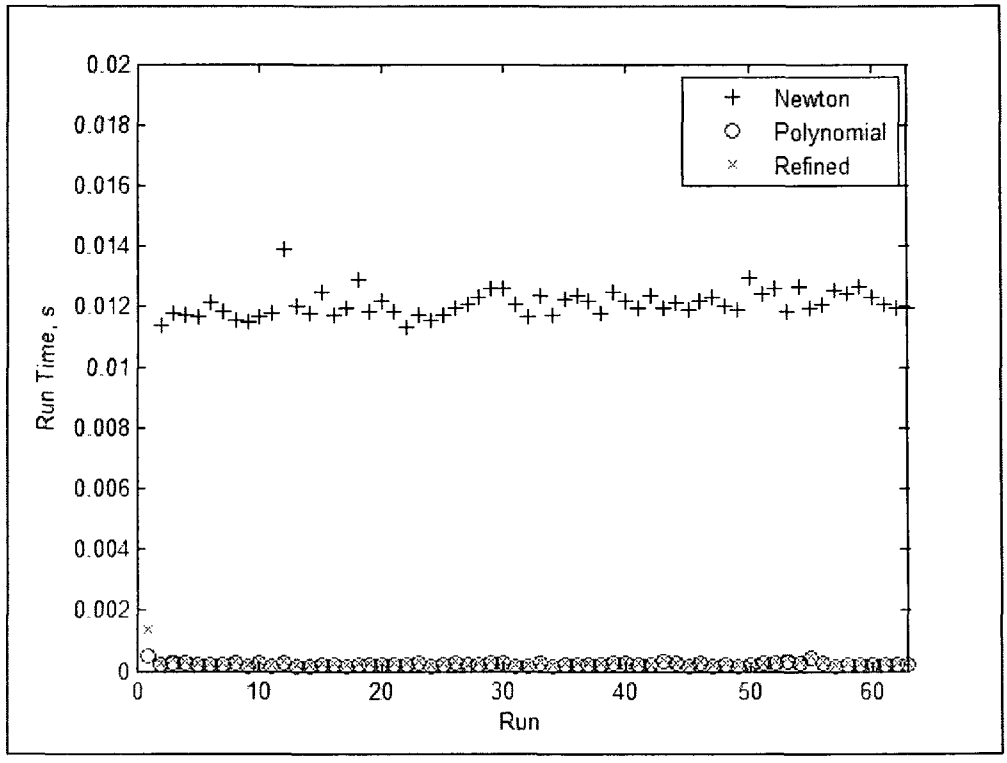

Figure 3.20 Computational Times for ERO, $\tau = 1/16$

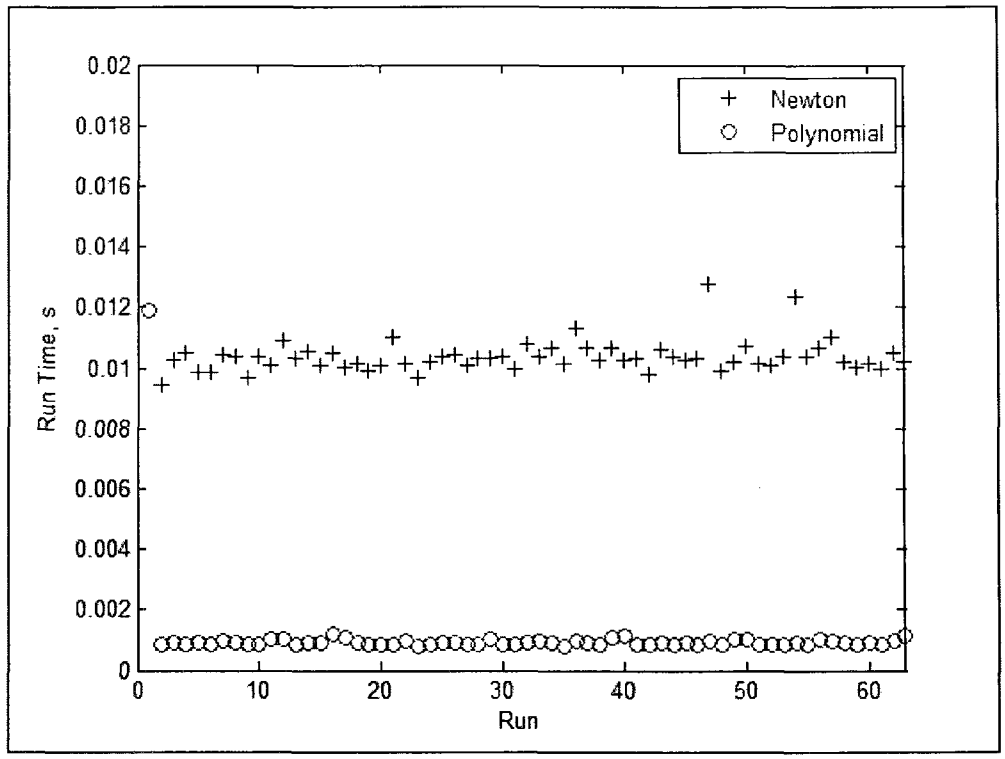

Figure 3.21 Computational Times for MFC, $\tau = 1/16$

3.3.3 Residual Comparison

Another consideration for evaluating repeat ground track methods is the value of the repeat ground track function, f, where by rearranging Equation (3.8) for the residual

$$f = \tau - \frac{\omega_E - \dot{\Omega}}{n + \dot{M}_o + \dot{\omega}} \tag{3.33}$$

For an ideal case, f is zero. For this case study, each method was evaluated using the appropriate form of Equation (3.33). The tolerance selected for the Newton method was 10^{-3} in order to maintain quick computing times. Tighter tolerances will produce smaller residual error with undesirable impact on run time. The same three cases for $\tau = ½$ (12 hour period), $\tau = ¼$ (6 hour period), and $\tau = 1/16$ (90 minute period) are presented in

comparing the function value. Also, identical gridding for inclination and eccentricity as that used in the semi-major axis comparison was employed here.

Figures 3.22-3.33 show the results for the FC, ERO, EROr, and MFC methods. Note the magnitude difference in the values. The EROr method consistently has the smallest error (10^{-13} to 10^{-16}) and is likely related to it being a refinement process of a previous solution. The ERO and MFC methods have comparable error (10^{-7} to 10^{-8}) and consistently outperform the FC method (10^{-3}). These differences in convergence between the FC and ERO/MFC methods are likely due to the differing function slopes at the semi-major axis zero due to the various J_4, J_2^2 perturbation terms present in the ERO/MFC methods and absent in the FC method.

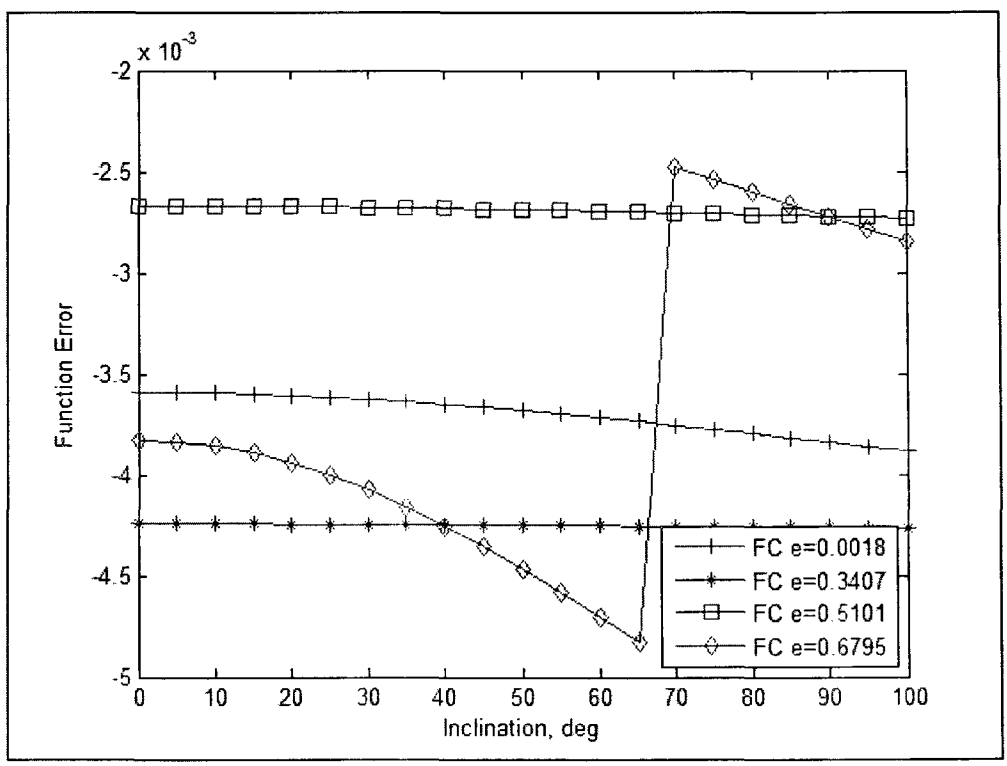

Figure 3.22 Function Value for FC, $\tau = ½$

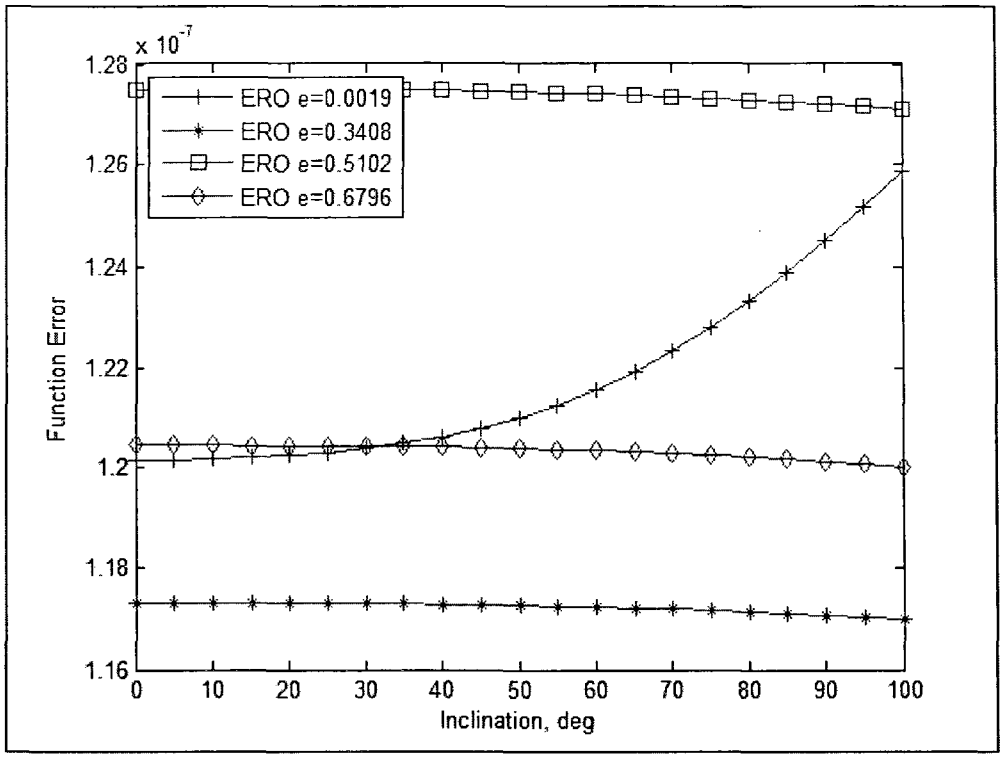

Figure 3.23 Function Value for ERO, $\tau = ½$

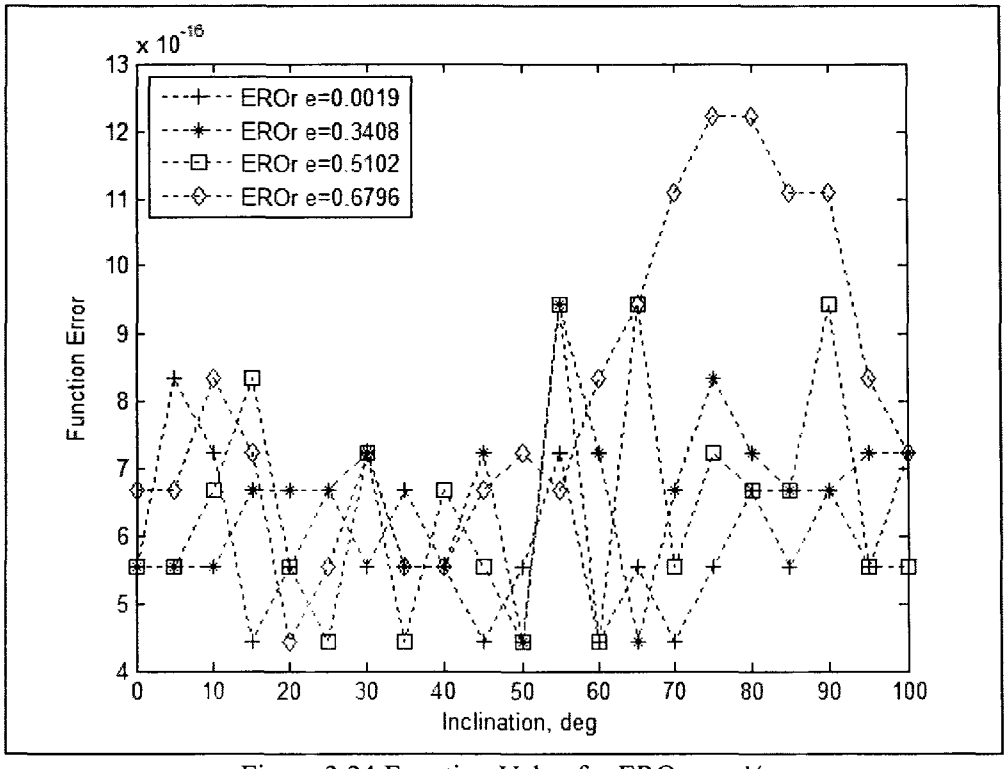

Figure 3.24 Function Value for EROr, $\tau = ½$

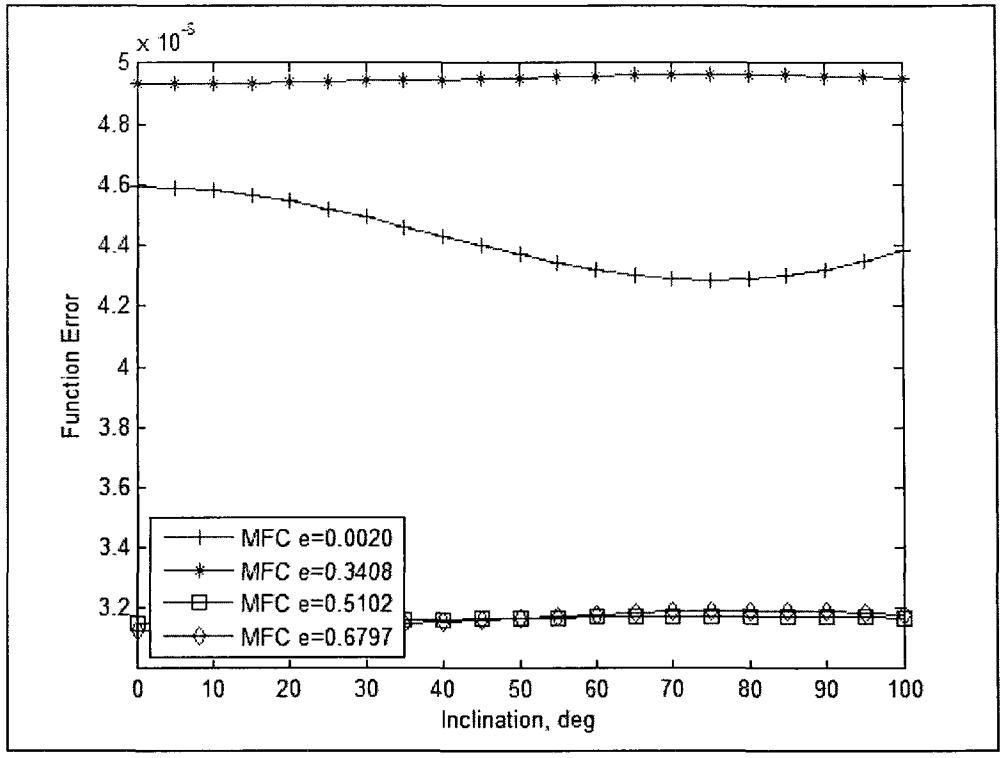

Figure 3.25 Function Value for MFC, $\tau = ½$

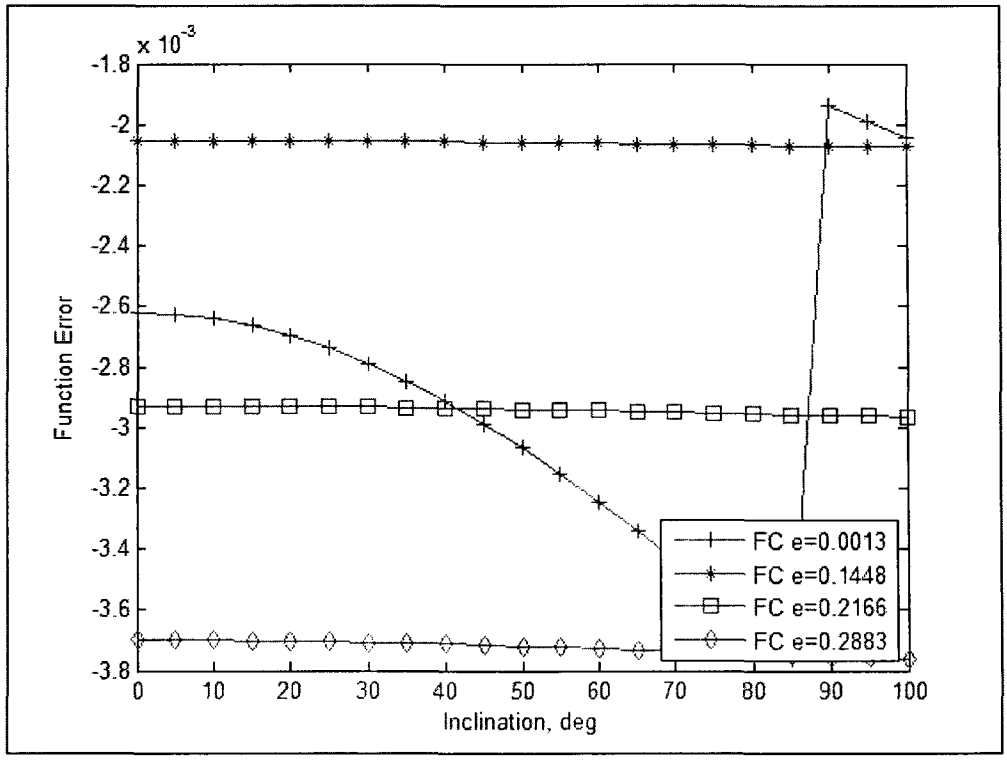

Figure 3.26 Function Value for FC, $\tau = ¼$

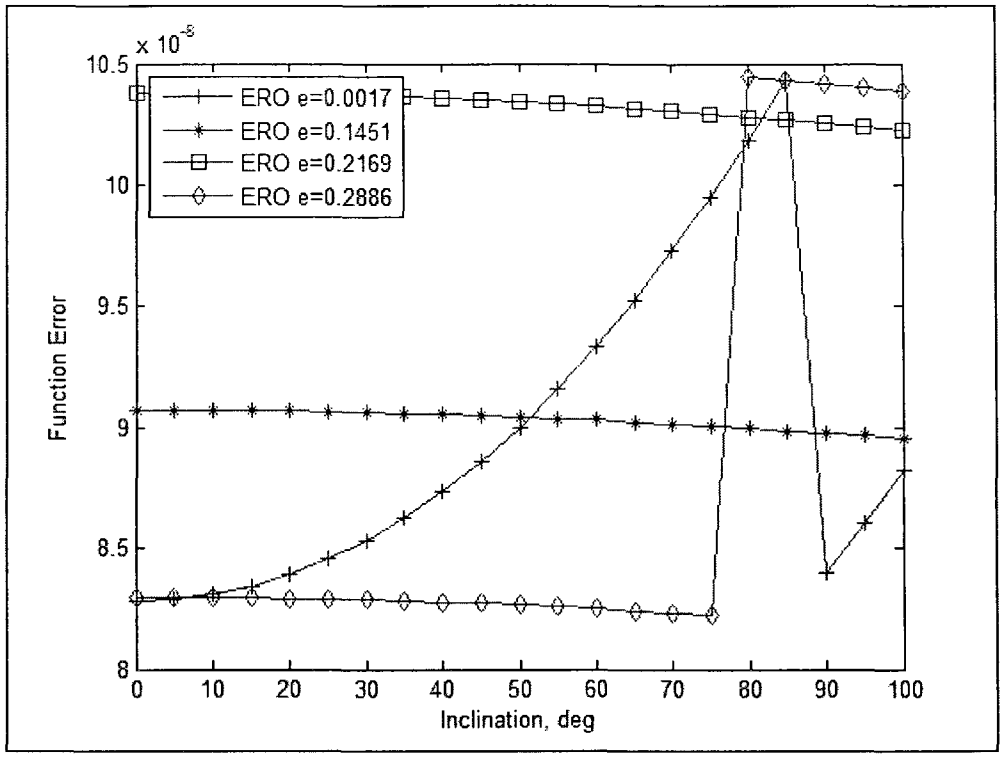

Figure 3.27 Function Value for ERO, $\tau = ¼$

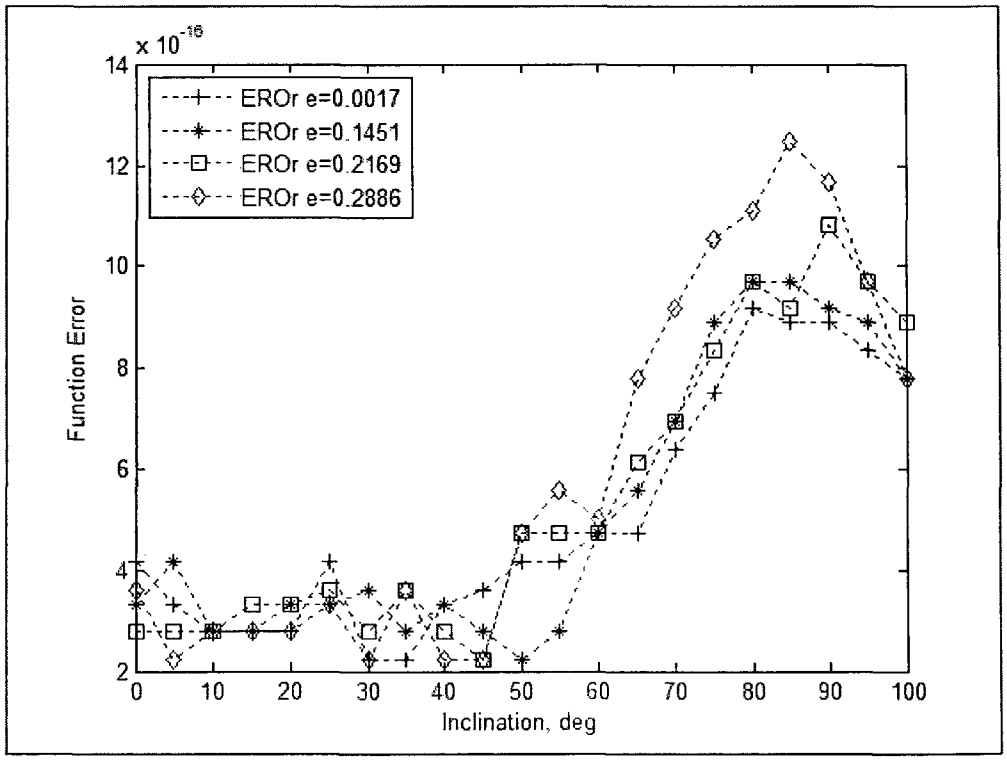

Figure 3.28 Function Value for EROr, $\tau = ¼$

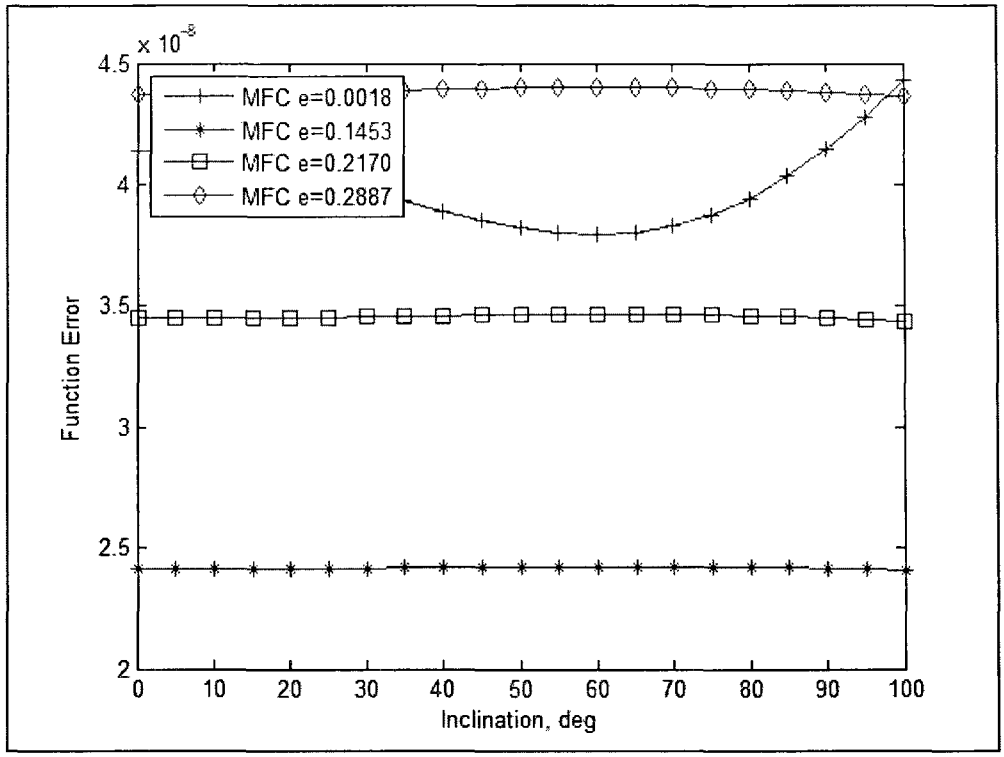

Figure 3.29 Function Value for MFC, $\tau = ¼$

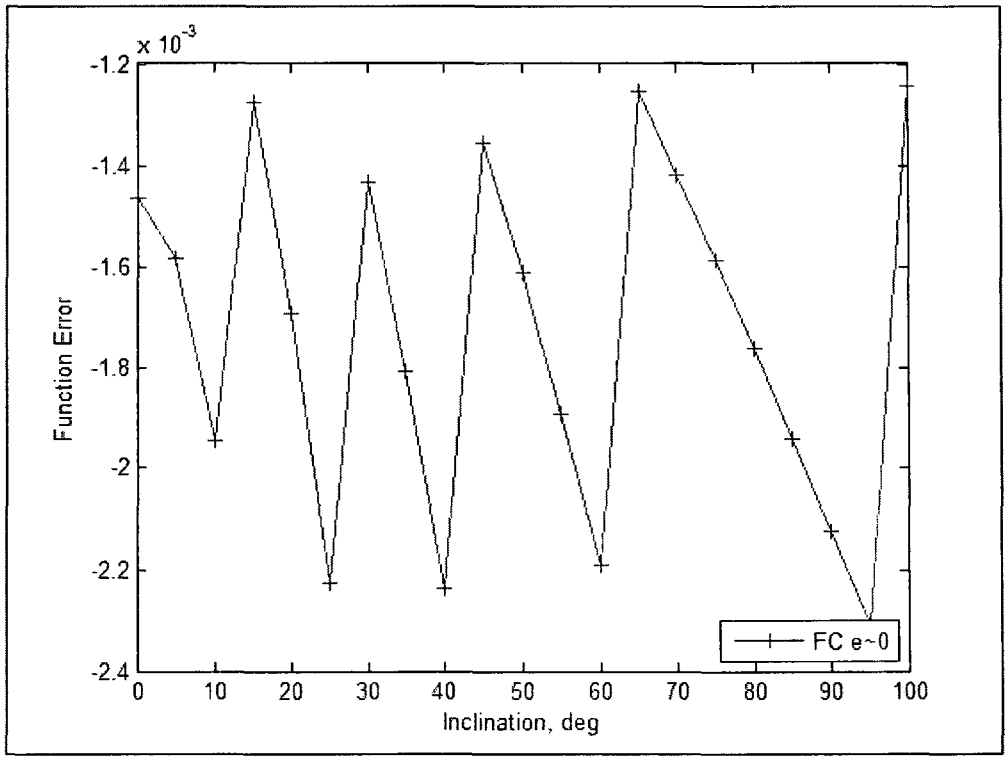

Figure 3.30 Function Value for FC, $\tau = 1/16$

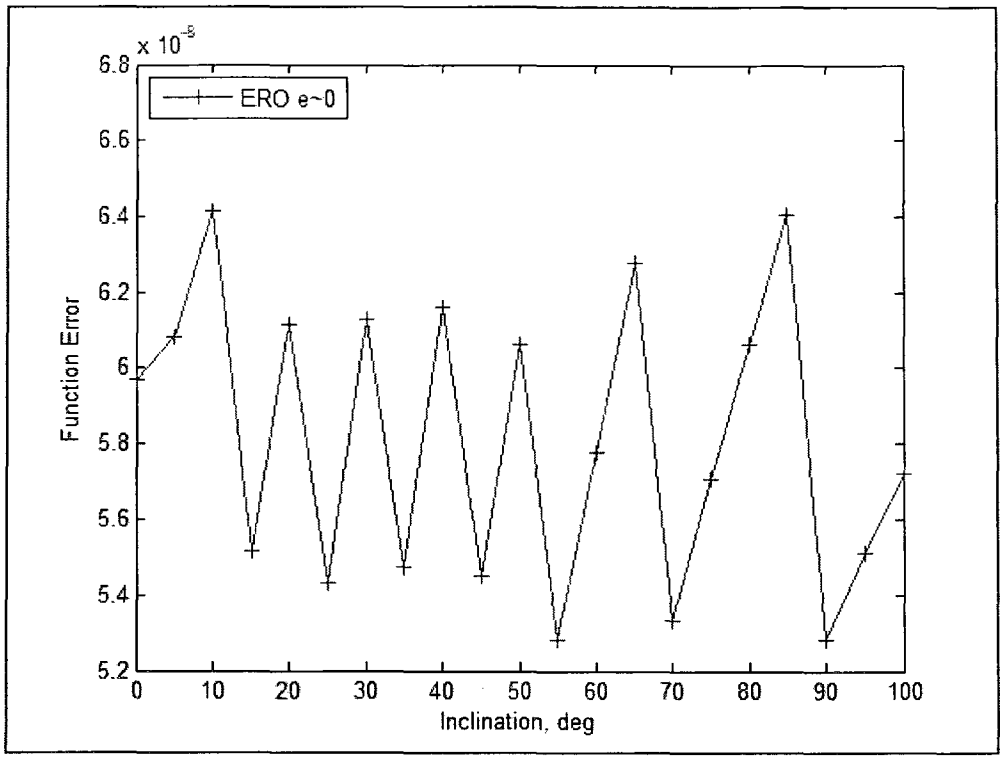

Figure 3.31 Function Value for ERO, $\tau = 1/16$

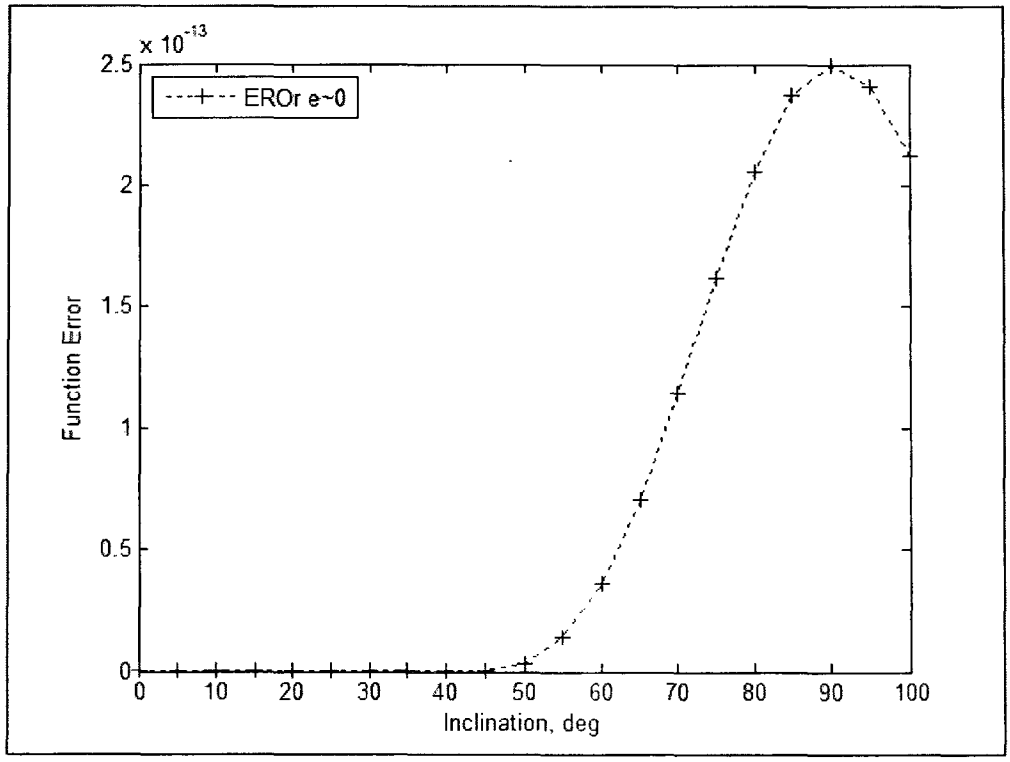

Figure 3.32 Function Value for EROr, $\tau = 1/16$

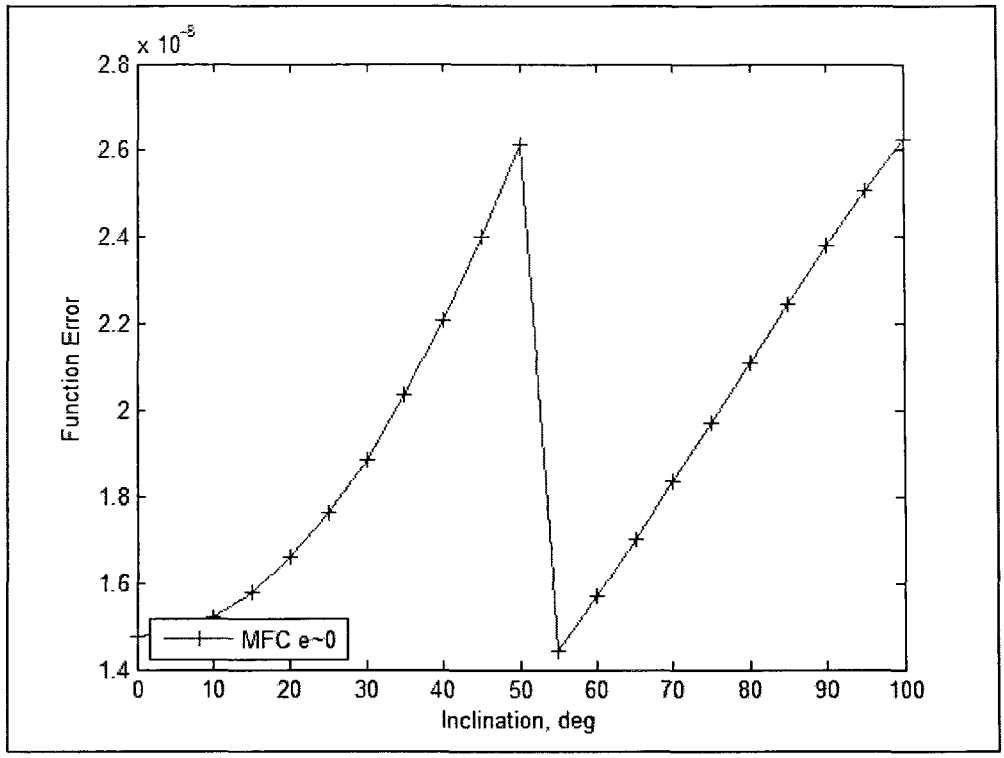

Figure 3.33 Function Value for MFC, $\tau = 1/16$

3.3.4 Comparison Conclusions

Four methods for numerically determining the condition for repeat ground tracks were investigated. Three recent methods, the FC, ERO, and MFC were reviewed. A fourth method, the SRG, was re-introduced and considered as a refinement process since a close guess semi-major axis and given eccentricity are necessary. A method comparison using three design orbits of various altitudes ($\tau = ½$, $\tau = ¼$, and $\tau = 1/16$) was investigated to better visualize the design space for each method.

Figures 3.4-3.12 show that the determined semi-major axis from the MFC and refined SRG methods are comparable. Therefore the ERO approach can be used with a SRG refinement to produce the equivalent MFC result. The ERO polynomial approach

only leads to a single valid, appropriate root where as the FC and MFC polynomial equations can lead to multiple valid roots which must be further examined to find the appropriate root. Therefore the ERO polynomial equation with the SRG is included in computational run time analysis for the polynomial equation strategy vs. traditional algebraic numerical solver. Figures 3.13-3.21 show the computational run times for the FC, ERO, and MFC methods. Overall, the polynomial equations are seen to be much less expensive than a traditional numerical solver. Also, the ERO approach shows a faster computational time over the FC and MFC approaches, even with the SRG refinement. In regard to Figures 3.22-3.33, the repeat ground track function values vary from thousandths with the FC method to 10^{-8} with the ERO and MFC methods to 10^{-13} for the ERO refined method. Clearly, the ERO refined method shows the function value closest to zero; zero being the ideal case.

For use in an optimization algorithm, each method was weighed based on reliability, performance, and computational ease. For reliability, the FC and MFC methods are not recommended because of the restricted solution space for near circular orbits. For performance, the FC and MFC methods use more variables than the ERO method. In regards to computational ease, the FC and MFC polynomial equations, Equations (3.16) and (3.28), can lead to multiple possible roots for a set of solutions which requires further investigation to find the appropriate viable, single solution. The ERO method polynomial equation, Equation (3.23), leads to only one viable root solution. Therefore, taking into consideration the overall reliability, performance, and computational ease exhibited by the ERO method with SRG refinement, the ERO

formulation is recommended over the FC and MFC approaches for finding initial orbital parameters. This research uses the ERO method with SRG refinement.

CHAPTER 4

OPTIMIZATION PROCESS

4.1 Optimization Cost Function

Selection of the cost function for the optimization process is critical. Abdelkhalik and Mortari[39] present two cost functions. The first cost function is observation resolution with the objective of achieving the highest value and the second is observation time for the site where attaining the largest possible value is the goal. The cost functions are mathematically expressed in such a way that a minimum numerical value over the design space is desired for each cost function. For the first cost function, the position vector for each site, k, is given in Equation (4.1) in an inertial reference frame. See Figure 4.1 for the satellite observation geometry.

$$r_k^{\ I} = R_E \begin{Bmatrix} \cos\phi_k \cos(\lambda_k + \omega_E t) \\ \cos\phi_k \sin(\lambda_k + \omega_E t) \\ \sin\phi_k \end{Bmatrix} \tag{4.1}$$

In Equation (4.1), several parameters are introduced where ϕ_k is the site latitude, λ_k is the site longitude, and t is time.

The cost function for highest resolution[39] is given in Equation (4.2)

$$J_R = \sum_k \alpha_k (r_k - r)^T (r_k - r) \tag{4.2}$$

where α_k is the priority weight for the kth site, r_k is the kth site's position vector, and r is the satellite's inertial position vector. The cost function for the maximum observation time[39] is provided in Equation (4.3)

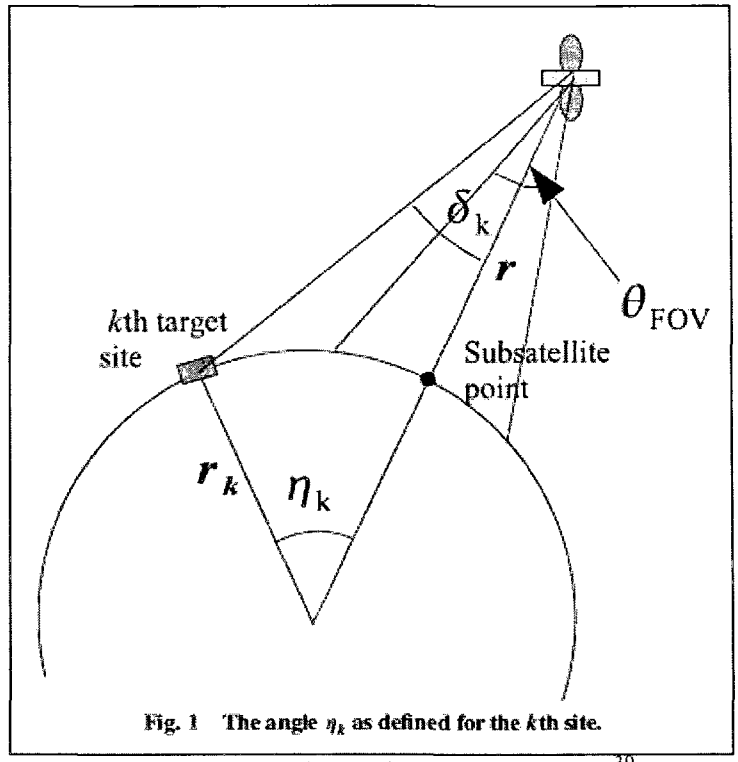

Figure 4.1 Satellite Position and Geometry[39]

$$J_T = \sum_k \alpha_k H(\upsilon_{FOV} - \delta_k)\left[t_f - \int_0^{t_f} \cos(\eta_k)dt\right] \tag{4.3}$$

where H is the Heaviside unit step function where $H(x) = 0$ if $x<0$ else $H(x) = 1$. δ_k is the angle measured at the satellite from nadir to the kth target, η_k is the angle measured at Earth's center from nadir to the kth target, and t_f is the overall reconnaissance time. An advantage of the two cost functions is that sites are weighted to establish priority. However, there are multiple limiting factors:

1. Sites are provided in geocentric coordinates and not transformed to more accurate geodetic coordinates which account for the non-spherical shape of the Earth.

2. By minimizing the distance between the satellite orbit and the sites, the semi-major axis must be first considered and fixed. Otherwise, the cost function would be optimized by an orbit that is close to the Earth's surface!
3. Best resolution is achieved only in the nadir direction. Sites within the slant range are still penalized in the cost functions.[54]
4. The orbit is assumed to be circular.

The first test case examined in Reference 39 included only two sites using the highest resolution cost function. Figure 4.2 shows how an appropriate orbit is easily achieved over only two sites. However, when the number of sites is increased to 20, the orbit does not visit all the sites as seen in Figure 4.3. When using a maximum observation time cost function, the 20 sites are observed by the optimized orbit as seen in Figure 4.4 where again all sites are not visited. The conclusion in the technical paper states that "As the number of sites increases, the solution orbit does not visit each site."[39]

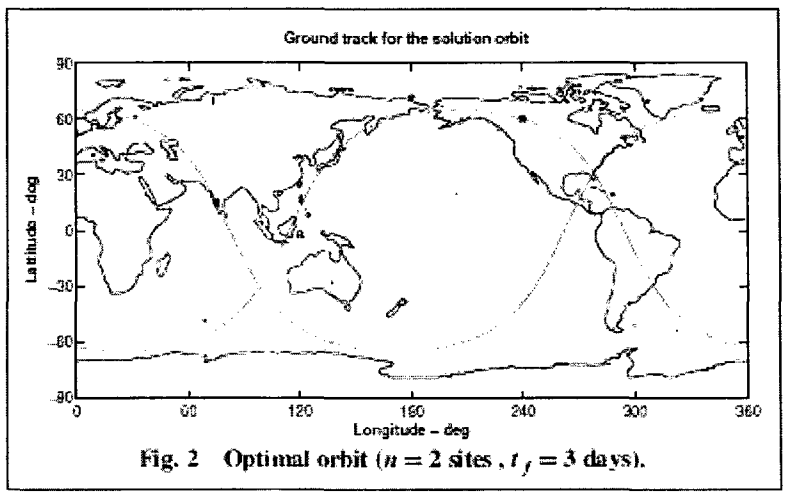

Fig. 2 Optimal orbit ($n = 2$ sites, $t_f = 3$ days).

Figure 4.2 Optimal Orbit for Highest Resolution Cost Function for Two Sites[39]

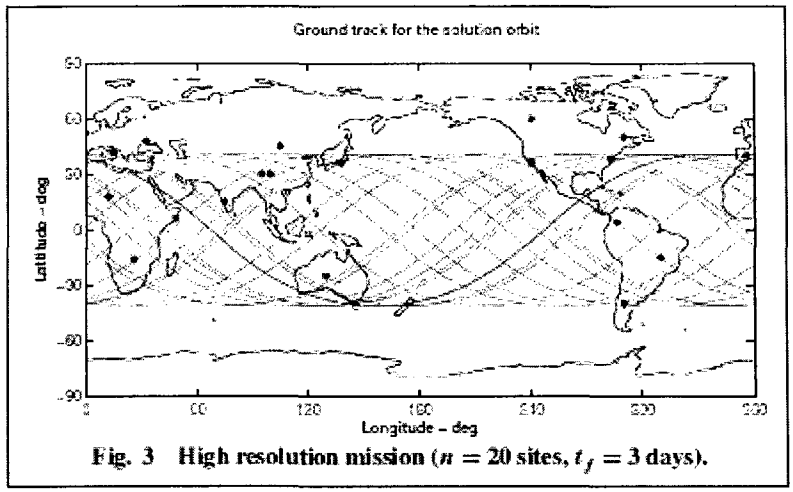

Figure 4.3 Optimal Orbit for Highest Resolution Cost Function for 20 Sites[39]

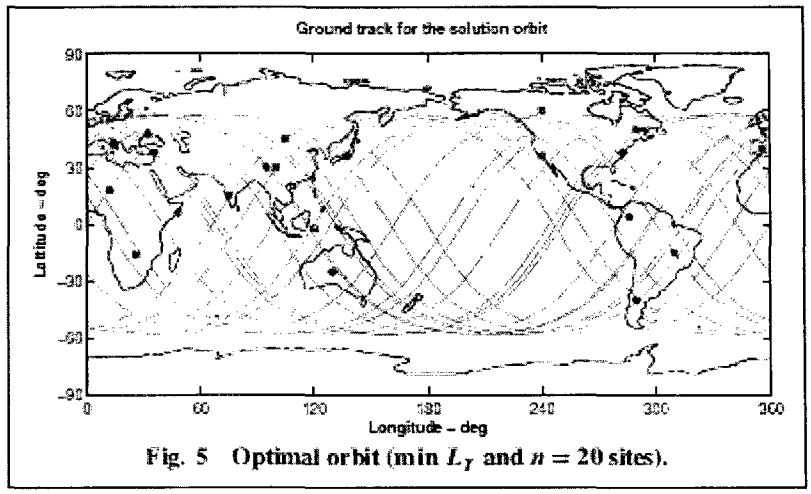

Figure 4.4 Optimal Orbit for Maximum Observation Time Cost Function for 20 Sites[39]

A more robust cost function for the repeating ground track problem is desired. The first cost function presented is based on maximum resolution for each site and the second cost function maximizes the observation time. However, these cost functions inherently include two limitations. For the maximum resolution, the semi-major axis must be first considered and fixed. This first limitation is already partially circumvented in this dissertation design methodology (see Chapter 2) by searching for the best semi-

major axis. The second limitation is the best resolution is considered only in the nadir direction so sites within the slant range that could have the needed observation data collected are still penalized. This limitation is overcome in the present work by the cost function selection itself.

Therefore, this work uses an enhanced cost function based on a Window-Constraint Packing Problem (WCP) which optimizes the opportunities for site observations depending on priority and windows.[30] The WCP method is an example of how satellites are currently tasked. The WCP method focuses on scheduling observations and eliminates the problem of needing to select the semi-major axis like in the maximum resolution cost function. The window method incorporates both minimum and maximum observation times and therefore negates the assumption of always desiring a maximum duration time like in the best observation time cost function. Also, the window method allows for off-nadir considerations by using the entire field of view. The WCP desires a maximum magnitude cost function value. One method of solving the WCP is to use a priority dispatch[30] cost function. The foundation of the cost function lies in the windows of opportunity, the time the observation sites are within view of the satellite, and all lighting conditions are met. Computations are based on propagating an initial state forward in time at discrete time element intervals using a fourth order Runge-Kutta scheme, with a 10 s step size, determining the cost function at each of those points. At each time element, each observation site is evaluated for feasible viewing opportunities. Once the viewing opportunities are determined, valid windows of opportunity are selected. To be a valid window of opportunity, the satellite must be within a given slant

range of the observation site and the length of the window must meet the minimum duration of coverage requirement.

The windows of opportunity are calculated for one period of repetition, T_r, which is related to the nodal period of the satellite, T_Ω, and nodal period of Greenwich,[46] $T_{\Omega G}$, by Equation (4.4).

$$T_r = kT_\Omega = dT_{\Omega G} \tag{4.4}$$

By expressing the nodal periods to depend on the orbital elements, Equation (4.4) is converted to a more useful form. The nodal period T_Ω is given by Equation (4.5) where κ denotes the secular rate of change in the argument of latitude and n_e is the epicycle frequency.[53]

$$T_\Omega = \frac{2\pi}{(1+\kappa)n_e} \tag{4.5}$$

Including J_2, J_4, and J_2^2 perturbations, κ is defined by Equation (4.6).[53]

$$\kappa = \kappa_2 + \kappa_4 + \kappa_{22} \tag{4.6}$$

where

$$\kappa_2 = \frac{3}{4}J_2\left(\frac{R_E}{a}\right)^2\left[4-5\sin(i)^2\right]$$

$$\kappa_4 = -\frac{3}{64}J_4\left(\frac{R_E}{a}\right)^4\left[136-500\sin(i)^2+385\sin(i)^4\right]$$

$$\kappa_{22} = \frac{3}{16}J_2^2\left(\frac{R_E}{a}\right)^4\left[14+17\sin(i)^2-35\sin(i)^4\right]$$

The nodal period of Greenwich is provided as in Equation (4.7)

$$T_{\Omega G} = \frac{2\pi}{\omega_E - \dot{\Omega}} \tag{4.7}$$

where the Earth's rotation is $\omega_E = 7.29211585530 \times 10^{-5}$ rad/s. The nodal regression of the orbital plane is $\dot{\Omega}$ given by Equation (4.8)[42]

$$\dot{\Omega} = \upsilon n \tag{4.8}$$

where υ is the secular change in the ascending node[53] and n is the satellite's mean motion. Again, including J_2, J_4, and J_2^2 perturbations, υ is defined by Equation (4.9).[53]

$$\upsilon = \upsilon_2 + \upsilon_4 + \upsilon_{22} \tag{4.9}$$

where

$$\upsilon_2 = -\frac{3}{2} J_2 \left(\frac{R_E}{a} \right)^2 \cos(i)$$

$$\upsilon_4 = \frac{15}{16} J_4 \left(\frac{R_E}{a} \right)^4 \cos(i) \left[4 - 7\sin(i)^2 \right]$$

$$\upsilon_{22} = \frac{3}{8} J_2^2 \left(\frac{R_E}{a} \right)^4 \cos(i) \left[11 - 20\sin(i)^2 \right]$$

The repetition period may be calculated using either kT_Ω or $dT_{\Omega G}$.

Once calculated, the repetition period is divided into discrete time elements. Each time element for each observation site is assigned a suitability function, s. The suitability function, s, contains three multiplicative parts. The first part is based on the altitude, h, of the satellite at observation. If the satellite is over the maximum altitude of sensor for desired resolution, the suitability function component for height, s_h, is penalized as shown in Equation (4.10)

$$s_h = 1 \text{ if } \chi \le 1$$

$$s_h = 1 - \log(\chi) \text{ if } 1 < \chi \le 2$$

$$s_h = 0 \text{ if } \chi > 2 \tag{4.10}$$

where χ is a percentage of resolution height given by Equation (4.11).

$$\chi = h/h_{pmax} \tag{4.11}$$

This factor allows for some margin above the resolution ceiling altitude for that observation point, but does not force the entire orbit below a certain altitude. The second part of the suitability function, s_r, depends on the sensor range angle, Θ. Observations on the edge of coverage are slightly penalized to encourage coverage near nadir as seen in Equation (4.12)

$$s_r = 1 \text{ if } \Theta < \Theta_{\max}\alpha$$

$$s_r = \beta \text{ if } \Theta > \Theta_{\max}\alpha \tag{4.12}$$

where $\alpha = 0.75$ and $\beta = 0.8$. The constants α and β may be any predetermined constants less than unity and Θ_{max} is the maximum range angle at the given time based on the satellite's altitude and sensor FOV and slew capability. Combining these two parts of the suitability function and multiplying by the observation site priority, p, provides an overall suitability function value for each time element of coverage during the window as given in Equation (4.13).

$$s = s_h s_r p \tag{4.13}$$

To find an overall window of opportunity suitability value, use the sum average of the suitability values for each time element for that window.

To create a schedule, the priority dispatch method ranks the targets first according to priority, a user defined requirement. Then the targets are ranked according to the number of window opportunities for scheduling, also called slack.[30] Finally, the window opportunities are ranked according to the quality of the observation based on the suitability function. The highest fitness window of opportunity is scheduled if the time

slot is available. If not, the algorithm checks the next window and so forth. When the target is scheduled, the scheduled time slot elements are assigned the corresponding suitability values. Once the schedule has been created, it is optimized for additional available times that expand each observation as suggested by Sorensen and Wolfe.[30] The evaluation function, Q, as given in Figure 2.1, is the negative sum of the time slot values based on suitability values, and is to be minimized by the optimization process.

$$Q = -\sum_{i=1}^{n_w} \sum_{j=1}^{n_{ti}} s_{ij} \tag{4.14}$$

In Equation (4.14), n_w is the number of windows scheduled and n_{ti} is the number of time elements within the i^{th} window. The negative is inserted to convert the problem from maximization to minimization in order to be compatible with the selected optimizer software package.

Now that the cost function for the optimization process has been defined, return to the overall goal of finding a constrained optimal orbit for an Earth observation satellite. This problem is very complex and may lead to multiple local minimums. To search through the parameter space to find a global minimum, the genetic algorithm was selected. This choice allows for a broader search and does not highly depend on the initial guess.[39] The genetic algorithm uses the primary six parameters: inclination, longitude of ascending node, argument of perigee, true anomaly, the height of perigee, and number of revolutions of the orbit in the period of repetition. The number of revolutions of the orbit in the period of repetition, k, must be an integer. To incorporate this restriction, the value for k is immediately truncated to an integer right after the genetic algorithm selects the value of k and before the cost function is processed. The genetic algorithm process referring to Figure 2.1 is seen in the iterative loop between the

selection of parameters and cost function evaluation. The evaluation function Q is calculated on the selected parameters. Using a coding for each of the parameters, the genetic algorithm evaluates Q using probabilistic transition rules to refine the parameters until an optimum state is found.[35] The optimality of the genetic algorithm is investigated in Section 4.3. The parameters for the genetic algorithm include a maximum generation limit of 100, function tolerance of 0.000001, population size of 100, crossover fraction of 0.85, infinite stall time limit, stall generation limit of 10, and with an initial population range bound as discussed in Chapter 2.

4.2 Optimization Process

Now that the cost function for the optimization process has been selected, return to the overall goal of finding an optimal orbit for an Earth observation satellite. This problem is very complex and may lead to multiple local minimums. To search through the parameter space to find a global minimum, the genetic algorithm (GA) has been selected. This selection allows for a broader search and does not highly depend on the initial guess.[39] GAs differ from the conventional search methods in four ways:[35]

1. GAs work with a coding of the parameter set, not the parameters themselves.
2. GAs search from a population of points, not a single point.
3. GAs use payoff (objective function) information, not derivatives or other auxiliary knowledge.
4. GAs use probabilistic transition rules, not deterministic rules.

GAs do not use design variables directly, instead the variables are coded into strings (a member). This codification allows the GA to exploit similarities in codes of multiple

members. Multiple members (a population) are used simultaneously to enable the GA to search a broader area with less chance of getting confined in a local minimum or maximum as with the calculus based methods. In each iteration of a population (a generation), an objective function value is assigned to each member. The objective function values are used in randomized operators to define the next generation. To create the next generation, the GA uses three main operators:[35]

1. Reproduction
2. Crossover
3. Mutation

Reproduction involves randomly copying a member of the previous generation based on a percentage of fitness which is determined by the objective function value of previous generation members. For example, a member who has a high objective function value will be given a higher percentage of fitness. All member fitness percentages will total to 100%. In this way, when a new member is randomly selected, it will more likely come from a previous member with a high objective function value. Once the next generation members have been selected, the next step is crossover.

Crossover randomly pairs up members of the generation pool. All or a percentage of the members may be paired. Once members are paired, they are mated by crossing a portion of each member at a randomly chosen point on the member. The newly crossed members are maintained as members of the current generation and replace the pair that was crossed. Crossover essentially enables members to exchange information to search for a better function value performance. Figure 4.5 demonstrates this concept.

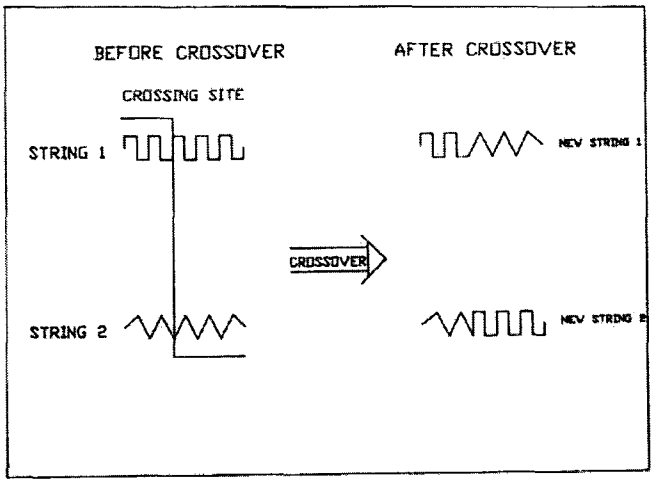

FIGURE 1.8 A schematic of simple crossover shows the alignment of two strings and the partial exchange of information, using a cross site chosen at random.

Figure 4.5 Crossover[35]

Mutation consists of a small percentage of members having a bit in their string changed (from 0 to 1 or vice versa) and ensures that the reproduction and crossover phases have not lost sight of an important aspect of the population. A GA with good results usually includes mutation occurring on the order of one per thousand bit transfers. Therefore mutation is considered a secondary mechanism when compared to reproduction and crossover.

The three phases of GA describe the operations performed on each member, but what does this mean to the overall goal of finding an optimum solution? That answer can be found in schemata. Members with the same characteristics in certain string positions are said to have similarity templates or schema. For example, two members that both begin with the same bit value share a schema. For a four binary bit code, the schema, for example, would be represented as 1*** where the star represents positions that could be

any characteristic. Schema enables the members to be grouped according to string characteristics. As generations progress, the most fit schema will emerge according to the Schema Theorem or Fundamental Theorem of Genetic Algorithms given in Equation (4.15).[35]

$$m(H,t+1) \geq m(H,t)\frac{f(H)}{\bar{f}}\left[1 - p_c \frac{\delta(H)}{l-1} - o(H)p_m\right] \qquad (4.15)$$

In this inequality relation, *m(H, t+1)* is the number of members with a particular schema, *H*, of population *t+1*, *m(H,t)* is the number of members with a particular schema, *H*, of population *t*, *f(H)* is the average fitness of the members with schema *H* of population *t*, $\bar{f}$ is the average fitness of the entire population *t*, p_c is the probability of crossover, and $\delta(H)$ is the defining length of schema *H*. Defining length is determined by the distance between the first and last specific member positions, *l* is the member length, *o(H)* is the order of schema *H* defined by the specific number of positions in the schema, and p_m is the probability of mutation.

The Schema Theorem clearly includes all three operators (reproduction, crossover, and mutation) and demonstrates how schema with high fitness will emerge with successive population generations. This theorem provides the fundamental power of genetic algorithms.

4.3 Genetic Algorithm Optimality

For each run of the algorithm, a different solution may be produced due to the probabilistic nature of the search logic. To characterize this solution randomness, this

section investigates the population size of the genetic algorithm, the runtime of the algorithm, and the cost value obtained for each solution. Additionally, the solutions are examined for any commonalities.

The default population size for the genetic algorithm in Matlab is 20.[55] This default is compared to population sizes of 100, 250, and 500. Four runs for each population are examined using the global case for no lighting conditions with the date midnight 1 January 1994 (see Chapter 6). Figures 4.6-4.8 shows the cost function value, number of generations, and run times in hours for the four runs of each population size.

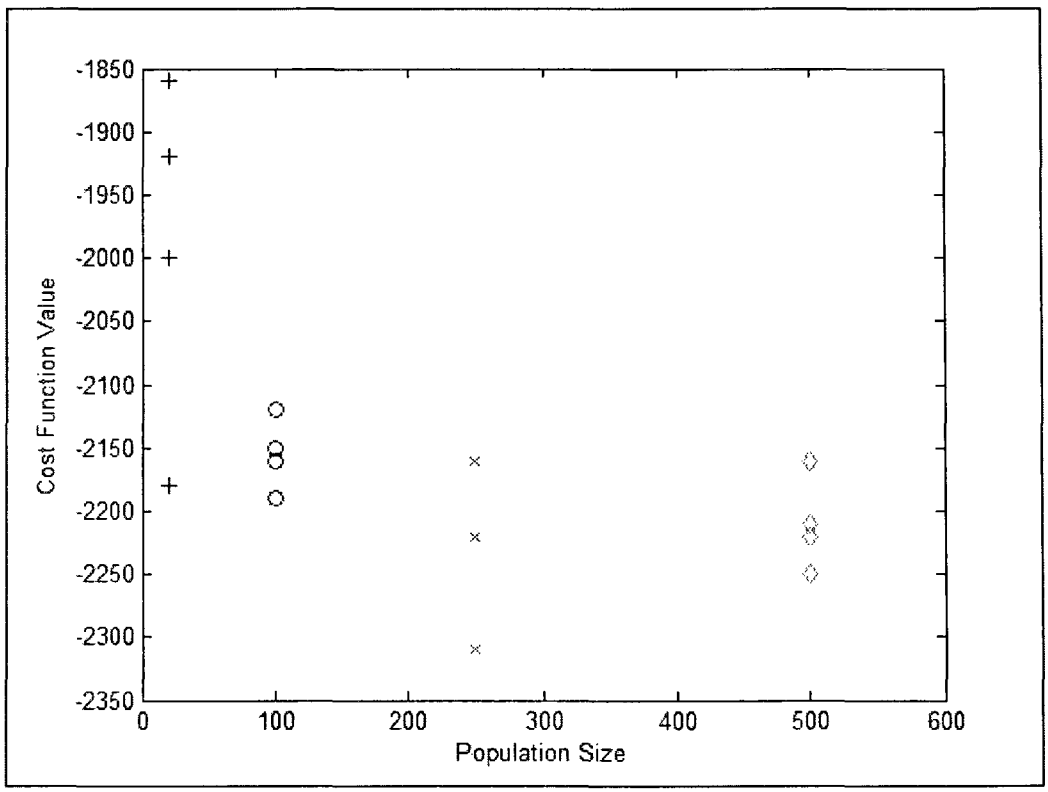

Figure 4.6 Cost Function Value for Population Sizes 20, 100, 250, and 500

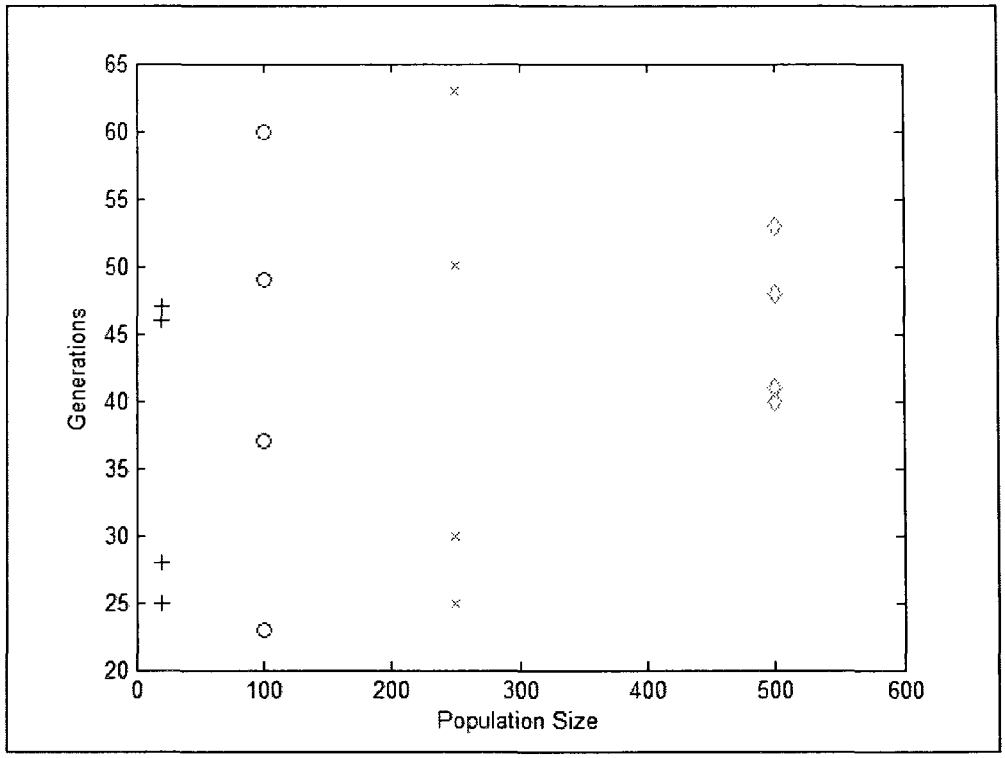

Figure 4.7 Generations for Population Sizes 20, 100, 250, and 500

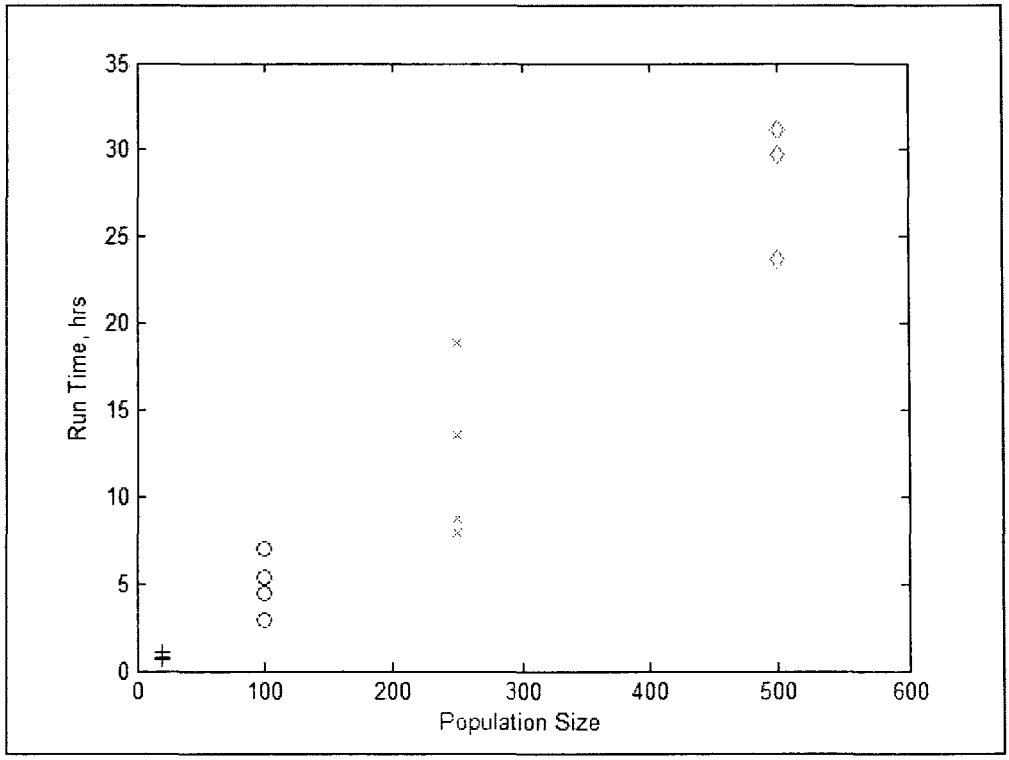

Figure 4.8 Run Times for Population Sizes 20, 100, 250, and 500

Figure 4.6 does not show a clear connection between the increased population size and a more optimal cost function value since the algorithm is designed to find the global minimum value. Ideally, an increase in population size to find a more optimal cost value would result in few needed generations since the search pool is more widespread. However, this is not necessarily the case as shown in Figure 4.7 where the generations range from 20 to 60. As expected, the time needed to run the algorithm increases with increased population size as shown in Figure 4.8. With a population size of 20, only an hour is needed for the genetic algorithm. When the population size increases to 250, the time increased from 8 hours to as much as 19 hours. A balance of time versus cost function value becomes apparent. The degree of "optimality" that is really needed in comparison to the time required to achieve the desired result is an open issue at this point.

Table 4.1 provides the orbital elements for the solutions for various population sizes. Although not shown, all these solutions successfully schedule all targets. Interestingly, the inclination tends toward 66 deg or a band of 80-85 deg. All h_p are within the resolution ceiling limit, 2000 km. Some solutions call for orbital locations above the ceiling limit as seen by a values that are above 8378 km. There is no clear overall repeatable answer which provides one unique optimal solution. Results suggest there are many different orbit designs which satisfy the constraints and have similar cost. The optimization process should continue to be investigated to find a more clear method to achieve at least a tight family of ideal solutions.

Table 4.1 Orbital Elements for Population Sizes 20, 100, 250, and 500

Population	Ω (deg)	ω (deg)	i (deg)	θ (deg)	h_p (km)	k	e	a (km)
20	57.19	61.63	82.08	49.97	1846.75	10	0.0945	9072.61
20	117.42	268.29	70.00	298.18	1788.31	11	0.0406	8502.36
20	76.41	273.17	103.34	320.19	1017.63	11	0.1344	8534.14
20	351.00	241.91	75.38	179.30	795.51	10	0.2097	9066.63
100	59.15	91.00	83.87	159.06	1815.68	10	0.0980	9073.99
100	164.20	208.66	66.58	234.74	1927.21	10	0.0844	9062.53
100	325.59	182.79	67.35	339.46	425.18	12	0.1523	8015.25
100	233.64	114.60	84.34	171.41	1900.18	10	0.0888	9074.39
250	111.05	10.59	85.60	169.57	207.19	12	0.1815	8033.23
250	87.06	126.74	80.30	202.10	1980.23	10	0.0796	9071.33
250	120.89	269.90	65.09	274.73	1946.51	10	0.0822	9061.75
250	227.43	194.33	66.84	109.33	192.09	12	0.1813	8014.24
500	131.08	110.44	79.84	147.15	1851.34	10	0.0938	9070.94
500	289.33	270.88	66.14	191.47	1792.44	11	0.0397	8499.74
500	151.85	270.87	68.67	253.65	1559.23	11	0.0674	8501.30
500	88.75	270.13	79.27	183.23	1951.10	10	0.0828	9070.58

CHAPTER 5

UNMODELED ON-ORBIT PERTURBATIONS

5.1 Introduction to Space Surveillance

The United States Space Surveillance program is an excellent example of how to realistically incorporate perturbations into orbital model predictions. The predictions are distributed to a wide array of sensors to collect observations. Once collected, the observations are sent back to a central processing facility to update the orbital elements. Figure 5.1 shows this information flow. This method of surveillance enables the U.S. military to maintain a catalog of all detectable Earth orbiting objects.

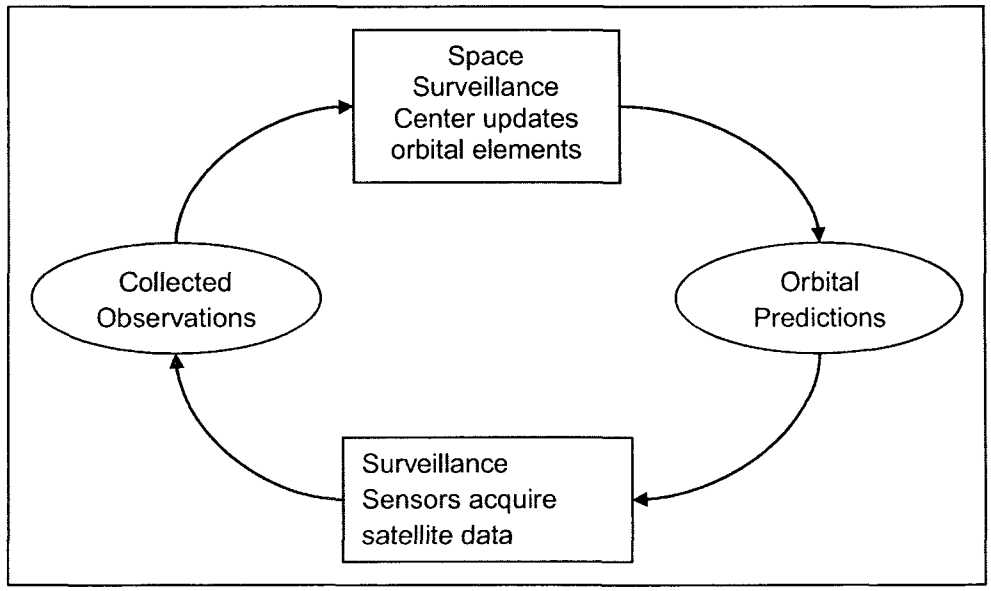

Figure 5.1 Orbital Model Information Flow

The requirement for a space surveillance program was identified shortly after the first artificial satellite was launched in 1957. The Air Force needed to prevent false missile warning threats while the Navy wanted to warn forces about overhead

reconnaissance satellites.[27] Today two main models developed over the years are still in use, the Position and Partials as functions of Time (PPT3) and the Simplified General Perturbations (SPG4). In 1959 each model started with a simple non-spherical Earth zonal harmonic solution by Brouwer. An atmospheric drag modification was added to the models in the early 1960s. In the 1970s the SPG4 added third body lunar and solar gravitational effects. The same terms were added to an original PPT to become the PPT3 in 1997. The main characteristics of each model are provided below:[27]

PPT3

1. Brouwer's solution includes J_2, J_3, J_4, and J_5 zonal harmonics.
2. Lyddane's modifications avoid small divisors of eccentricity and the sine of inclination.
3. Critical inclinations are handled with a special 12 term series expansion.
4. Smith's semi-empirical atmospheric drag model represents the mean motion effect as a quadratic time function.
5. Hujsak adapted Bowman's lunar and solar gravitational effects and Earth tesseral harmonics resonance effects and provided an extension to geosynchronous satellites.

SGP4

1. Brouwer's solution with long and short periodic terms that do not include eccentricity as a factor are included.
2. Lane and Crawford developed an atmospheric drag model with only the secular terms.

3. Hujsak adapted Bowman's lunar and solar gravitational effects and Earth tesseral harmonics resonance effects and provided an extension to geosynchronous satellites.

The Navy and Air Force space surveillance centers' models still use foundations from the orbital models developed in the 1950s and 1960s. These orbital models used by the U.S. military have evolved from a simplified, analytical non-spherical Earth zonal harmonic solution to include special perturbations of aerodynamic drag and third-body effects. This development was made possible by the improvement of computational techniques and facilities.[27] One computational method of adding perturbations is Cowell's Formulation.

5.2 Cowell's Formulation

This numerical technique enables any disturbing acceleration to be included in the formulation of a problem. For example the two body like equation is shown in Equation (5.1)[16] where $\vec{r}$ is the position vector and $\vec{a}_{perturbed}$ is the perturbing acceleration vector.

$$\ddot{\vec{r}} = -\frac{\mu}{r^3}\vec{r} + \vec{a}_{perturbed} \tag{5.1}$$

The acceleration is divided into the traditional two body acceleration plus perturbing accelerations. Each perturbing acceleration can now be linearly added as appropriate and even turned on or off accordingly in the problem. Cowell's formulation of the problem is then numerically integrated to propagate the orbit. Perturbations of consideration for an Earth observation problem include non-spherical Earth, aerodynamic drag, solar radiation, and third body effects. The perturbed acceleration can be expressed in Equation (5.2).

$$\vec{a}_{perturbed} = \vec{a}_{ns} + \vec{a}_{drag} + \vec{a}_{sr} + \vec{a}_{3body} \tag{5.2}$$

Outlined below are four perturbations of main concern for the Earth surveillance application. These disturbances include the non-spherical Earth, aerodynamic drag, solar radiation, and third body effects. These perturbations (except the low order zonal effects) are not modeled in the optimization design problem for finding an orbital solution covering the target set. However, the following perturbations are modeled in the lifecyle portion of this research showing the effective life cycle of the determined orbit. Other perturbations exist, but are not discussed.

5.3 Disturbing Functions

5.3.1 Non-Spherical Earth

Since the Earth is not a perfect sphere, its gravitational potential is not uniform. An aspherical potential function U is defined and then used to determine the gravitational acceleration (by taking the gradient) at a particular point.[16] Figure 5.2 shows the geometry of the non-spherical Earth.

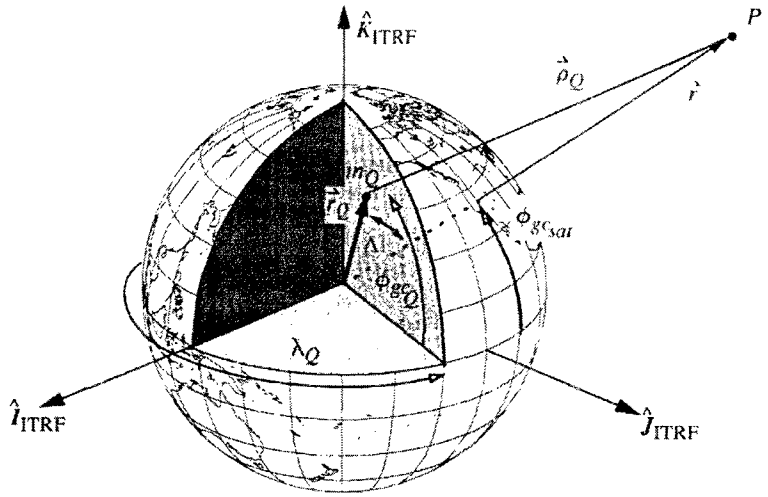

Figure 8-3. Deriving the Gravitational Potential. We consider each point in the Earth, m_Q, when determining the gravitational potential at P. The latitude is a geocentric value. Λ is the angle between the vectors r_Q and r.

Figure 5.2 Non-Spherical Earth Geometry[16]

The potential function is given by Equation (5.3)

$$U = G\sum_{Q=1}^{\infty}\frac{m_Q}{\rho_Q} \tag{5.3}$$

where G is the gravitational constant, m_Q is the Earth mass at point Q, P is the satellite point, and ρ_Q is the distance from Q to P. As the sum of the masses (a large but finite number) approaches an integral, Equation (5.3) becomes Equation (5.4) where m_E denotes Earth mass.

$$U = G\int_{body}\frac{1}{\rho_Q}dm_E \tag{5.4}$$

The geocentric distance from the Earth's center to the point of interest P is Equation (5.5).

$$r = \sqrt{x^2 + y^2 + z^2} \tag{5.5}$$

The distance from center of the Earth to an elemental mass of the Earth, located at Q, is provided in Equation (5.6).

$$r_Q = \sqrt{\varepsilon^2 + \eta^2 + \zeta^2} \tag{5.6}$$

The total range angle Λ between position vectors $\vec{r}$ and $\vec{r}_Q$ is given by Equation (5.7).

$$\cos(\Lambda) = \frac{\vec{r} \bullet \vec{r}_Q}{r r_Q} \tag{5.7}$$

Finally, the distance ρ_Q between the elemental mass and the satellite is shown in Equation (5.8).

$$\rho_Q^2 = r^2 + r_Q^{\ 2} - 2 r r_Q \cos(\Lambda) \tag{5.8}$$

Substituting ρ_Q into the potential equation yields Equation (5.9).

$$U = G \int_{body} \frac{dm_E}{r\sqrt{1 - 2\alpha\cos(\Lambda) + \alpha^2}} \tag{5.9}$$

where

$$\alpha = \frac{r_Q}{r}$$

Since cos (Λ) is less than or equal to 1 and α is less than 1 for a point outside the Earth, use Legendre Polynomials to express part of Equation (5.9) as Equation (5.10).

$$\frac{1}{\sqrt{1 - 2\alpha\cos(\Lambda) + \alpha^2}} = \sum_{l=0}^{\infty} \alpha^l P_l[\cos(\Lambda)] \tag{5.10}$$

The potential Equation (5.9) then becomes Equation (5.11).

$$U = \frac{G}{r} \int_{body} \sum_{l=0}^{\infty} \alpha^l P_l[\cos(\Lambda)] dm_E \tag{5.11}$$

Use the cosine law of spherical trigonometry to find an expression for the range angle Λ in terms of latitude ϕ and longitude λ as in Equation (5.12).

$$\cos(\Lambda) = \sin(\phi_{gc_Q})\sin(\phi_{gc_{sat}}) + \cos(\phi_{gc_Q})\cos(\phi_{gc_{sat}})\cos(\lambda_Q - \lambda_{sat}) \tag{5.12}$$

Following a spherical harmonics approach, expand the Legendre Polynomials using the addition theorem shown in Equation (5.13)

$$\begin{aligned}
&P_l[\cos(\Lambda)] = P_l[\sin(\phi_{gc_Q})]P_l[\sin(\phi_{gc_{sat}})] + \sum_{m=1}^{l}\frac{(l-m)!}{(l+m)!}\{A_{l,m}A'_{l,m} + B_{l,m}B'_{l,m}\} \\
&A_{l,m} = P_{l,m}[\sin(\phi_{gc_Q})]\cos(m\lambda_Q) \\
&A'_{l,m} = P_{l,m}[\sin(\phi_{gc_{sat}})]\cos(m\lambda_{sat}) \\
&B_{l,m} = P_{l,m}[\sin(\phi_{gc_Q})]\sin(m\lambda_Q) \\
&B'_{l,m} = P_{l,m}[\sin(\phi_{gc_{sat}})]\sin(m\lambda_{sat})
\end{aligned} \tag{5.13}$$

where l indicates degree and m indicates order.

Isolate terms that are independent of the satellite's location (for m=1 to l) in Equation (5.14).

$$\begin{aligned}
C'_{l,m} &= \int_{body} r_Q^l \frac{(l-m)!}{(l+m)!} P_{l,m}[sin(\phi_{gc_Q})]cos(m\lambda_Q)dm_E \\
S'_{l,m} &= \int_{body} r_Q^l \frac{(l-m)!}{(l+m)!} P_{l,m}[sin(\phi_{gc_Q})]sin(m\lambda_Q)dm_E
\end{aligned} \tag{5.14}$$

For the special case of zonal harmonics (where m=0), the C' coefficient in Equation (5.14) reduces to Equation (5.1.5)

$$C'_{l,0} = \int_{body} r_Q^l P_{l,0}[sin(\phi_{gc_Q})]dm_E \tag{5.15}$$

so that the potential Equation (5.11) can now be expressed as Equation (5.16).

$$U = \frac{G}{r}\sum_{l=0}^{\infty}\frac{P_l[sin(\phi_{gc_{sat}})]}{r^l}C'_{l,0} + \frac{G}{r}\sum_{l=1}^{\infty}\sum_{m=1}^{l}\frac{P_{l,m}[sin(\phi_{gc_{sat}})]}{r^l}\{C'_{l,m}cos(m\lambda_{sat}) + S'_{l,m}sin(m\lambda_{sat})\} \tag{5.16}$$

Non-dimensionalize the C' and S' coefficients of Equation (5.14) into Equation (5.17)

$$C'_{l,m} = C_{l,m} R_E{}^l m_E$$
$$S'_{l,m} = S_{l,m} R_E{}^l m_E \tag{5.17}$$

where R_E is the mean equatorial radius of the Earth. The potential Equation (5.16) then becomes Equation (5.18) where $\mu = Gm_E$.

$$U = \frac{\mu}{r}\sum_{l=0}^{\infty} P_l\left[sin\left(\phi_{gc_{sat}}\right)\right]\left(\frac{R_E}{r}\right)^l C_{l,0} + \frac{\mu}{r}\sum_{l=1}^{\infty}\sum_{m=1}^{l} P_{l,m}\left[sin\left(\phi_{gc_{sat}}\right)\right]\left(\frac{R_E}{r}\right)^l \left\{C_{l,m}\, cos\left(m\lambda_{sat}\right) + S_{l,m}\, sin\left(m\lambda_{sat}\right)\right\} \tag{5.18}$$

However, $C_{l,0}$, $C_{l,1}$, and $S_{l,1}$ are all zero for $l \geq 1$. Separating the 0^{th} term (ideal spherical potential) from the rest allows the potential Equation (5.18) to be written as Equation (5.19).

$$U = \frac{\mu}{r}\left[1 + \sum_{l=2}^{\infty}\sum_{m=1}^{l} P_{l,m}\left[sin\left(\phi_{gc_{sat}}\right)\right]\left(\frac{R_E}{r}\right)^l \left\{C_{l,m}\, cos\left(m\lambda_{sat}\right) + S_{l,m}\, sin\left(m\lambda_{sat}\right)\right\}\right] \tag{5.19}$$

The terms in Equation (5.19) comprise the types of spherical harmonics, which are discussed next.

Spherical Harmonics (Zonal):

Zonal Harmonics, 0-order (m=0), represent bands of latitude and is commonly notated as "J" where $J_l = -C_{l,0}$. The normalized, second-degree, zonal gravitational coefficient $C_{2,0}$ represents the Earth's equatorial bulge and is the strongest perturbation.[16] Thus, $J_2 = -C_{2,0} = 0.0010826269$. Figure 5.3 shows the zonal harmonics.

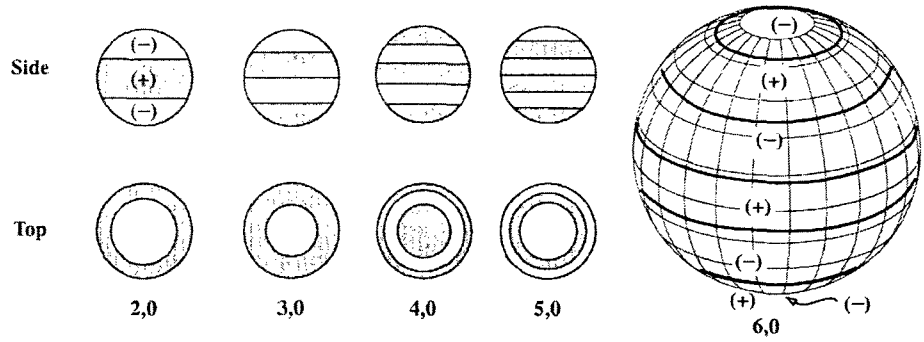

Figure 8-4. **Zonal Harmonics.** J_2 accounts for most of the Earth's gravitational departure from a perfect sphere. This band (and others) reflects the Earth's oblateness. The shading indicates regions of additional mass. The third harmonic appears similar to the J_2 from the top but is reversed for the bottom view.

Figure 5.3 Zonal Harmonics[16]

Spherical Harmonics (Sectorial):

Sectorial harmonics occur when $l=m$ and represent bands of longitude which look like "orange-slice" sectors.[16] Figure 5.4 shows the sectorial harmonics.

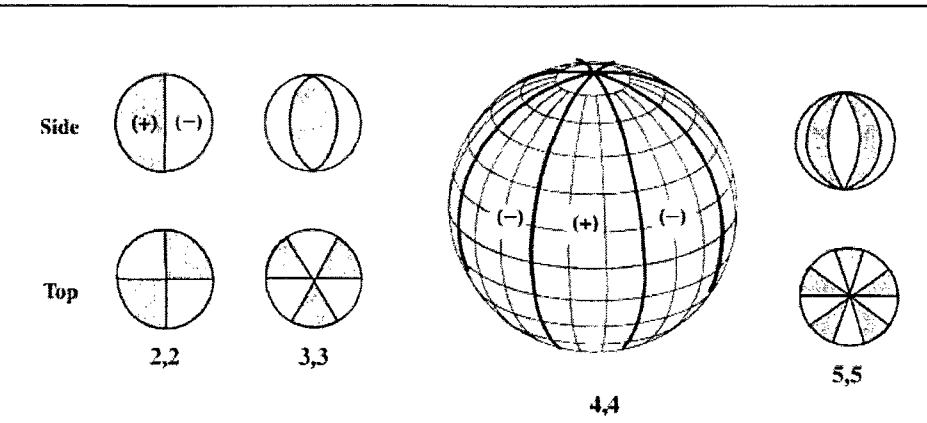

Figure 8-5. **Sectorial Harmonics.** Sectorial harmonics take into account the extra mass distribution in longitudinal regions.

Figure 5.4 Sectorial Harmonics[16]

Spherical Harmonics (Tesseral):

Tesseral harmonics look like tiles carved out with a number of circles (*l-m*) of latitude and 2*m* meridians of longitude.[16] Figure 5.5 shows tesseral harmonics.

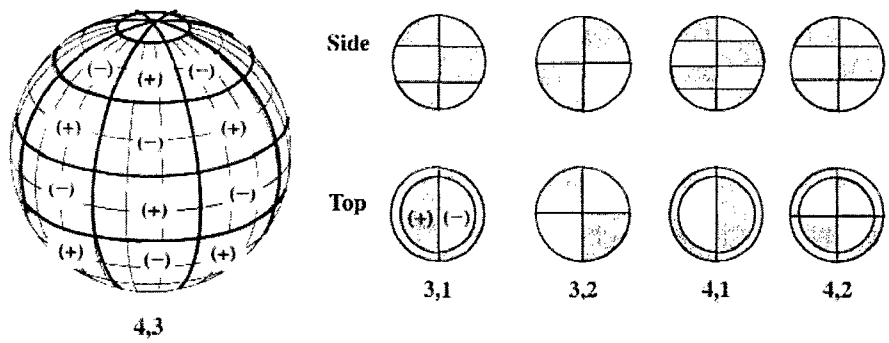

Figure 8-6. Tesseral Harmonics. Tesseral harmonics attempt to model specific regions on the Earth which depart from a perfect sphere.

Figure 5.5 Tesseral Harmonics[16]

Non-Spherical Acceleration:

The gravitational potential is used to find the gravitational acceleration by taking the gradient of the potential. Since the potential is expressed in spherical coordinates, use the chain rule to find the non-spherical acceleration in Cartesian coordinates as shown in Equation (5.20).[16]

$$\vec{a}_{ns} = \frac{\partial U}{\partial r}\left(\frac{\partial r}{\partial \vec{r}}\right)^T + \frac{\partial U}{\partial \phi_{gc_{sat}}}\left(\frac{\partial \phi_{gc_{sat}}}{\partial \vec{r}}\right)^T + \frac{\partial U}{\partial \lambda_{sat}}\left(\frac{\partial \lambda_{sat}}{\partial \vec{r}}\right)^T \tag{5.20}$$

The Cartesian components (I J K) of the non-spherical perturbative acceleration vector, $\vec{a}_{ns}$, are thus found to be in terms of the potential function U and the satellite position vector $\vec{r}$ and its components r_I, r_J, and r_K.

$$
\begin{aligned}
a_{nsI} &= \left\{ \frac{1}{r}\frac{\partial U}{\partial r} - \frac{r_K}{r^2\sqrt{r_I^2 + r_J^2}}\frac{\partial U}{\partial \phi_{gc_{sat}}} \right\} r_I - \left\{ \frac{1}{r_I^2 + r_J^2}\frac{\partial U}{\partial \lambda_{sat}} \right\} r_J \\
a_{nsJ} &= \left\{ \frac{1}{r}\frac{\partial U}{\partial r} - \frac{r_K}{r^2\sqrt{r_I^2 + r_J^2}}\frac{\partial U}{\partial \phi_{gc_{sat}}} \right\} r_J + \left\{ \frac{1}{r_I^2 + r_J^2}\frac{\partial U}{\partial \lambda_{sat}} \right\} r_I \\
a_{nsK} &= \frac{1}{r}\frac{\partial U}{\partial r} r_K + \frac{\sqrt{r_I^2 + r_J^2}}{r^2}\frac{\partial U}{\partial \phi_{gc_{sat}}}
\end{aligned}
\tag{5.21}
$$

The effects of non-spherical acceleration on an orbit include:[16]

1. Secular perturbations induced by even zonal harmonics on Ω, ω, and M.
2. No secular effects are seen in a, e, and i.
3. Periodic perturbations induced by all harmonics on all elements.

Another important aspect of the non-spherical Earth is the coordinate system used to describe points on the surface of the Earth. Coordinates used to describe locations based on a perfect sphere model are called geocentric coordinates. Geodetic coordinates are based on the geoid, or reference ellipsoid, model. The difference between geocentric and geodetic coordinates can be up to 20 km[16] and is shown in Figure 5.6.

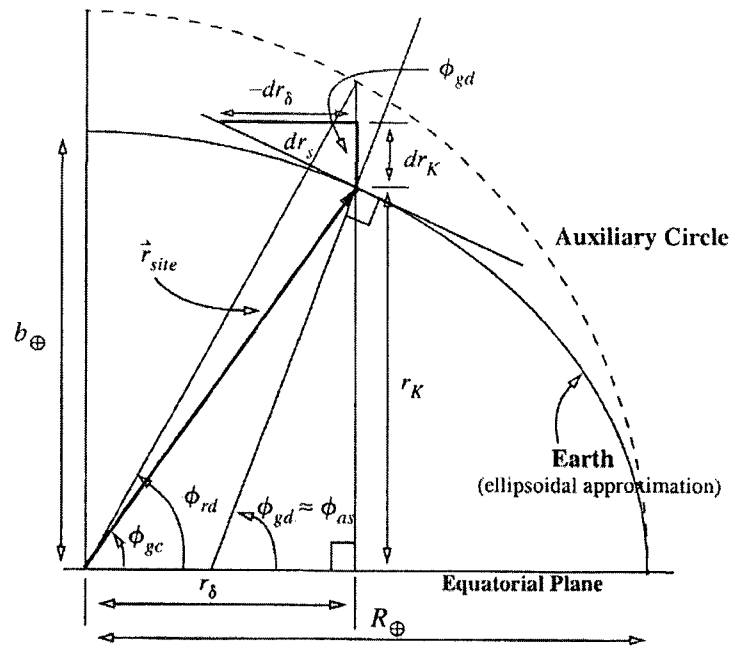

Figure 3-3. Latitude Geometry (exaggerated scale). The geodetic latitude, ϕ_{gd}, makes an angle perpendicular to the surface and the equatorial plane, whereas the geocentric latitude, ϕ_{gc}, is referenced to the center of the Earth. Astronomic latitude, ϕ_{as}, is very close to ϕ_{gd}. The center of the ellipsoid differs slightly for ϕ_{gd} and ϕ_{as}. Reduced latitude, ϕ_{rd}, is used only to derive relations.

Figure 5.6 Geocentric vs. Geodetic Coordinates[56]

Fortunately, a simple transformation between geocentric and geodetic coordinates for latitude is available.[16] The difference between longitude coordinates is very small. For very accurate coordinates, the National Geospatial-Intelligence Agency provides a model called the World Geodetic System 1984 (WGS84). This model, updated in 1996, is of degree n = 360 and order m = 360 with 130,317 coefficients and provides accuracy on the order of 1.0 m or better.[25] This research uses geodetic latitude and geocentric longitude coordinates.

In addition to the surface coordinates, calculating the altitude height of the satellite perpendicular to the Earth's surface also needs to take into consideration the

perturbed shape of the Earth. Figure 5.7 shows the geometry involved in finding the height of the satellite based on the ellipsoid.

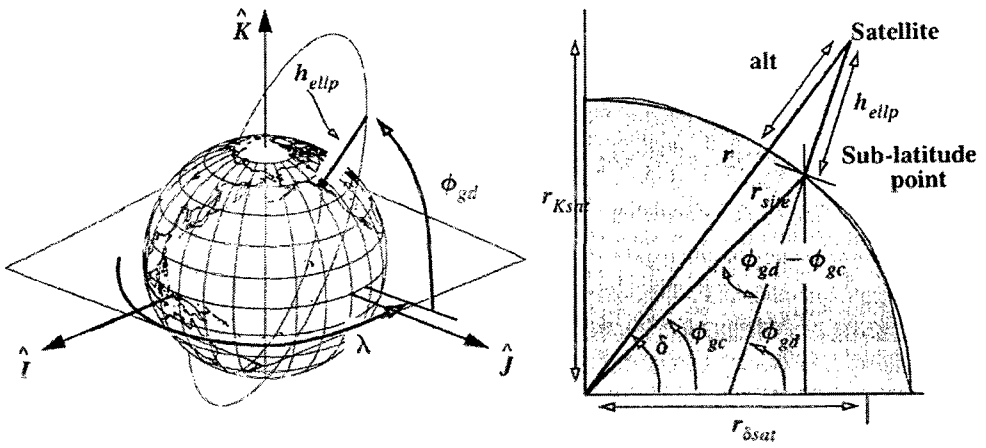

Figure 3-21. Determining a Satellite's Sub-latitude Point. Notice h_{ellp} is used for the altitude, and not H_{MSL}. The difference between the geodetic and geocentric angles is helpful in setting up the iteration for the problem.

Figure 5.7 Satellite Altitude[56]

5.3.2 Aerodynamic Drag

This non-conservative perturbation is the second strongest influence for near Earth satellites. The atmospheric density is difficult to model because of the large molecular mean free path and changes due to the atmosphere's molecular structure, incident solar flux, and geomagnetic interactions. Accurately modeling the atmosphere includes characteristics such as: molecular chemistry, thermodynamics, aerodynamics, hypersonics, meteorology, electromagnetics, planetary sciences, and orbital mechanics. Models may include static or time-varying variations.[16]

Static Variations:

1. Latitudinal: The Earth's bulge effects actual altitude and hence atmospheric density.
2. Longitudinal: These effects are caused by atmospheric changes due to land formations such as mountains and oceans.

Time-Varying Variations:

1. Diurnal: These changes take place every day as the Earth rotates and the atmosphere is heated and cooled by the Sun. The maximum atmospheric bulge (warmest) is around 2PM where as the minimum value is about 4AM.
2. 27-day Solar Rotation Cycle: These irregular effects come from the Sun's rotational period where active solar regions grow and decay.
3. 11-year Sun Spots Cycle: The intensity of the Sun's magnetic field slowly oscillates in localized regions. This effect is actually a 22-year cycle.
4. Semi-Annual/Seasonal: These variations last approximately six months due to the varying distance of the Earth from the Sun and the Sun's declination.
5. Cyclical: The exact cause of this effect is not fully understood but is most likely related to Sun spots and parallels but lags the 11-year Sun spot cycle.
6. Rotating Atmosphere: The atmosphere rotates with the Earth. The velocity is larger closer to the surface due to friction.
7. Miscellaneous: Additionally, winds, magnetic storms, and even the tides can cause the atmospheric density to fluctuate.

Various models have been developed for the atmosphere from the very basic to more complex. Most models are valid for a specific range of altitude or for certain assumptions.

The basic equation for atmospheric drag is provided in Equation (5.22)[16]

$$\vec{a}_{drag} = -\frac{C_D A}{m}\frac{\rho v_{rel}^{\ 2}}{2}\frac{\vec{v}_{rel}}{|\vec{v}_{rel}|} \tag{5.22}$$

where C_D is the drag coefficient which is approximately 2.2 for a flat plate or 2 for a sphere, ρ is the density, A is the cross sectional area, m is the satellite mass, and $\vec{v}_{rel}$ is the velocity vector relative to the atmosphere.

A summary of the effects of drag on an orbit includes[16]

1. Large secular changes in a and e and small change in i.
2. Large periodic changes in i, Ω, and ω and small changes in a and e.
3. Perigee remains approximately constant but can be coupled with third-body or central body effects.

5.3.3 Solar Radiation

This effect is a non-conservative perturbation which shares the same time-varying variations caused by the Sun as aerodynamic drag. The effects are more pronounced at higher altitudes. Solar radiation is also difficult to model because of varying satellite cross-sectional area, solar cycles and variations, and accurate representation of the coefficients to model the satellite's reflectivity.[16]

A basic solar radiation model is developed starting with the solar-radiation constant, or solar flux, SF = 1353 W/m^2. The average solar pressure is the solar flux divided by the speed of light given in Equation (5.23).

$$p_{sr} = \frac{SF}{c} = \frac{1353 W/m^2}{3\times 10^8 \, m/s} = 4.51\times 10^{-6} \; N/m^2 \tag{5.23}$$

The acceleration due to solar radiation is given by Equation (5.24)[16]

$$\bar{a}_{sr} = \frac{p_{SR} c_R A_{sun}}{m} \frac{\bar{r}_{sun-sat}}{|\bar{r}_{sun-sat}|} \tag{5.24}$$

where c_R is the reflectivity which is 0 for translucent material, 1 when all radiation is absorbed, and 2 when all radiation is reflected; A_{sun} is the area exposed to the Sun, and $\bar{r}_{sun-sat}$ is the vector from the Sun to satellite.

The effect of the solar radiation pressure on an orbit includes[16]

1. Periodic changes in all orbital elements; approximately equal to drag at 800 km.
2. Changes in perigee height can seriously effect satellite's lifetime.
3. Period for variations can be as long as a year.
4. Effects are usually small except for low mass/large surface area satellites.
5. Need to account for time in Earth's shadow.

5.3.4 Third Body Effects

These conservative perturbations effect satellites in higher altitude orbits and are more noticeable where the effects of aerodynamic drag start to diminish.[16] Third body effects are usually caused by the Sun and Moon for Earth satellites. The acceleration of a

satellite with the influence of a third body, denoted by subscript 3, is given as in Equation (5.25).[16]

$$\ddot{\vec{r}} = -\frac{\mu_E \vec{r}}{r^3} + \mu_3 \left(\frac{\vec{r}_{sat3}}{r_{sat3}^3} - \frac{\vec{r}_{E3}}{r_{E3}^3} \right) \tag{5.25}$$

Subscript sat3 denotes direction from satellite to third body while subscript E3 denotes direction from Earth to third body. This equation includes the two body gravitational term as the first term. Removing this term and summing over k bodies concludes the acceleration due to the disturbing bodies, $\vec{a}_{3body}$, is seen in Equation (5.26).

$$\vec{a}_{3body} = \sum_{i=1}^{k} \mu_i \left(\frac{\vec{r}_{sati}}{r_{sati}^3} - \frac{\vec{r}_{Ei}}{r_{Ei}^3} \right) \tag{5.26}$$

This research focuses on the affects from the Sun and Moon as the additional bodies of influence. The Moon, because of its closer proximity has a larger influence than that of the Sun by a ratio of about 2.2.[16] The Moon's influence has even been used to help change the orbits of satellites.[57]

The third body effects on an orbit can be summarized:[16]

1. No secular, long-periodic, or monthly variations in a.
2. Secular perturbations in Ω and ω.
3. Long-periodic variations in e, i, Ω and ω are associated with the satellite's perigee and disturbing body motion.
4. For near Earth orbits oblateness dominates orbital plane regression about polar axis.
5. For higher orbits the orbital plane regression is about a pole between the polar axis and ecliptic pole.

5.4 Employing Perturbations

These four perturbations, non-spherical Earth, aerodynamic drag, solar radiation pressure, and third body effects, are modeled in the lifecycle analysis portion of the design method. This research includes the simple models presented in Section 5.3 for each perturbation. More sophisticated perturbation models may be available and could be incorporated at a later time. The lifecycle analysis simulation employs Cowell's method to linearly add each perturbation component to the general two-body equation of motion.

CHAPTER 6

CASE STUDY RESULTS

6.1 Global Case Study

The global case study includes twenty observation sites worldwide given in Table 6.1. Observation site location is from the National Geospatial-Intelligence Agency GEOnet Names Server.[58] The global case was evaluated first using a baseline condition, then variations of the baseline are investigated. Table 6.2 shows the case study baseline and variations. The start date chosen is midnight 1 April 1994.

Table 6.1 Global Observation Sites

Country	Capital	Lat (deg)	Long (deg)	Priority	Target
Argentina	Buenos Aires	-34.5875	-58.6725	1	16
Australia	Canberra	-35.283333	149.216667	4	2
Brazil	Brasilia	-15.783333	-47.916667	2	10
Canada	Ottawa	45.416667	-75.7	5	7
China	Beijing	39.928889	116.388333	1	8
Costa Rica	San Jose	9.93333	-84.0833	2	11
Cote d Ivoire	Yamoussoukro	6.816667	-5.283333	3	9
Egypt	Cairo	30.05	31.25	2	12
Germany	Berlin	52.516667	13.4	2	1
Iceland	Reykjavík	64.15	-21.95	1	18
India	New Delhi	28.6	77.2	3	13
Indonesia	Jakarta	-6.174444	106.829444	3	14
Japan	Tokyo	35.685	139.751389	2	5
Mexico	Ciudad de Mexico	19.434167	-99.138611	3	3
Morocco	Rabat	34.02	-6.83	4	17
New Zealand	Wellington	-41.3	174.783333	2	20
Qatar	Doha	25.286667	51.533333	3	4
South Africa	Pretoria	-25.706944	28.229444	2	15
The Bahamas	Nassau	25.083333	-77.35	3	19
United Kingdom	London	51.5	-0.116667	1	6

Table 6.2 Case Study Baseline and Variations

Conditions / User Requirements	Baseline	Min Duration	Revisit Rate	Lighting	Max Sun Angle	FOV	Slew	Resolution
Min Duration (s)	60	360	60	60	60	60	60	60
Revisit Rate (day)	1	1	2	1	1	1	1	1
Lighting	Off	Off	Off	On	On	Off	Off	Off
Max Sun Angle (deg)	N/A	N/A	N/A	45	60	N/A	N/A	N/A
FOV (deg)	30	30	30	30	30	10	30	30
Slew (deg)	15	15	15	15	15	15	5	15
Resolution (km)	2000	2000	2000	2000	2000	2000	2000	1000

6.1.1 Global Baseline

For the global case study baseline condition, an orbit was found that met all the user requirement conditions. However, note this orbit in not a unique solution as there are ample design freedoms to meet all user requirements as discussed in Section 4.3. The resulting primary and auxiliary parameters for the baseline condition are

$\Omega = 59.48$ deg $\quad \omega = 272.40$ deg $\quad i = 68.66$ deg $\quad a = 8501.45$ km

$\theta = 197.06$ deg $\quad h_p = 1837.53$ km $\quad k = 11 \quad e = 0.0347$

The evaluation function has a value of Q = -2199.62. Table 6.3 shows the schedule for each target assuming time is zero at the start of the parameters given. All schedules are listed by targets according to priority and slack. Start and stop times are given in seconds from start of propagation. Figure 6.1 shows the ground trace for a satellite flying the designed orbit with repeat ground track.

Table 6.3 Global Baseline Schedule

Target	Start Time (s)	Stop Time (s)	Priority
7	37380	37990	5
2	25620	26060	4
17	55160	55750	4
3	78970	79530	3
4	5720	6240	3
9	55830	56280	3
13	83840	84410	3
14	32740	33230	3
19	70980	71490	3
10	72160	72450	2
11	36630	37090	2
12	47490	48040	2
15	4510	4970	2
5	68380	68890	2
20	17920	18290	2
1	46850	47470	2
16	72460	72810	1
8	76300	76900	1
6	21960	22570	1
18	30080	30700	1

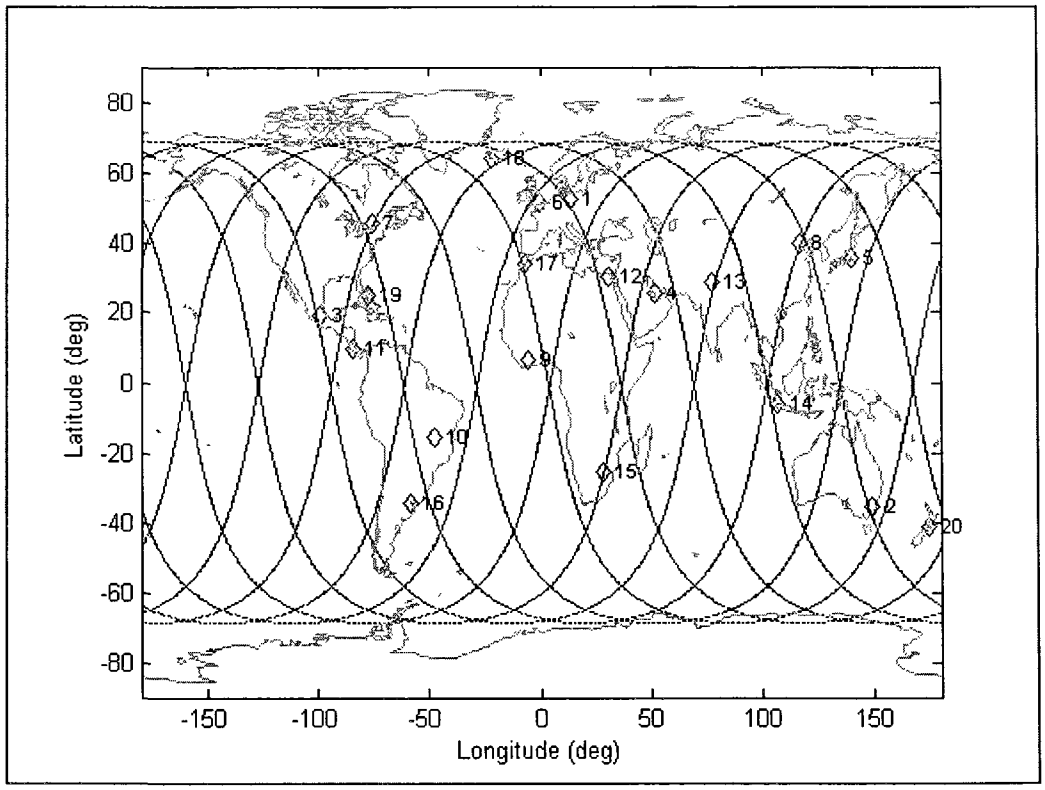

Figure 6.1 Global Baseline Ground Trace

This orbit has interesting characteristics. The inclination constraint of a minimum 64 deg dictated by Target 18 was met. The height of perigee at 1837.53 km stays under the resolution ceiling of 2000 km. However, all orbital positions do not remain under the 2000 km limit, an example of an orbit that would not be considered by traditional methods of focusing on orbits that remain fully under the ceiling. The spacecraft makes 11 revolutions in each repetition period. Each target is viewed at some point with either near direct overflight or sensor slew capability and is scheduled for much more than the 60 seconds required by the minimum duration of coverage. Note the highest priority targets are observed by near direct overflight. Also, the minimum schedule is 290 s but most observations are 450 s or larger.

6.1.2 Minimum Duration Variation

The minimum duration was extended to 360 s from the baseline 60 s. The resulting primary and auxiliary parameters for the minimum duration condition are

$\Omega = 19.92$ deg $\omega = 174.24$ deg $i = 86.71$ deg $a = 8034.66$ km

$\theta = 188.92$ deg $h_p = 373.01$ km $k = 12$ $e = 0.1610$

The evaluation function has a value of $Q = -2208.73$. Table 6.4 shows the target schedule while Figure 6.2 shows the ground track.

Table 6.4 Minimum Duration Variation Schedule

Target	Start Time (s)	Stop Time (s)	Priority
7	22240	22840	5
2	55980	56720	4
17	7580	8270	4
3	28660	29470	3
4	79010	79770	3
9	6820	7570	3
13	71940	72670	3
14	63840	64690	3
19	21690	22230	3
1	940	1470	2
5	57800	58490	2
10	13470	14220	2
12	410	930	2
15	84870	85660	2
20	48660	49410	2
11	67750	68110	2
8	65120	65720	1
16	20180	20860	1
6	45640	46000	1
18	52570	52930	1

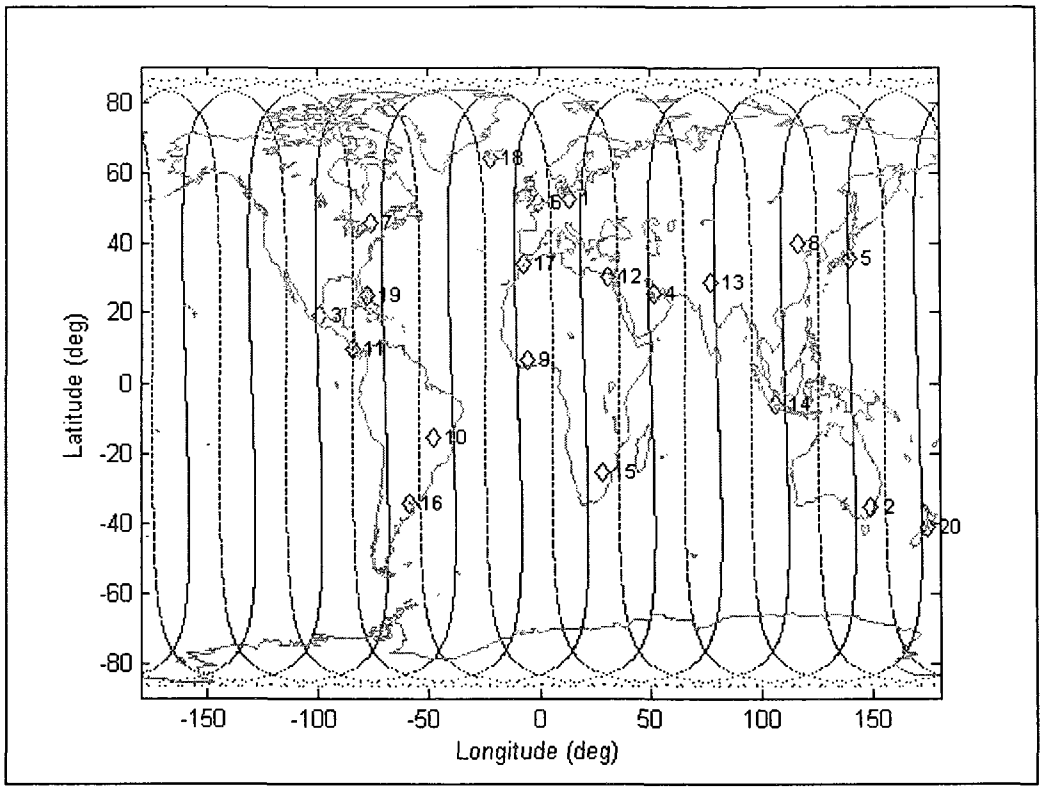

Figure 6.2 Minimum Duration Variation Ground Trace

Interestingly, here is another orbit that easily meets the minimum inclination of 64 deg with an inclination in the mid 80s. The orbit is quite elliptical for such a low Earth orbit, k being 12 or approximately a two hour orbital period, with a height of perigee only at 373 km. Although in a different order than the targets scheduled in the baseline condition, all targets were able to be scheduled for the extended minimum duration of 360 s while most targets are scheduled for 500 to 700 s. The cost function value is very close to the baseline value and is slightly larger (magnitude). Changing the minimum duration for a global case is fairly easy to accommodate for only 20 targets. A higher number of targets may produce a much different solution where the cost function value would be expected to be lower than the baseline. Note the longer duration requirement

does not allow near direct over flights of the highest priority targets, when ground tracks in Figures 6.1 and 6.2 are compared.

6.1.3 Revisit Rate Variation

The revisit rate was extended to 2 days from the baseline 1 day. However, when the algorithm was employed, the computer did not have enough memory to process the request. In order to run the algorithm on the available computer, the discreet time interval was doubled to 20 s for propagation purposes. The resulting primary and auxiliary parameters for the revisit rate condition are

$\Omega = 74.18$ deg $\quad \omega = 268.55$ deg $\quad i = 68.94$ deg $\quad a = 8771.75$ km

$\theta = 142.85$ deg $\quad h_p = 1979.52$ km $\quad k = 21 \quad e = 0.0482$

The evaluation function has a value of $Q = -1189.23$. Table 6.5 shows the target schedule while Figure 6.3 shows the ground track.

Table 6.5 Revisit Rate Variation Schedule

Target	Start Time (s)	Stop Time (s)	Priority
7	40500	41260	5
2	28240	28740	4
17	59200	59900	4
9	105040	105680	3
14	35700	36280	3
3	84240	84800	3
4	133180	133800	3
19	75780	76460	3
13	124820	125520	3
10	158740	159280	2
15	142620	143140	2
11	166300	166920	2
12	51160	51820	2
20	110280	110760	2
5	108220	108940	2
1	50460	51140	2
16	167680	167860	1
8	26220	26920	1
6	140580	141340	1
18	32840	33620	1

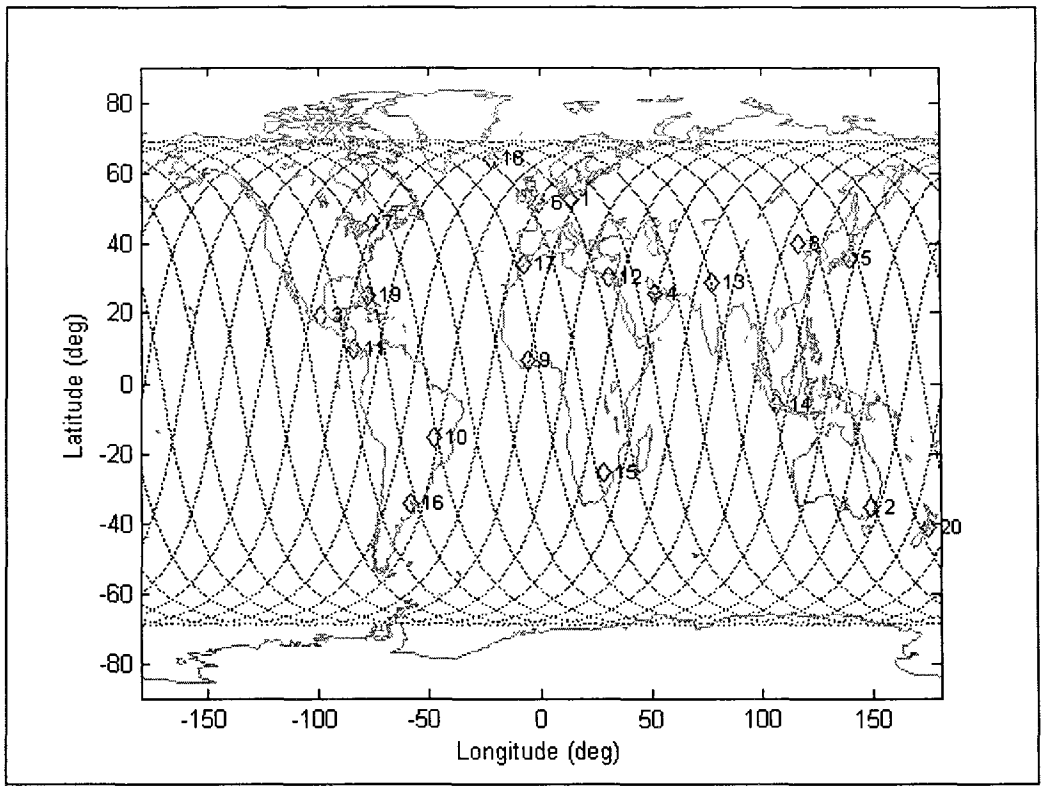

Figure 6.3 Revisit Rate Variation Ground Trace

Even though the amount of available viewing time was doubled in the revisit rate variation compared to the baseline condition, the overall quality of the solution was about the same. While the cost function value was -1189, this included half the number of points along the timeline; therefore half the opportunity to calculate the cost value since it is a sum of the quality at each point. So, doubling the revisit rate value to -2378, shows only a slight increase (magnitude) in the value of the solution as compared to the baseline. The inclination of 68 deg meets the required 64 deg. The height of perigee stays under the 2000 km ceiling resolution altitude. All targets are scheduled; all much more than the minimum duration of 60 s. Near direct overflight behavior of high priority targets has also returned.

6.1.4 Lighting Condition Variation

The lighting condition variation as part of the user requirements includes a maximum Sun angle on the observation sites at 45 deg. While only 16 of 20 observation sites are able to be covered, keep in mind the short duration of only a one day revisit rate is challenging to achieve. An expanded revisit rate would provide more flexibility to find a solution covering more sites. Additionally, the Sun angle requirement for the time of year specified makes it geometrically unobtainable to reach parts of the southern hemisphere. The targets not scheduled are all in the southern hemisphere with the exception of one which is designated with low priority. Once again the solution presented is not a unique solution as multiple runs provide other solutions that also meet user requirements. The parameters found for the lighting condition variation are

$\Omega = 223.53$ deg $\quad \omega = 347.87$ deg $\quad i = 92.92$ deg $\quad a = 8042.17$ km

$\theta = 204.18$ deg $\quad h_p = 343.75$ km $\quad k = 12$ $\quad e = 0.1654$

The evaluation function has a value of Q = -1775.80. Table 6.6 shows the schedule of each observation site. Sites with zero times were not able to be scheduled. Figure 6.4 below shows the ground trace for a satellite flying the designed orbit with repeat ground track.

Table 6.6 Lighting Condition Variation Schedule

Target	Start Time (s)	Stop Time (s)	Priority
7	26860	27320	5
2	0	0	4
17	12720	13400	4
3	34600	35480	3
4	84710	85590	3
9	13410	14190	3
13	77470	78340	3
14	71170	72010	3
19	27330	27790	3
20	0	0	2
1	5190	5660	2
5	62940	63780	2
10	21190	21990	2
11	27800	28510	2
15	120	600	2
12	5670	6360	2
16	0	0	1
18	0	0	1
6	12340	12710	1
8	70010	70810	1

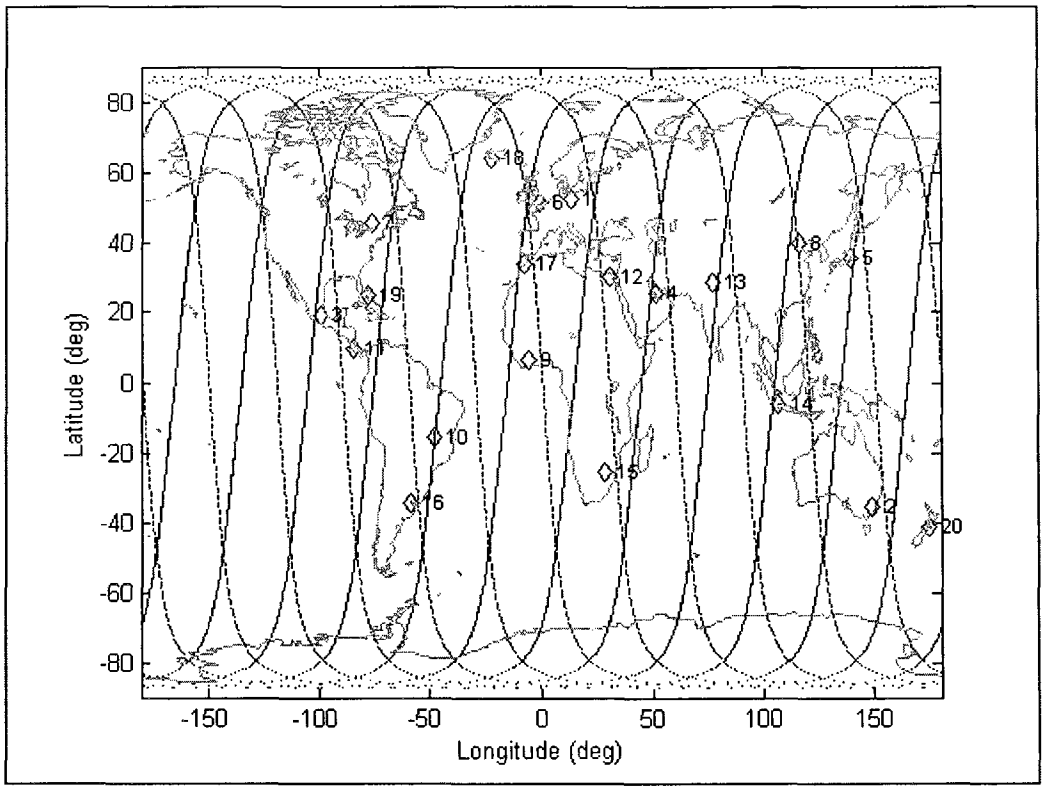

Figure 6.4 Lighting Condition Variation Ground Trace

The orbit for lighting condition variation is quite different from the baseline. The orbit has a lower height of perigee than the baseline and not all orbital position heights remain within the resolution ceiling. The orbit is more inclined at 92 deg and is much more elliptical. With the lighting restriction, only 16 sites are observed in the short repetition cycle. This performance is mostly due to the angle of the Sun for the given time of year. A different choice of day would make a noticeable difference in which targets are able to be viewed. The top priority target can only be viewed certain days of the year. While the top priority target is scheduled, only one of the two next level priority targets is scheduled. The magnitude of the evaluation function value for the

lighting condition variation is less (magnitude) than the baseline as expected in a more restrictive case study.

6.1.5 Maximum Sun Angle Variation

The maximum Sun angle was extended to 60 deg from the baseline 45 deg. The resulting primary and auxiliary parameters for the maximum Sun angle condition are

$\Omega = 178.68$ deg $\quad \omega = 358.67$ deg $\quad i = 83.52$ deg $\quad a = 8030.77$ km

$\theta = 112.08$ deg $\quad h_p = 151.18$ km $\quad k = 12$ $\quad e = 0.1882$

The evaluation function has a value of $Q = -2231.42$. Table 6.7 shows the target schedule while Figure 6.5 shows the ground track.

Table 6.7 Maximum Sun Angle Variation Schedule

Target	Start Time (s)	Stop Time (s)	Priority
7	14600	15070	5
2	52610	53360	4
17	500	1130	4
3	22350	23310	3
4	72460	73390	3
9	1140	2120	3
13	65210	66110	3
14	58910	59880	3
19	15080	15590	3
1	79050	79590	2
5	50690	51540	2
10	8980	9820	2
15	81040	81860	2
20	45580	46320	2
11	15600	16180	2
12	79600	80350	2
8	57810	58580	1
16	16730	17440	1
18	7190	7470	1
6	180	490	1

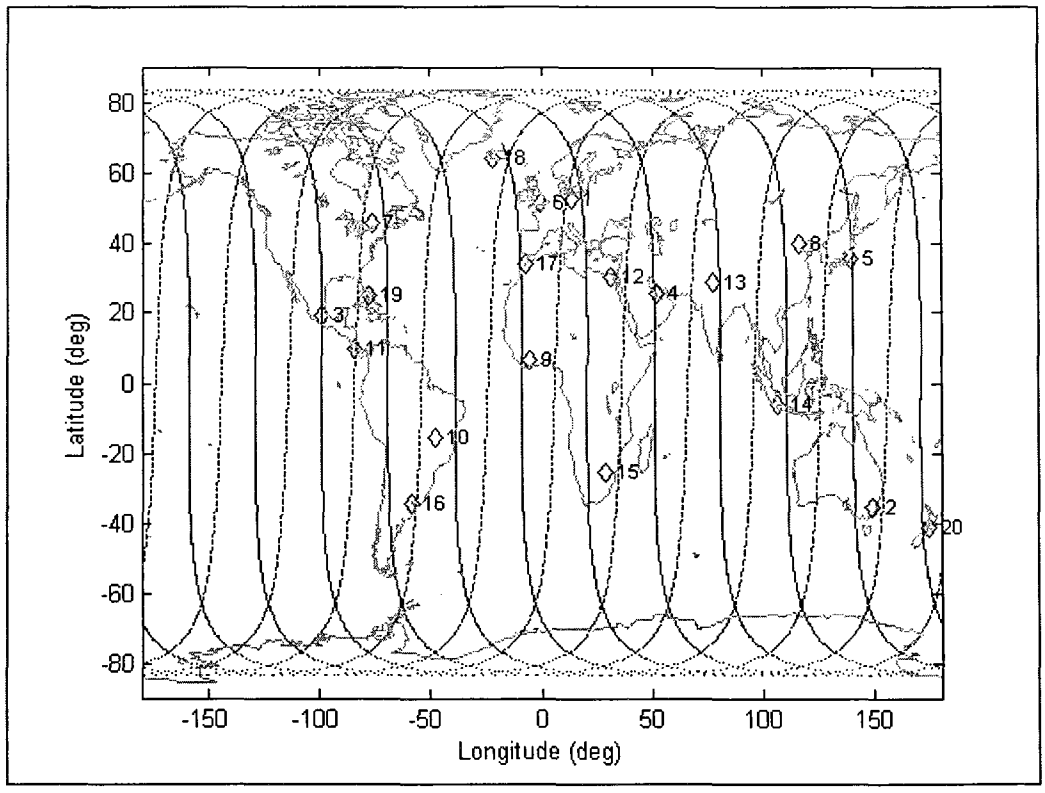

Figure 6.5 Maximum Sun Angle Variation Ground Trace

By relaxing the Sun angle restriction in the lighting condition case, a higher value cost function value was obtained as expected. Additionally, all targets are within range limits and were therefore scheduled.

6.1.6 Field of View Variation

The field of view was confined to 10 deg from the baseline 30 deg. The resulting primary and auxiliary parameters for the field of view condition are

$\Omega = 208.23$ deg $\omega = 15.93$ deg $i = 83.77$ deg $a = 8034.66$ km

$\theta = 99.34$ deg $h_p = 554.12$ km $k = 11$ $e = 0.1868$

The evaluation function has a value of Q = -1000.42. Table 6.8 shows the target schedule while Figure 6.6 shows the ground track.

Table 6.8 Field of View Variation Schedule

Target	Start Time (s)	Stop Time (s)	Priority
7	23750	24190	5
2	57260	57990	4
17	8360	8850	4
3	32340	32640	3
4	79030	79640	3
9	9060	9680	3
13	71200	71590	3
14	64460	64740	3
19	24210	24650	3
1	0	0	2
20	0	0	2
5	55440	55600	2
10	17500	18260	2
11	24660	25240	2
12	720	1020	2
15	2190	2850	2
6	0	0	1
18	0	0	1
8	63020	63510	1
16	18330	18590	1

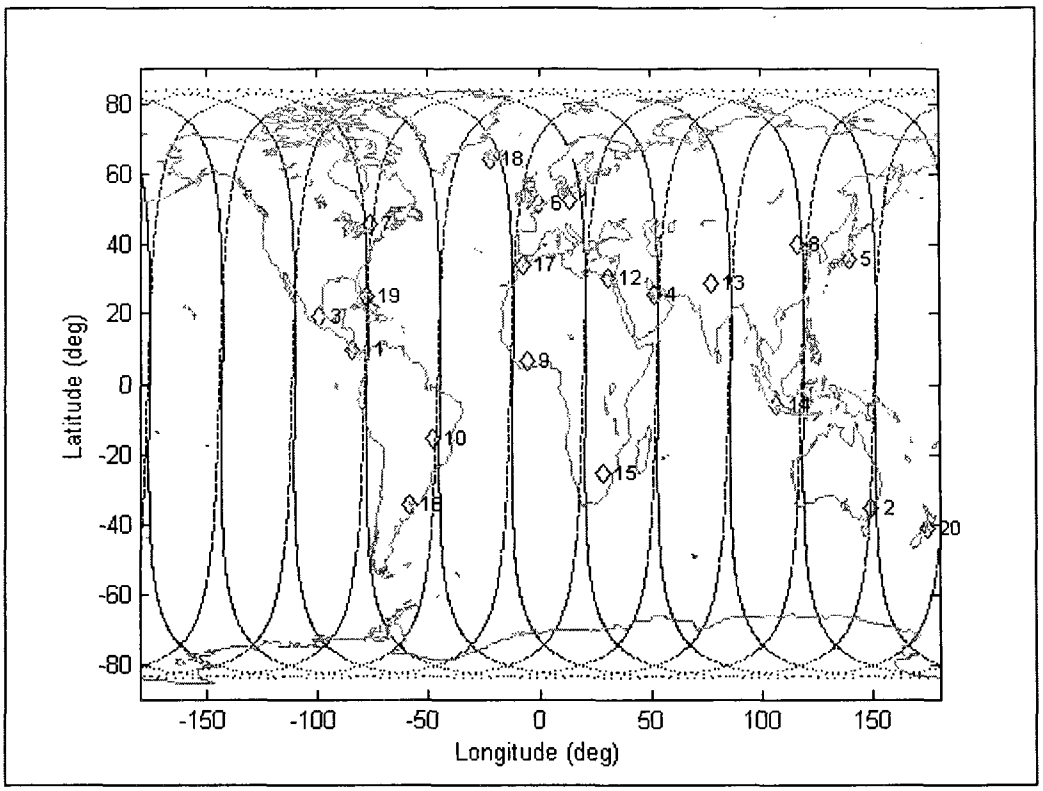

Figure 6.6 Field of View Variation Ground Trace

As expected, limiting the field of view had a noticeable impact on the cost function value, approximately half of the baseline value. The field of view parameter has a greater impact on the cost function value than imposing the lighting condition. Indeed, four targets were not able to be scheduled, but these four targets were of the lowest and next to lowest priority. Interestingly, here is another orbit that meets the requirement of 64 deg dictated by Target 18 with an inclination in the mid 80s. Also, this is another elliptical orbit where all orbital positions do not remain under the resolution ceiling. Even with the limited viewing angle, the targets scheduled were scheduled for more than 300 s. much more than the minimum required 60 s.

6.1.7 Slew Variation

The slew angle was confined to 5 deg from the baseline 15 deg. The resulting primary and auxiliary parameters for the slew angle condition are

$\Omega = 58.84$ deg $\quad \omega = 282.17$ deg $\quad i = 84.27$ deg $\quad a = 9074.33$ km

$\theta = 143.73$ deg $\quad h_p = 1897.01$ km $\quad k = 10$ $\quad e = 0.0013$

The evaluation function has a value of $Q = -1345.61$. Table 6.9 shows the target schedule while Figure 6.7 shows the ground track.

Table 6.9 Slew Variation Schedule

Target	Start Time (s)	Stop Time (s)	Priority
7	33660	34210	5
2	21020	21310	4
17	16160	16580	4
3	79880	80420	3
4	45290	45780	3
9	15540	15940	3
13	36560	37100	3
14	75610	75880	3
19	33180	33640	3
10	23720	23950	2
11	32890	33170	2
12	7450	7930	2
15	6250	6550	2
20	57620	57890	2
1	53110	53720	2
5	67890	68390	2
8	27600	28220	1
16	72680	73000	1
6	16590	17150	1
18	25620	26140	1

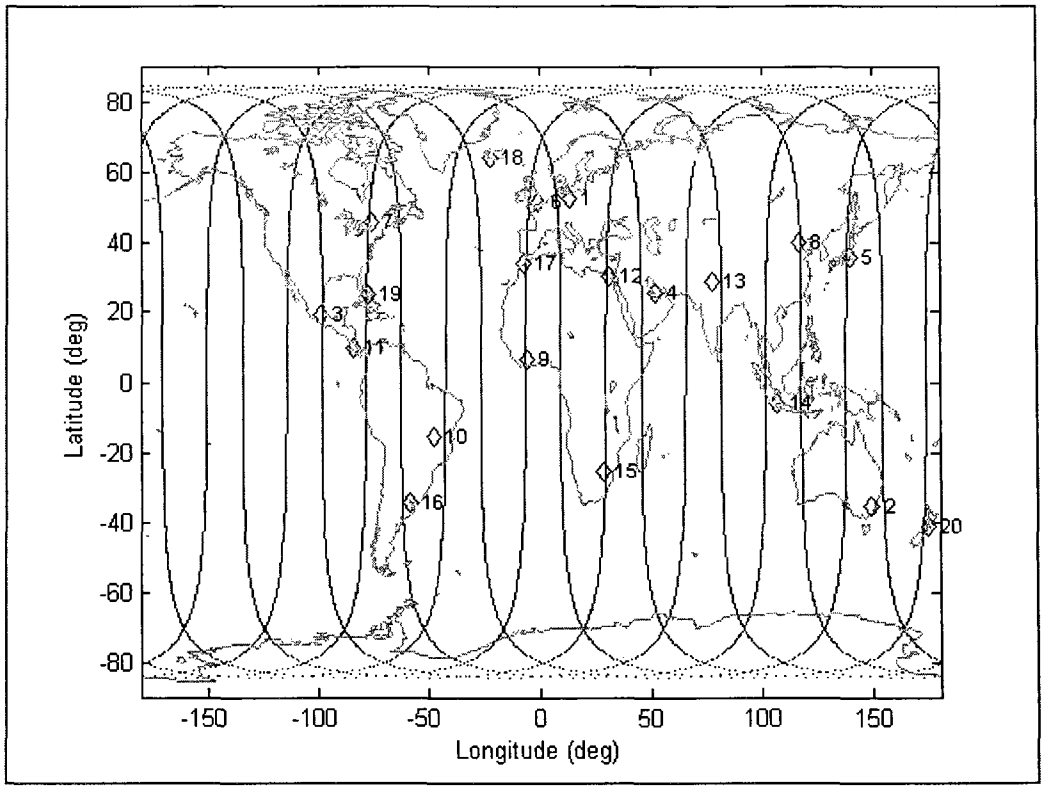

Figure 6.7 Slew Variation Ground Trace

Like the field of view restriction, limiting the slew angle has a noticeable effect on the cost value function as compared with the baseline condition. This orbit is much closer to the resolution height overall and is nearly circular. The height of perigee at 1897 km is approaching resolution ceiling of 2000 km. The spacecraft makes 10 revolutions in the repetition period. Again, the inclination requirement is met and the orbital inclination is in the mid 80s. However, even with the limited slewing capability, the solution provides for a schedule that covers all targets. Also, the targets are scheduled for more than the minimum duration required time. So while all the targets are scheduled, the quality of the observations must be less for the magnitude of the cost value to be so low. Thus slew capability is an effective design freedom to enhance observation quality, and the baseline case exploited this feature.

6.1.8 Resolution Altitude Variation

The resolution altitude was confined to 1000 km from the baseline 2000 km. The resulting primary and auxiliary parameters for the resolution altitude condition are

$\Omega = 146.22$ deg $\omega = 304.70$ deg $i = 73.70$ deg $a = 8034.66$ km

$\theta = 235.49$ deg $h_p = 975.74$ km $k = 13$ $e = 0.0034$

The evaluation function has a value of $Q = -772.28$. Table 6.10 shows the target schedule while Figure 6.8 shows the ground track.

Table 6.10 Resolution Altitude Variation Schedule

Target	Start Time (s)	Stop Time (s)	Priority
7	56640	56890	5
17	78340	78550	4
2	81550	81710	4
3	12660	12860	3
13	58660	58880	3
19	56310	56480	3
4	23320	23490	3
9	36150	36350	3
14	9580	9750	3
10	0	0	2
5	3720	3950	2
12	29990	30220	2
15	72880	73130	2
1	37010	37270	2
11	56000	56200	2
20	74850	75010	2
6	71280	71570	1
16	7160	7310	1
8	10400	10640	1
18	50490	50760	1

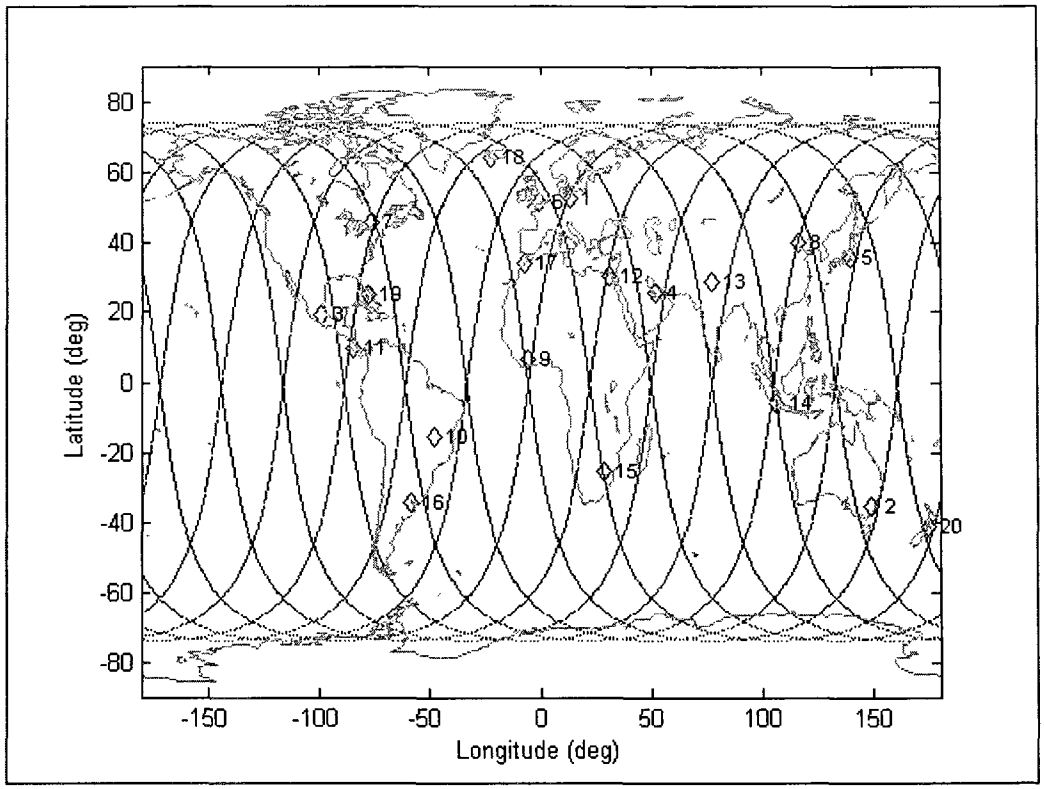

Figure 6.8 Resolution Altitude Variation Ground Trace

Altering the minimum resolution definitely makes a difference in the outcome of the orbital solution in comparison to the baseline condition. This orbit has an inclination of 73 deg, different from the other solutions with inclinations in the 80s. This solution is the lowest orbit with 13 revolutions in the repetition cycle, to be expected with the limitation of 1000 km ceiling resolution altitude. The orbit is near circular with the height of perigee and most orbital positions being very close to the resolution ceiling. The cost function is highly degraded at only -772 in comparison to the baseline value of -2199. This solution provides viewing opportunity for all but one target with relatively low priority. While all target viewings meet the 60 s requirement, most are only scheduled for 200 s, not much more than the minimum due to the higher velocity flybys.

6.2 Regional Case Study

In addition to the global case study, this research optimization algorithm was employed for a regional set of observation sites. The purpose of the regional target set was to see how well the algorithm performed when stressed with a cluster of targets. Table 6.11 shows the target selection for a regional case study including ten sites. The same baseline conditions given in Table 6.2 are used in the regional case study. To ensure viewing opportunities for this target set, the start date selected was midnight 1 January 1994.

Table 6.11 Regional Observation Sites

Country	City	Lat (deg)	Long (deg)	Priority	Target
New Zealand	Auckland	-36.866667	174.766667	4	8
New Zealand	Christchurch	-43.533333	172.633333	3	3
New Zealand	Dunedin	-45.866667	170.5	2	10
New Zealand	Hastings	-39.65	176.833333	1	6
New Zealand	Invercargill	-46.4	168.35	2	1
New Zealand	New Plymouth	-39.066667	174.083333	1	7
New Zealand	Queenstown	-45.033333	168.666667	5	2
New Zealand	Westport	-41.75	171.566667	3	4
New Zealand	Wellington	-41.3	174.783333	2	5
New Zealand	Whangarei	-35.816667	174.5	3	9

In the regional case, an orbit was found that met all the user requirement conditions. However, note this orbit in not a unique solution as there are ample design freedoms to meet all user requirements. Like the global case study and variations, repeated runs may produce different resulting parameters that also meet the user requirements. The resulting parameters for the regional case are

$\Omega = 155.51$ deg $\quad \omega = 71.03$ deg $\quad i = 71.50$ deg $\quad a = 8019.21$ km

$\theta = 159.78$ deg $\quad h_p = 607.90$ km $\quad k = 12 \quad e = 0.1300$

The evaluation function has a value of Q = -416.68. Table 6.12 shows the schedule for each target. Figure 6.9 shows the ground trace for a satellite flying the designed orbit with repeat ground track.

Table 6.12 Regional Case Schedule

Target	Start Time (s)	Stop Time (s)	Priority
2	80540	80660	5
8	42340	43030	4
4	80670	80730	3
9	80890	80990	3
3	80740	80810	3
5	73350	73410	2
1	73180	73240	2
10	73250	73340	2
6	73420	73660	1
7	80820	80880	1

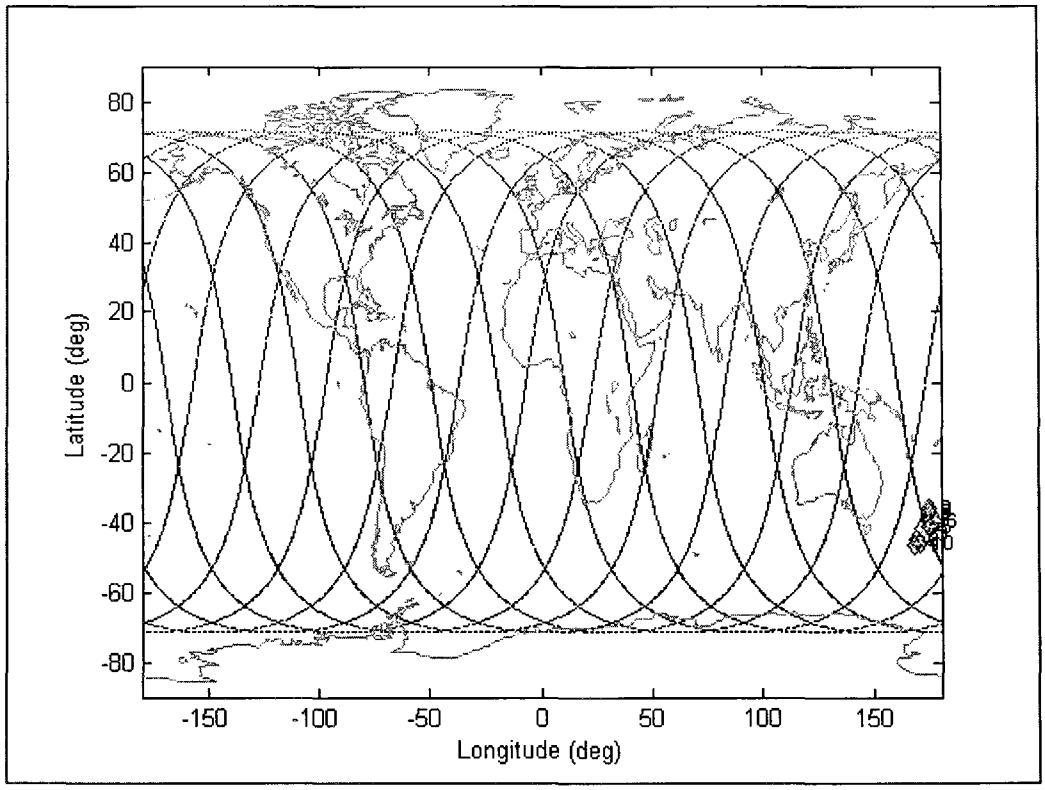

Figure 6.9 Regional Case Ground Trace

The inclination value of 71.50 deg meets the minimum inclination 46.4 deg determined by Target 1. While the height of perigee is much less than the required ceiling altitude, here is another example of an orbit that has orbital positions above the resolution ceiling altitude. An elliptical solution is not unexpected as it can provide intensive coverage over a selected geographical area.[59] All targets are scheduled but note the schedule reflects four minimum observation times of 60 s where the global case schedule times were expanded well beyond the minimum requirement. In general, the regional observation times are shorter than the global case, as expected with a set of clustered targets. Note all but one target are viewed on two specific flybys, also expected for high target density. The cost value for the regional case study is much less than the global case; however, the target set is based on half the number of targets.

6.3 Lifecycle Analysis

One way to evaluate the feasibility of the optimization solution is to see how significant the orbital parameters and cost function value change over time considering perturbation influences. The optimization solution is determined using only limited zonal effects. Additional perturbations such as aerodynamic drag, solar radiation pressure, and third body effects should be considered in a more realistic simulation. This section employs the perturbations as described in Section 5.3 using Cowell's Formulation as described in Section 5.2. The satellite description is provided in Table 6.13.

Table 6.13 Satellite Description

Mass	100 kg
Coefficient of Drag	2
Coefficient of Reflectivity	1.2
Cross Sectional Area	2 m^2

Figures 6.10-6.17 show the changes in the orbital elements and cost function given over time for 10 repetition cycles. The global baseline initial orbital elements are

$\Omega = 59.48$ deg $\quad \omega = 272.40$ deg $\quad i = 68.66$ deg $\quad a = 8501.45$ km

$\theta = 197.06$ deg $\quad h_p = 1837.53$ km $\quad k = 11 \quad e = 0.0347$

The ideal evaluation function has a value of $Q = -2199.62$.

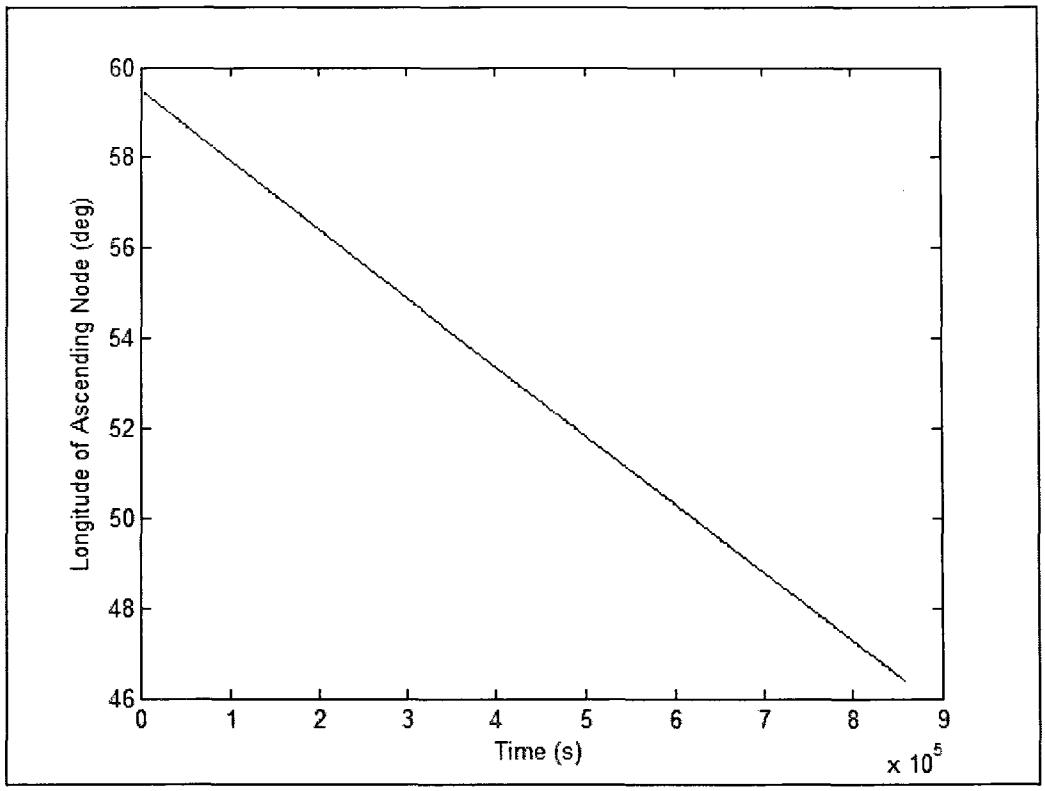

Figure 6.10 Longitude of Ascending Node over Time

The drift in the longitude of ascending node shows a long term secular change towards the West. Over the 10 repetition cycle time period, the change is about 13 degrees. This variation is in good agreement with the nodal regression behavior documented in Figure 3.1-5 in Reference 60, which in some sense validates the higher fidelity lifecycle analysis propagation simulator. A zoomed view of this graph shows very small periodic variances, not even noticeable at this level of detail.

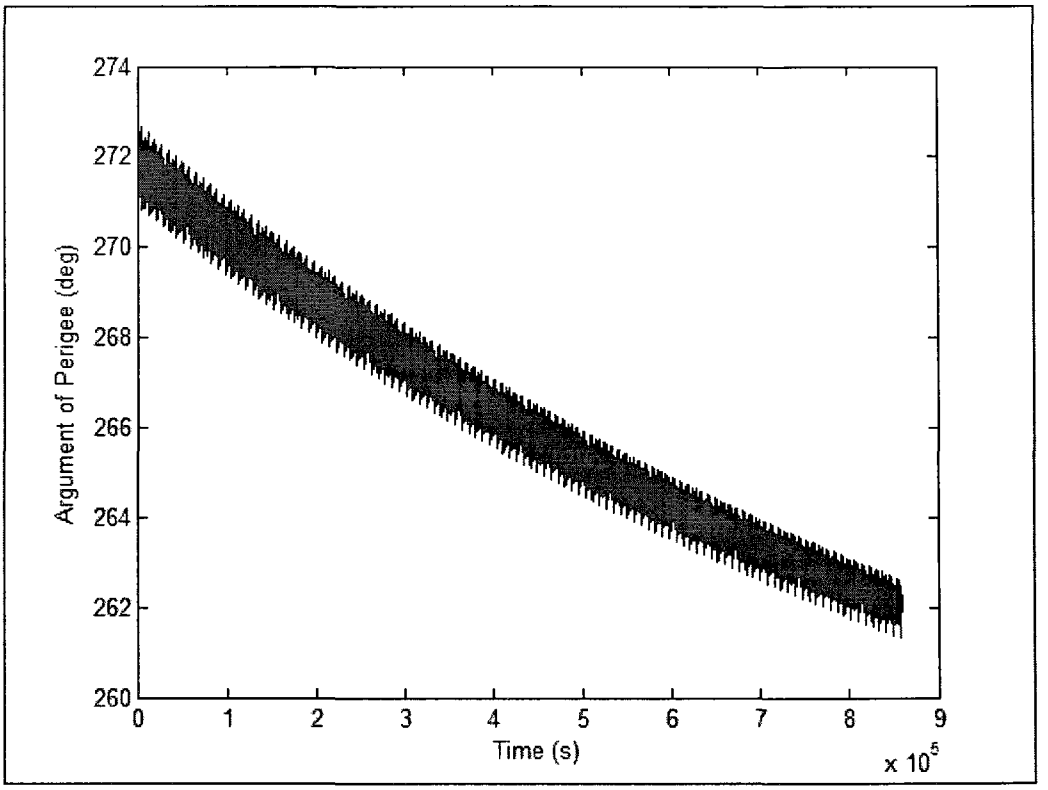

Figure 6.11 Argument of Perigee over Time

The argument of perigee shows much more noticeable short term periodic effects of the perturbations. The overall secular change which is in the retrograde direction is still more pronounced than the periodic effects. The total change in the argument of perigee over the 10 repetition period is about 10 degrees. Results here are also consistent with the apsidal rotation data given in Reference 60 in Figure 3.1-6, providing further validation of the lifecycle propagator accuracy.

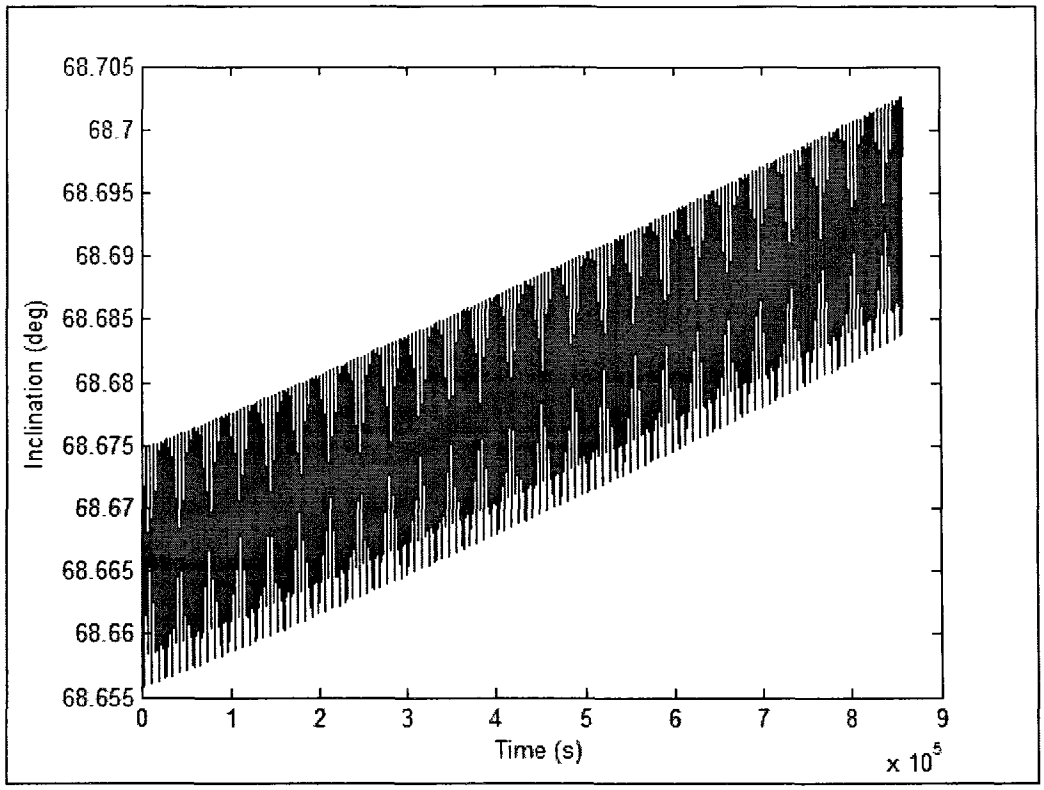

Figure 6.12 Inclination over Time

The inclination of the orbital period slightly increases over time with a small change of only 0.03 degrees. Here, both periodic and secular changes are apparent with an appropriately chosen scale.

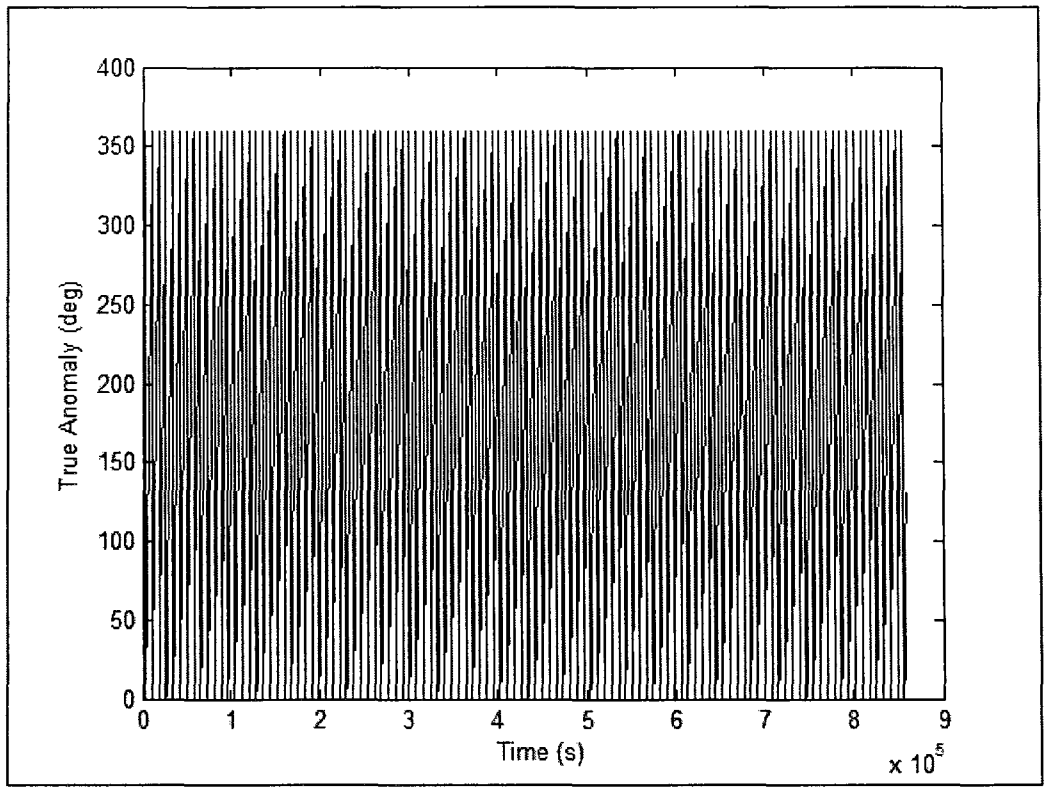

Figure 6.13 True Anomaly over Time

This graph shows the motion of the satellite along the orbit for 110 orbital cycles, as excepted since there are 11 revolutions per repetition cycle and this graph covers 10 repetition cycles. As expected the true anomaly passed through all 360 degrees in a cyclic motion.

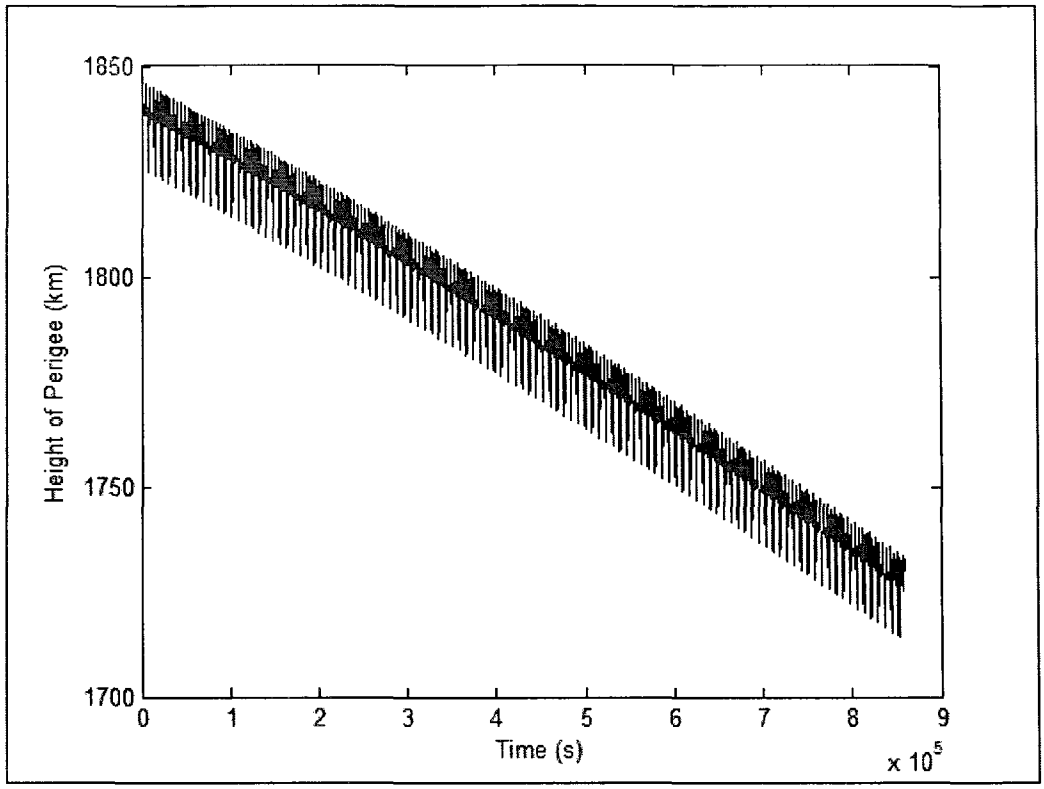

Figure 6.14 Height of Perigee over Time

The height of perigee looses a noticeable amount of altitude over the 10 repetition period timeframe with a loss of approximately 100 km. The short term periodic affects show an interesting pattern. However, the secular changes dominate the overall direction of change in the height of perigee.

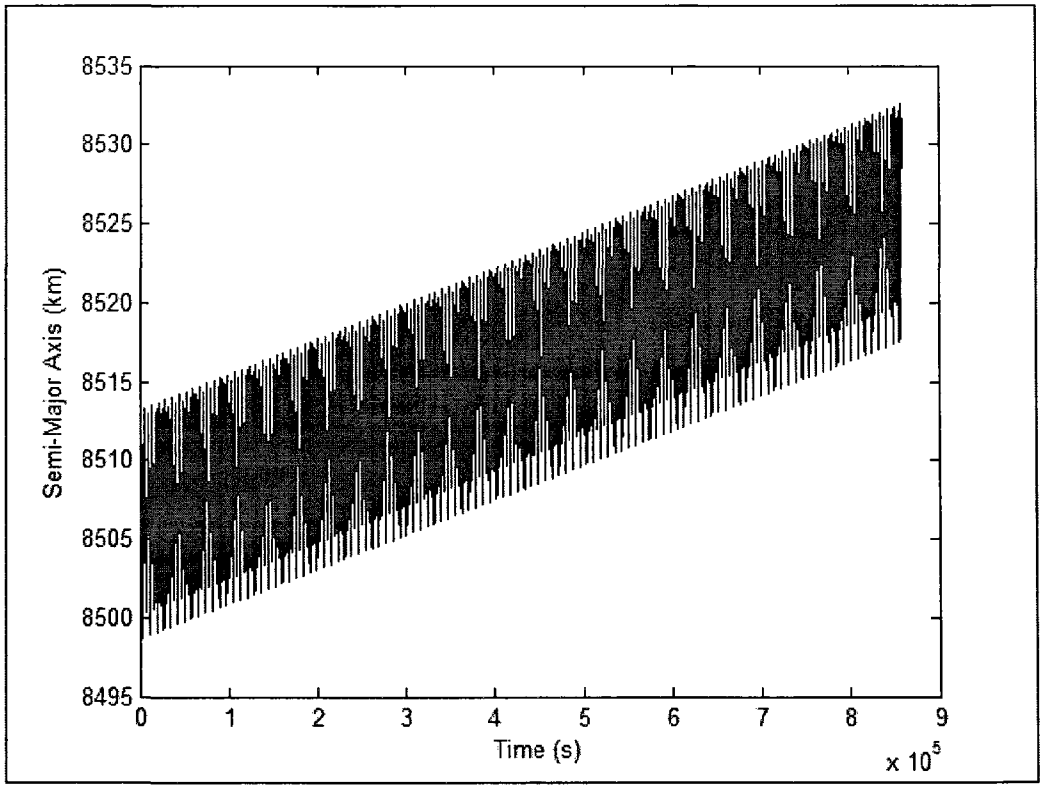

Figure 6.15 Semi-Major Axis over Time

The semi-major axis shows a slight overall increase in orbital size of 20 km. There are 110 periodic cycles shown that correspond to each orbital revolution like true anomaly in Figure 6.13. These short term periodic cycles are due mostly to the harmonic zonal affects. The increasing of the orbital period is most likely a long term periodic harmonic zonal effect.

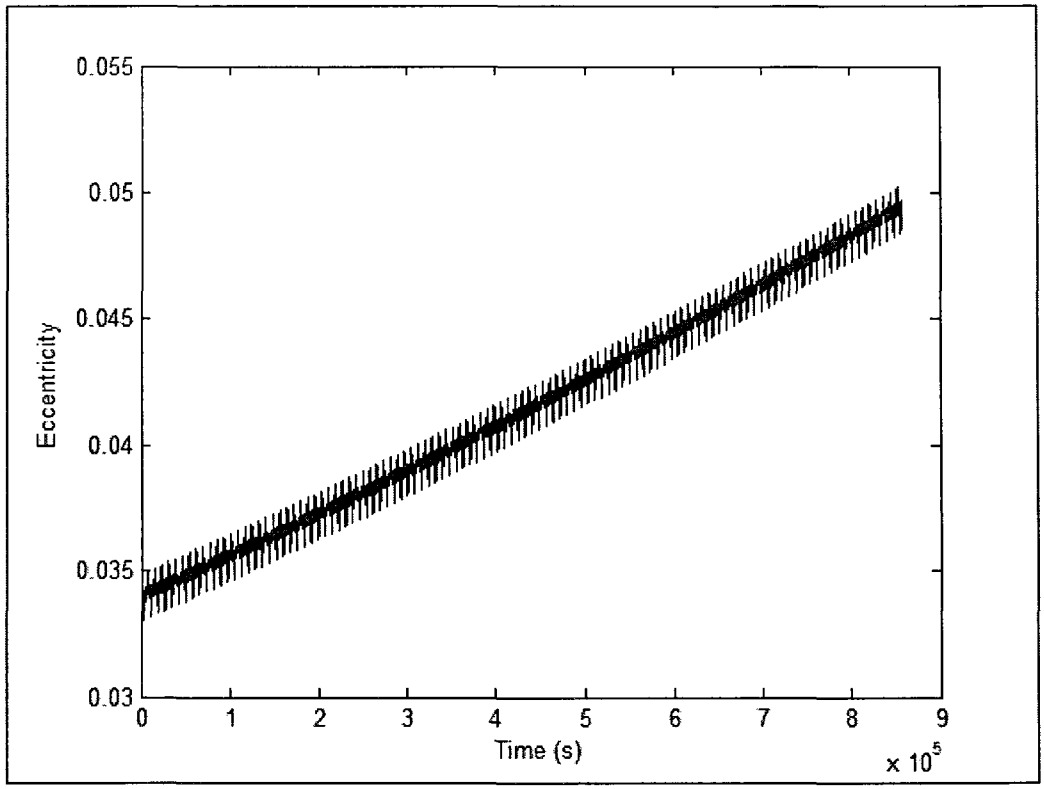

Figure 6.16 Eccentricity over Time

The eccentricity of the orbit shifts from 0.034 to 0.049 which corresponds to the decreasing height of perigee and increasing semi-major axis. Here the periodic variations seen in each orbital revolution are obvious, as well as the overall secular change.

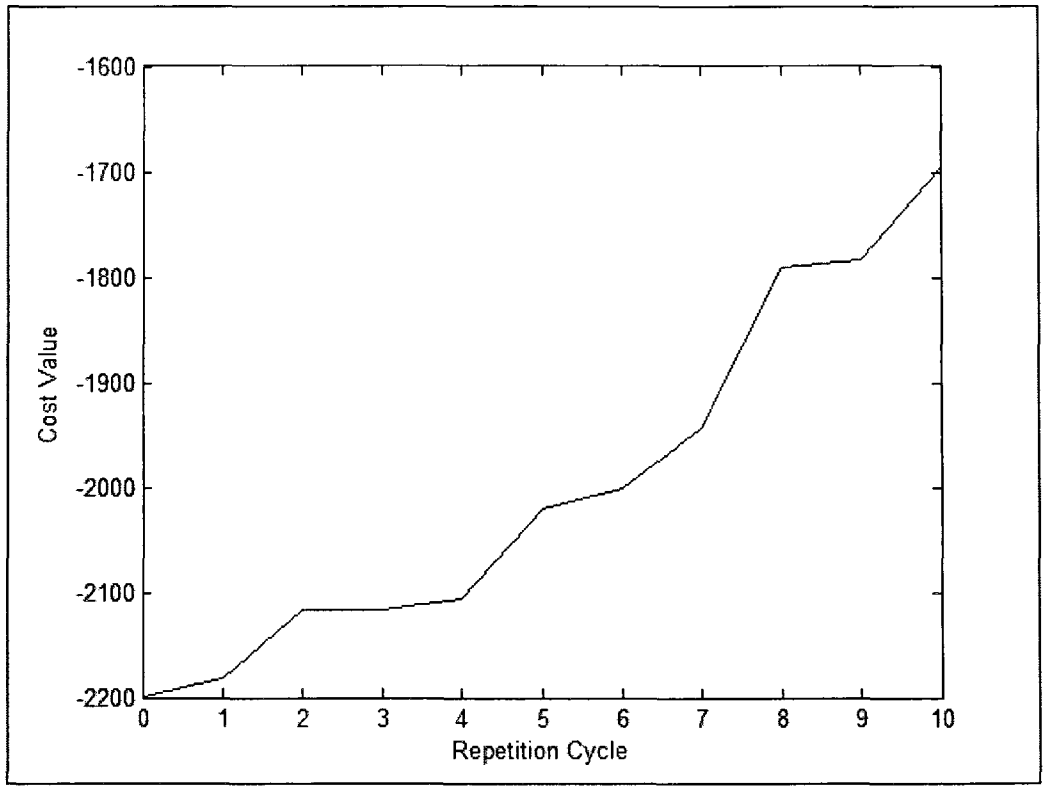

Figure 6.17 Cost Function Value over Time

The ideal cost function value is plotted as the 0 repetition cycle. The significant change of the cost function value over time is quite apparent. However, looking at the first few repetition cycles, it could be argued that keeping the orbital elements near the original initial elements through orbital maintenance would keep a cost function value near the ideal cost function value even in the full perturbation environment.

To estimate how much impulsive velocity change would be required to achieve orbital maintenance, simple two body expressions can be used. For elliptic orbits, the specific energy of the satellite, E, is related to the semi-major axis by $E = -\mu/2a$. Using the initial semi-major axis a_1 = 8501 km where subscript 1 indicates the beginning value, the energy level is E_1 = -23.44 km^2/s^2. After 10 repetition cycles, Figure 6.15 indicates an approximate 20 km increase or a_2 = 8521 km yielding the ending energy E_2 = -23.39

km^2/s^2. The energy change over the 10 day period due to perturbations is $\Delta E = E_2 - E_1 =$ 0.05 km^2/m^2. Now recall the general energy relation $E = v^2/2-\mu/r$, which can be used to find the initial velocity $v_1 = 7.083$ km/s at perigee where $r_1 = 8215$ km. Assuming orbital maintenance is executed at perigee, the required velocity v_2 to restore the original energy level is thus $v_2 = 7.090$ km/s. Therefore, every 10 days an impulsive velocity change of $\Delta v = v_2 - v_1 = 7$ m/s is required for orbital maintenance. This maintenance level is consistent with existing technologies and deployed satellites.

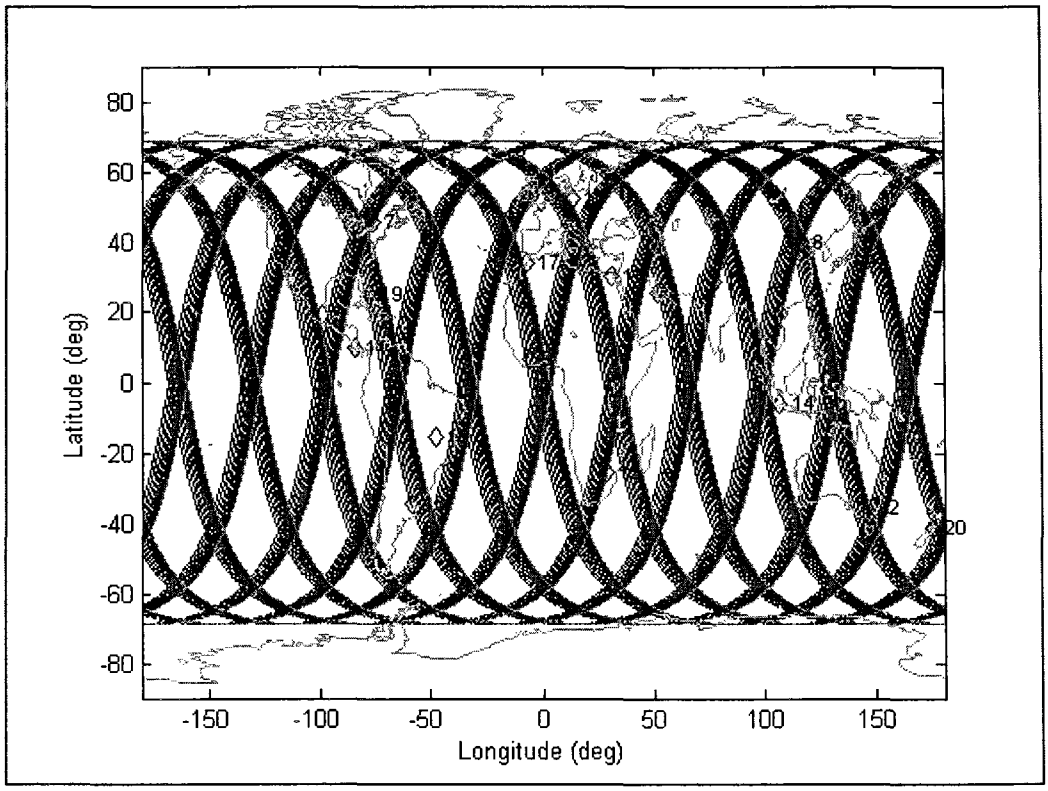

Figure 6.18 Perturbed Ground Trace

Figure 6.18 shows the ground trace over the 10 period repetition cycle timeframe. The magenta color is the first repetition cycle. The blue shows the rest of the 9 cycles. As expected from Figure 6.10, the shift of the longitude of ascending node is to the West. The change in inclination is not noticeable.

Figures 6.19 and 6.20 show the inertial position of the orbit over the 10 repetition cycles from a polar viewpoint and a more equatorial view. The red line shows the direction of the last position of the Sun while the blue line shows the direction of the last position of the Moon.

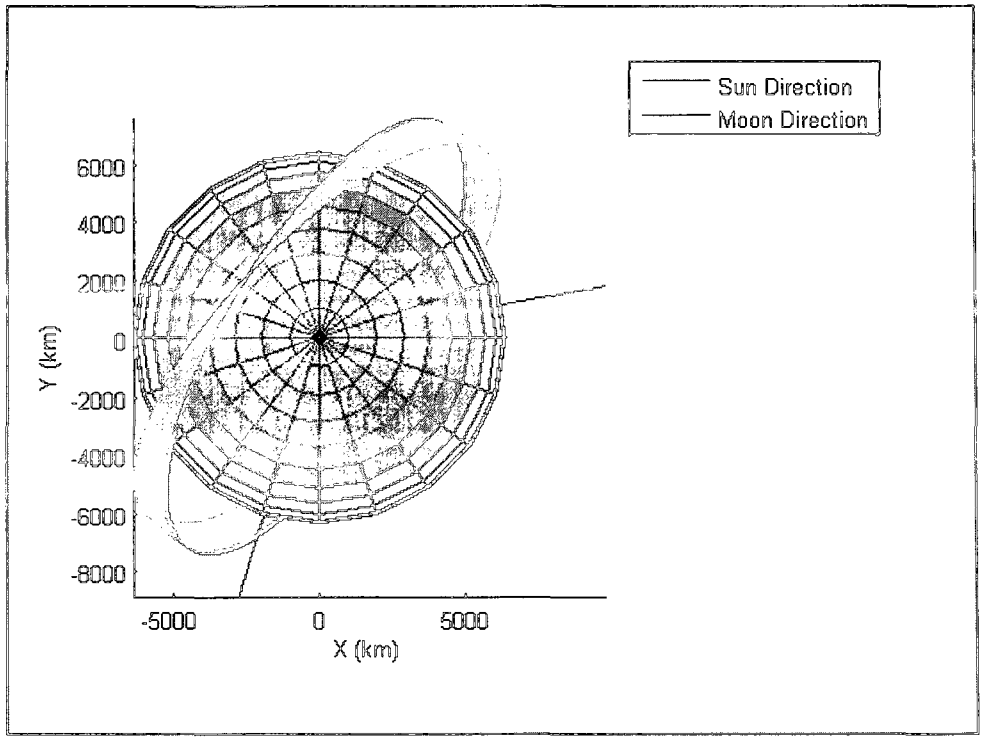

Figure 6.19 Perturbed Orbit Polar View

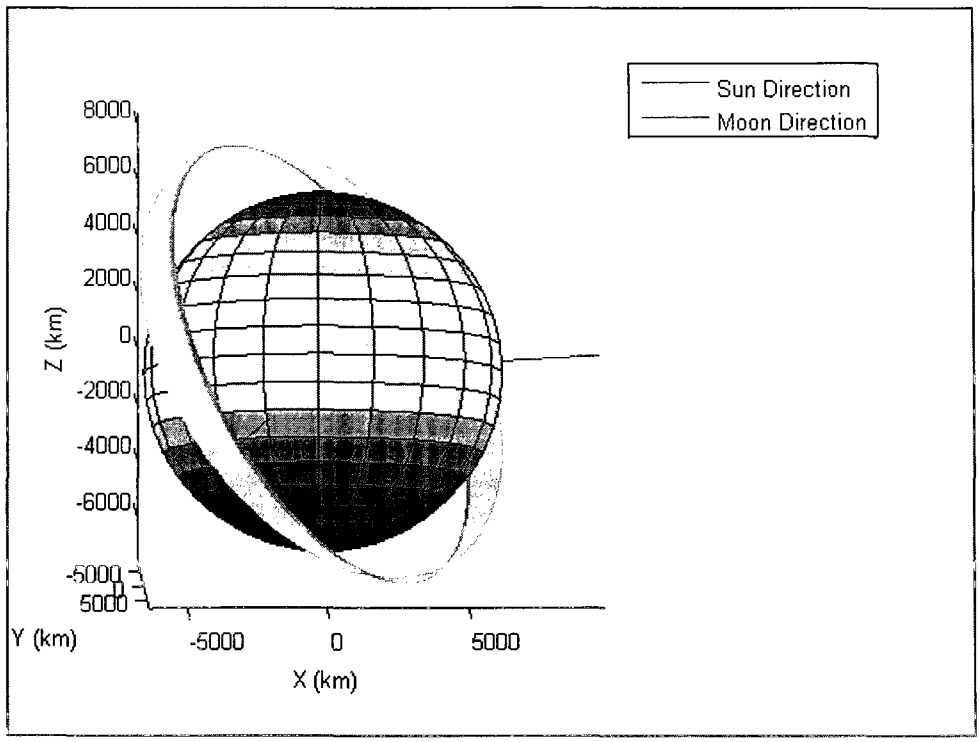

Figure 6.20 Perturbed Orbit Equatorial View

Also of interest is the change in the scheduling of targets over time. Tables 6.14 and 6.15 show the first repetition cycle schedule and the tenth repetition cycle respectively. Notice the difference between Table 6.14 and Table 6.3, the global baseline schedule built in an ideal limited zonal model simulator (Table 6.3) where as the first repetition cycle schedule here (Table 6.14) is developed in the full perturbation model simulator. Only the first three targets (first two priority levels) are scheduled in the same order in the first and tenth repetition cycles. In Table 6.15 there is one target (Jakarta) not scheduled in the tenth repetition cycle. The scheduled time of each target in the first repetition cycle ranges from 290-630 s. The scheduled time of each target in the tenth repetition cycle ranges from 110-590 s. While the schedules show the decreased observation times in the repetition cycles, the schedules do not reflect the quality of the

observation. The cost function is based on both the length of observation times and the quality of the observations.

Table 6.14 First Repetition Cycle Schedule

Target	Start Time (s)	Stop Time (s)	Priority
7	37380	37990	5
2	58960	59360	4
17	55160	55750	4
3	78980	79530	3
4	5720	6240	3
9	55830	56290	3
13	83840	84410	3
14	32750	33230	3
19	70990	71490	3
10	72160	72450	2
11	36630	37090	2
12	47490	48040	2
15	4510	4970	2
5	68370	68890	2
20	17920	18290	2
1	46850	47480	2
16	72460	72810	1
8	76300	76900	1
6	21960	22570	1
18	30080	30710	1

Table 6.15 Tenth Repetition Cycle Schedule

Target	Start Time (s)	Stop Time (s)	Priority
7	72530	72910	5
2	27510	27770	4
17	57130	57590	4
14	0	0	3
19	72920	73310	3
3	81070	81390	3
4	41540	42120	3
9	57710	58220	3
13	33600	34140	3
10	22010	22430	2
11	73320	73650	2
5	17730	18300	2
12	7370	7910	2
15	50640	50980	2
20	19660	20060	2
1	48750	49330	2
8	25540	26130	1
16	21600	21910	1
6	48630	48740	1
18	48200	48620	1

CHAPTER 7

CONCLUSIONS

7.1 Conclusions

This research has shown that user requirements can be brought to the forefront of mission planning for Earth observation missions. The observation site requirements and restraints along with the sensor characteristics can be used to find an appropriate orbit for the satellite. The design methodology presented in this research mapped mission requirements into parameters and uses a cost function based on the Window-Constraint Packing Problem to create a schedule based on the priority dispatch method. The genetic algorithm was used to find optimized parameters that best meet the user requirements and constraints. A case study demonstrated the effectiveness of this design methodology and showed the design methodology leads to an orbit satisfying the user specified requirements and constraints. Additionally, the global baseline was varied to show how each of the user requirements can change the quality of the cost function and the scheduling of the targets. The case study demonstrated elliptical orbits and orbits with altitudes above the resolution ceiling should be explored in mission designs to maximize system performance. The lifecycle analysis results provided insight into how each of the orbital elements changes under perturbations assuming no corrective measures are taken to maintain the repeating ground track orbit.

7.2 Recommendations

While the goal of this research is to find an optimal orbit for the given user requirements, the cost function and search process do not provide a fully unique solution. Further investigation to refine the cost function and/or search process is needed. The cost function could be expanded to include more constraints ranging from launch site restrictions on the types of available orbits, to the space environment areas of concern such as the Van Allen radiation belt, to the amount of energy or fuel required to maintain the desired repeating ground track orbit over a specific mission timeframe. Also, further work envisioned includes adapting the design method for use with other software programs such as Satellite Tool Kit to take advantage of more sophisticated perturbation models and propagation algorithms.

REFERENCES

1. Porter, R., *The Versatile Satellite*, Oxford University Press, Oxford , 1977.

2. Fink, D., "Earth Observation - Issues and Perspectives," AIAA 16th Annual Meeting and Technical Display, Baltimore, Maryland, May, 1980.

3. Anderson, J., *Introduction to Flight,* 3rd Edition, McGraw-Hill, New York, 1989.

4. Crouch, T., *Wings A History of Aviation from Kites to the Space Age*, W.W. Norton & Company, New York, 2003.

5. Scott, P., *The Shoulder of Giants A History of Human Flight to 1919*, Addison-Wesley Publishing Company, Reading, 1995.

6. Lambert, W., *Reconnaissance & Bomber Aircraft of the 1914-1918 War*, Aero Publishers, Los Angeles, 1962.

7. Smith, M., *Ten Propositions Regarding Spacepower*, Air University Press, Maxwell Air Force Base, 2002.

8. Taubman, P., *Secret Empire Eisenhower, the CIA, and the Hidden Story of America's Space Espionage*, Simon & Schuster, New York, 2003.

9. Campbell, J., *Introduction to Remote Sensing*, 2nd Edition, The Guilford Press, New York, 1996.

10. Diebert, R., "Unfettered Observation," Lambright, W., *Space Policy in the 21st Century*, The Johns Hopkins University Press, Baltimore, 2003.

11. Booth, N., *The Encyclopedia of Space*, Mallard Press, New York, 1990.

12. *Air Force Doctrine Document 2-2, Space Operations*, U.S. Air Force, 1998.

13. Geller, M., "Earth Observations in the Twenty-First Century," AIAA-86-2345, AIAA Space Station in the Twenty-First Century Meeting, Reno, Nevada, September, 1986.

14. Sellers, J., *Understanding Space An Introduction to Astronautics*, McGraw-Hill, New York, 1994.

15. Ohlemacher, R. and Johnson, D., "Establishing a Policy Framework for Global Change Earth Observations," AIAA-2008-7796, AIAA Space 2008 Conference and Exposition, San Diego, California, September, 2008.

16. Vallado, D., *Fundamentals of Astrodynamics and Applications*, 3rd Edition, Microcosm Press, Hawthorne, 2007.

17. Wiesel, W., *Spaceflight Dynamics*, McGraw-Hill, New York, 1989.

18. Griffen, M. and French, J., *Space Vehicle Design*, American Institute of Aeronautics and Astronautics, Reston, 2004.

19. Battin, R., *An Introduction to the Mathematics and Methods of Astrodynamics*, Revised Edition, American Institute of Aeronautics and Astronautics, Reston, 1999.

20. Zill, D. and Cullen, M., *Differential Equations with Boundary-Value Problems*, 3rd Edition, PWS-KENT Publishing Company, Boston, 1993.

21. Larson, W. and Wertz, J., *Space Mission Analysis and Design*, 2nd Edition, Microcosm, Torrance, 1992.

22. Wilkins, C., Wong, H., and Kapila, V., "Symmetric Orbits in the Presence of J2 Perturbation," AIAA-2007-6843, AIAA Guidance, Navigation and Control Conference and Exhibit, Hilton Head, South Carolina, August, 2007.

23. Cefola, P., "Equinoctial Orbit Elements - Application to Artificial Satellite Orbits," AIAA-72-937, Palo Alto, California, September, 1972.

24. Vallado, D. and Finkleman, D., "A Critical Assessment of Satellite Drag and Atmospheric Density Modeling," AIAA-2008-6442, AIAA/AAS Astrodynamics Specialist Conference and Exhibit, Honolulu, Hawaii, August, 2008.

25. *Department of Defense World Geodetic System 1984*, NIMA TR8350.2, National Geospatial-Intelligence Agency, January, 2000.

26. Marcos, F., Burke, W., and Lai, S., "Thermospheric Space Weather Modeling," AIAA-2007-4527, 38th AIAA Plasmadynamics and Lasers Conference, Miami, Florida, June, 2007.

27. Hoots, F. and Glover, R., "History of Analytical Orbit Modeling in the U.S. Space Surveillance System," *Journal of Guidance, Control, and Dynamics*, Vol. 27, No. 2, March-April, 2004, pp. 174-185.

28. Ravanbakhsh, A., Mortazavi, M., and Roshanian, J., "Multidisciplinary Design Optimization Approach to Conceptual Design of a LEO Earth Observation Microsatellite," AIAA-2008-3259, SpaceOps 2008 Conference, Heidelberg, Germany, May, 2008.

29. Harris, R., *Satellite Remote Sensing An Introduction*, Routledge & Kegan Paul, New York, 1987.

30. Wolfe, W. and Sorensen, S., "Three Scheduling Algorithms Applied to the Earth Observing Systems Domain," *Management Science*, Vol. 46, No. 1, January, 2000, pp. 148-166.

31. Frank, J., Jonsson, A., Morris, R., and Smith, D., "Planning and Scheduling for Fleets of Earth Observing Satellites," 6th International Symposium on Artificial Intelligence, Robotics, Automation, and Space 2002, Montreal, June, 2002.

32. Bensana, E., Lemaitre, M., and Verfaillie, G., "Earth Observation Satellite Management," *Constraints*, Vol. 4, 1999, pp. 293-299.

33. Cordeau, J. and Laporte, G., "Maximizing the Value of an Earth Observation Satellite Orbit," *Journal of the Operational Research Society*, Vol. 56, 2005, pp. 962-968.

34. Globus, A., Crawford, J., Lohn, J., and Morris, R., "Scheduling Earth Observing Fleets Using Evolutionary Algorithms: Problem Description and Approach," Proceedings of the 3rd International NASA Workshop on Planning and Scheduling for Space, Houston, Texas, October, 2002.

35. Goldberg, D., *Genetic Algorithms in Search, Optimization, and Machine Learning*, Addison-Wesley Publishing Company, New York, 1989.

36. Nocedal, J. and Wright, S., *Numerical Optimization*, 2nd Edition, Springer, USA, 2006.

37. Rao, S., *Engineering Optimization*, 3rd Edition, John Wiley & Sons, New York, 1996.

38. Pontani, M. and Conway, B., "Particle Swarm Optimization Applied to Space Trajectories," *Journal of Guidance, Control, and Dynamics*, Vol. 33, No. 5, September-October, 2010, pp. 1429-1441.

39. Abdelkhalik, O. and Mortari, D., "Orbit Design for Ground Surveillance Using Genetic Algorithm," *Journal of Guidance, Control, and Dynamics*, Vol. 29, No. 5, September-October, 2006, pp. 1231-1235.

40. Vtipil, S. and Newman, B., "Constrained Optimal Orbit Design for Earth Observation Satellites Based on User Requirements," AAS-09-427, AAS/AIAA Astrodynamics Specialist Conference, Pittsburgh, Pennsylvania, August, 2009.

41. Stratton, A., "Earth Resources Satellites: Capabilities Versus Requirements," Ford, C., *Space Technology and Earth Problems*, American Astronautical Society, Washington D.C., 1970.

42. Aorpimai, M. and Palmer, P., "Repeat-Groundtrack Orbit Acquisition and Maintenance for Earth-Observation Satellites," *Journal of Guidance, Control, and Dynamics*, Vol. 30, No. 3, May-June, 2007, pp. 5654-659.

43. Vtipil, S. and Newman, B. "Determining an Efficient Repeat Ground Track Method for Earth Observation Satellites: For Use in Optimization Algorithms," AIAA-2010-8266, AIAA/AAS Astrodynamics Specialists Conference, Toronto, Ontario, August, 2010.

44. Collins, S. K. "Computationally Efficient Modelling for Long Term Prediction of Global Positioning System Orbits," M.S. Thesis, Department of Aeronautics and Astronautics, Massachusetts Institute of Technology, February, 1977.

45. Vincent, M., "The Inclusion of Higher Degree and Order Graviy Terms in the Design of a Repeat Ground Track," AIAA/AHS Astrodynamics Conference, Vol. I, Portland, Oregon, 1990, pp. 201-207.

46. Mortari, D., Wilkins, M., and Bruccoleri, C., "The Flower Constellations," *Journal of Astronautical Sciences*, Vol. 52, January-June, 2004, pp. 107-127.

47. Tonetti, S., "Optimization of Flower Constellations: Applications in Global Navigation System and Space Interferometry," AIAA-2009-205, 47th AIAA Aerospace Sciences Meeting Including The New Horizons Forum and Aerospace Exposition, Orlando, Florida, January, 2009.

48. Hashida, Y. and Palmer, P., "Epicyclic Motion of Satellites Under Rotating Potential," *Journal of Guidance, Control, and Dynamics*, Vol. 25, No. 3, May-June, 2002, pp. 571-581.

49. Vtipil, S. and Newman, B., "Designing a Constrained Optimal Orbit for Earth Observation Satellites Based on User Requirements," AIAA-2010-7520, AIAA/AAS Astrodynamics Specialist Conference, Toronto, Ontario, August, 2010.

50. Vtipil, S. and Newman, B., "Repeat Ground Track Methods for Earth Observation Satellites: For Use in Optimization Algorithms," AAS-09-193, 19th AAS/AIAA Spaceflight Mechanics Meeting, Savannah, Georgia, February, 2009.

51. Wilkins, M., and Mortari, D., "Constellation Design Via Projection of an Arbitrary Shape onto a Flower Constellation Surface," AIAA-2004-4975, AIAA/AAS Astrodynamics Specialist Conference and Exhibit, Providence, Rhode Island, August, 2004.

52. Aorpimai, M. and Palmer, P., "Analysis of Frozen Conditions and Optimal Frozen Orbit Insertion," *Journal of Guidance, Control, and Dynamics*, Vol. 26, No. 5, September-October, 2003, pp. 786-793.

53. Hashida, Y. and Palmer, P., "Epicyclic Motion of Satellites About an Obate Planet," *Journal of Guidance, Control, and Dynamics*, Vol. 24, No. 3, May-June 2001, pp. 586-596.

54. Abdelkhalik, O., "Orbit Design and Estimation for Surveillance Mission Using Genetic Algorithms," Ph.D. Dissertation, Department of Aerospace Engineering, Texas A&M University, College Station, Texas, December, 2005.

55. Matlab & Simulink. Student Version R2009a, Version 7.8.0.347, February, 2009.

56. Vallado, D., *Fundaments of Astrodynamics and Applications*, 2nd Edition, McGraw-Hill, New York, 2001.

57. Mathur, R. and Ocampo, C., "An Algorithm for Computing Optimal Earth Centered Orbit Transfers via Lunar Gravity Assist," AIAA-2010-7521, AIAA/AAS Astrodynamics Specialist Conference, Toronto, Ontario, August, 2010.

58. NGA GEOnet Names Server (GNS), National Geospatial-Intelligence Agency, http://earth-info.nga.mil/gns/html.

59. Draim, J. and Castiel, D., "Elliptic Constellations for Optimal Coverage of Selected Geographical Areas," AIAA-96-1075, AIAA International Communications Satellite Systems Conference, Washington D.C., February, 1996.

60. Bate, R. R., Mueller, D. D., and White, J. E., *Fundamentals of Astrodynamics*, Dover Publications, New York, 1971.

VITA

Sharon Vtipil earned her Bachelor of Science degree in Aerospace Engineering from the United States Naval Academy in 1997. She commissioned into the United States Air Force and worked for eight years in the areas of space operations and program management. During her time in the Air Force, she earned her Master's of Engineering degree in Aerospace Engineering from the University of Florida in 2000. In 2006, she joined Old Dominion University to pursue a Doctorate degree in Aerospace Engineering.